

The composition of Mars

Takashi Yoshizaki^{*1} and William F. McDonough^{1,2,3}

¹Department of Earth Science, Graduate School of Science, Tohoku University, Sendai, Miyagi 980-8578, Japan

²Department of Geology, University of Maryland, College Park, MD 20742, USA

³Research Center of Neutrino Sciences, Tohoku University, Sendai, Miyagi 980-8578, Japan

January 10, 2020

Abstract

Comparing compositional models of the terrestrial planets provides insights into physicochemical processes that produced planet-scale similarities and differences. The widely accepted compositional model for Mars assumes Mn and more refractory elements are in CI chondrite proportions in the planet, including Fe, Mg, and Si, which along with O make up >90% of the mass of Mars. However, recent improvements in our understandings on the composition of the solar photosphere and meteorites challenge the use of CI chondrite as an analog of Mars. Here we present an alternative model composition for Mars that avoids such an assumption and is based on data from Martian meteorites and spacecraft observations. Our modeling method was previously applied to predict the Earth's composition. The model establishes the absolute abundances of refractory lithophile elements in the bulk silicate Mars (BSM) at 2.26 times higher than that in CI carbonaceous chondrites. Relative to this chondritic composition, Mars has a systematic depletion in moderately volatile lithophile elements as a function of their condensation temperatures. Given this finding, we constrain the abundances of siderophile and chalcophile elements in the bulk Mars and its core. The Martian volatility trend is consistent with ≤ 7 wt% S in its core, which is significantly lower than that assumed in most core models (i.e., >10 wt% S). Furthermore, the occurrence of ringwoodite at the Martian core-mantle boundary might have contributed to the partitioning of O and H into the Martian core.

^{*}Corresponding author. E-mail: takashiy@tohoku.ac.jp

1 Introduction

Mars is the second best-explored planet in our Solar System, given multiple space missions and cosmochemical studies on Martian meteorites (McSween and McLennan, 2014). Therefore comparison of physical and chemical properties of Mars with those of the Earth can provide important insights into the origin and evolution of the rocky planets, especially conditions for habitable planet formation. Radioisotope dating of Martian meteorites demonstrates that its accretion and evolution occurred earlier than that of the Earth (Dauphas and Pourmand, 2011; Kruijer et al., 2017b; Bouvier et al., 2018). The rapid formation of Mars is consistent with a pebble accretion and/or runaway and oligarchic growth model, depending upon model assumptions (Dauphas and Pourmand, 2011; Johansen et al., 2015; Levison et al., 2015). Thus, a comparison of the composition of Mars and the Earth (McDonough and Sun, 1995; McDonough, 2014) will provide insights into processes of planetary formation and evolution.

Compositional modeling of terrestrial planets requires determining the abundances and distribution of elements, given limited chemical data from their silicate shell, knowledge of the behavior of elements in different P-T-composition- $f\text{O}_2$ conditions (Table 1), and constraints from their geodetic properties. A compositional model for the bulk planet and its core and mantle can be used to understand the many and markedly different processes involved in its accretion and differentiation. Models for the chemical composition of Mars (e.g., Morgan and Anders, 1979; Longhi et al., 1992; Wänke and Dreibus, 1994; Lodders and Fegley, 1997; Sanloup et al., 1999; Halliday et al., 2001; Burbine and O'Brien, 2004; Taylor, 2013) have been reviewed recently by Taylor (2013). Limited cosmochemical constraints and seismic data from Mars make it difficult to evaluate critically these competing models. Importantly, most existing models assume Mars' major element composition equates to that in CI carbonaceous chondrites. Chondrites are undifferentiated assemblage of metal and silicate (Scott and Krot, 2014). Chondritic meteorites, especially the CI carbonaceous chondrites, are chemically similar to the solar photosphere (e.g., Palme et al., 2014), which is taken to reflect the Sun's abundances of non-gaseous elements. At >99% of mass of the Solar System, understanding the Sun's composition and that of chondrites, the building blocks of the terrestrial planets, is key to understanding the sources and processes involved in making the planets.

The Wänke and Dreibus family of models (Wänke, 1981, 1987; Dreibus and Wänke, 1984, 1987; Wänke and Dreibus, 1988, 1994) is the most widely accepted compositional model of Mars. It is based on the chemical composition of Martian meteorites and assumes that Mn and more refractory elements (Table 1) are in CI-like proportions in Mars, and considers CI chondrites as one of the components of Mars' building materials. Abundances of other less refractory elements are determined from chemical correlations with refractory or major elements. Many studies use a similar approach (Longhi et al., 1992; Halliday et al., 2001; Taylor, 2013). Taylor (2013) revisited and updated the Wänke and Dreibus model using the more abundant, recent chemical data for Martian meteorites and spacecraft observations, and found no significant difference with the Wänke

and Dreibus model. This model is the standard for most geochemical and geophysical modeling (e.g., Sohl and Spohn, 1997; Khan et al., 2018) and experimental work (e.g., Bertka and Fei, 1997, 1998a).

As an alternative approach, Morgan and Anders (1979) determined Martian refractory and moderately volatile element abundances based on K/Th (i.e., volatile/refractory) ratio of 620, which was measured for the Martian surface by a gamma-ray survey (GRS) in the Mars 5 orbiter mission in 1970s (Surkov, 1977). This K/Th value is significantly lower than recently observed values (~ 5300 ; Taylor et al., 2006a,b). The Morgan and Anders (1979) model also assumes CI-like Mg/Si ratio for Mars as did by Wänke and Dreibus (1994).

The chemical composition of Mars has also been estimated using a mixing ratio of chondritic meteorites that can reproduce the O-isotopic composition of Martian meteorites (Lodders and Fegley, 1997; Sanloup et al., 1999; Burbine and O'Brien, 2004). This approach estimates high volatile abundances for the terrestrial planets (e.g., K/Th ~ 16400 for Mars; Lodders and Fegley, 1997), which are not consistent with the measured planetary surface compositions (Surkov et al., 1986, 1987; McDonough and Sun, 1995; Taylor et al., 2006a,b; Peplowski et al., 2011; Prettyman et al., 2015).

Here we present an alternative compositional model for Mars. Given the recent improvements in our understandings on the composition of the solar photosphere and meteoritic samples (Section 2), we avoid the CI chondrite assumption. We base our model on data from Martian meteorites and spacecraft observations and use a method that was previously applied to predict the Earth's composition. We determine a unique composition for bulk silicate Mars (BSM) and a best fit, non-unique model for its core composition. By establishing the systematic depletion in volatile elements in the BSM, we show that the core has ≤ 7 wt% S along with O and H as light elements. We discuss similarities and differences between the Earth and Mars and possible causes of these differences elsewhere.

2 Recent developments in understanding the Solar System

Over the last decade technological advances and insights have revealed markedly new perspectives about the Sun's composition and restrictions in the radial distribution of certain chondritic materials. Multiple challenges have been advanced regarding the solar photosphere's composition, weakening the use of CI chondrites as a proxy for the bulk solar composition. Spectroscopic observations of the solar photosphere and assumptions about local thermodynamic equilibrium in modeling the photosphere's composition are used to constrain its elemental abundances (e.g., Asplund et al., 2009). The *solar metallicity problem* notes the significant difference in estimates of the sun's metallicity (Z_{\odot} , abundance of elements in the Sun heavier than He) from spectroscopic observations versus helioseismology (e.g., Basu and Antia, 2008; Haxton et al., 2013; Bergemann

and Serenelli, 2014). The former method suggests 30 to 40% lower metal content in the Sun and the finding is at 5σ to 15σ outside the limits set by helioseismology for the Sun’s surface He abundance, the sound speed in the convective zone, and the depth of the convective zone boundary. Data from experiments on the opacity of metals in high temperature plasma (Bailey et al., 2015; Nagayama et al., 2019), the composition of solar wind particles (Schmelz et al., 2012), and measurements of the solar neutrino flux (Haxton et al., 2013; Agostini et al., 2018) are in mutual agreement with findings from helioseismology, regarding the Sun’s metallicity. One solution to the problem is to have a significant increase in the Sun’s abundance of Mg, Si, S and Fe, which leads to a hotter core temperature (Basu and Antia, 2008; Asplund et al., 2009; Bergemann and Serenelli, 2014).

It is also important to recognize the accretion settings of different chondritic parent bodies. Isotopic distinctions (e.g., O, Ni, Cr, Ti, Mo, W) are now clearly established for the non-carbonaceous and carbonaceous (NC and CC, respectively) meteorite groups, including the chondrites (Warren, 2011; Dauphas and Schauble, 2016; Kruijer et al., 2017a). These differences likely originated because of a limited radial transport in the accretion disk, which may have been controlled by an early-formed young Jupiter (Walsh et al., 2011; Kruijer et al., 2017a; Raymond and Izidoro, 2017; Desch et al., 2018). As members of the inner Solar System NC group, Mars and Earth are isotopically most similar to ordinary and enstatite chondrites, respectively, whereas CI chondrites are isotopically a part of the CC group meteorites, which are taken to sample the outer Solar System building blocks. Trace element chemistry of NC and CC meteorites supports this isotopic divide of two groups (Dauphas and Pourmand, 2015; Barrat et al., 2016). The $<10\%$ variation in relative abundances of refractory elements among NC and CC chondrites (e.g., Masuda, 1957; Coryell et al., 1963; Larimer and Wasson, 1988; Wasson and Klemmeyn, 1988; Bouvier et al., 2008b) is used to constrain compositional models of the Earth by accepting these chondritic refractory element ratios (McDonough and Sun, 1995; Palme and O’Neill, 2014). Thus, we recommend not using a CI-chondrite compositional model for the inner terrestrial planets, including Mars, especially for non-refractory elements. Here we develop a compositional model for Mars that is based on Martian rocks and is free of the CI chondrite assumption for non-refractory elements. As a reference frame for comparing meteorites and planetary compositions, including for the production of chondrite-normalized patterns (e.g., rare earth element (REE) diagrams), the CI composition provides a useful standard. In this paper, we use the CI reference frame without it having any implications for the origin of materials that formed Mars and other terrestrial planets.

3 Data

A compilation of chemical and isotopic data of Martian meteorites was used in this study, with most data coming from the Martian Meteorite Compendium (Righter, 2017) and the online Met-Base database (<https://metbase.org/>). Shergottites, especially poikilitic (previously identified as lherzolitic) samples, were used to estimate the composition of the bulk silicate Mars (BSM). These samples have experienced crystal accumulation, but their composition maintain critical imprints of

their primordial origins. We complement this suite of rocks with data from olivine and basaltic shergottites in order to elucidate melt-residue correlations. In most cases we excluded nakhlites, chassignites and other ungrouped Martian meteorites (e.g., Allan Hills (ALH) 84001) from our analyses because these samples are variably thermally modified cumulates, or show more complex lithologies rather than being simple melt-derived rocks (McSween, 2008; Day et al., 2018). Paired Martian meteorites (e.g., Northwest Africa (NWA) 2975 and NWA 2986) are treated as one sample. Several analyses which are unrepresentative due to sample heterogeneity or terrestrial contamination are also excluded from our dataset. Average values of elemental abundances in each Martian meteorite are calculated and used in the compositional modeling. We also use data from the Martian surface as measured by spacecraft missions using GRS (Taylor et al., 2006a,b; Boynton et al., 2008). For some elemental abundances, we adopted estimates by recent studies (e.g., Yang et al., 2015; Wang and Becker, 2017; Tait and Day, 2018; see Section 4). Errors are reported as 1 standard deviations, unless otherwise noted. For a CI chondritic composition (Table 2), we adopted the value proposed by Palme et al. (2014) for most elements, with some modifications for halogens (Clay et al., 2017), Mo, Tl, Bi (Wang et al., 2015), highly siderophile elements (Day et al., 2016), and U (Wipperfurth et al., 2018).

We note that our compositional modeling of Mars is based on limited chemical data from Martian rocks that might not be representative samples of the Martian crust or mantle (e.g., Taylor, 2013 and references therein). As is likely the case for the Earth, there is likely no residual domain of the primitive BSM remaining. In addition, multiple evidence indicate compositional heterogeneity in the Martian mantle and crust. Incompatible element compositions (McLennan, 2003), radiogenic isotope systematics (e.g., initial $^{87}\text{Sr}/^{86}\text{Sr}$ and $^{143}\text{Nd}/^{144}\text{Nd}$; Norman, 1999; Blichert-Toft et al., 1999; Symes et al., 2008) and redox state (Wadhwa, 2001; Hui et al., 2011) of shergottites indicate the presence of at least two distinct sources in the Martian mantle, whose origin remains unconstrained (e.g., Symes et al., 2008; Brandon et al., 2012; McSween, 2015). Furthermore, radiogenic isotope systematics of nakhlites and chassignites indicate a third reservoir which was moderately depleted in incompatible elements (Jones, 2003; Foley et al., 2005; Treiman, 2005; McCubbin et al., 2013; Day et al., 2018; Udry and Day, 2018). Lower K, Th and Fe abundances and the lower K/Th ratio of shergottites than that of the Martian crust measured by Mars Odyssey GRS, are also consistent with diverse sources in the Martian mantle (McLennan, 2003; Taylor et al., 2006a). These observations may reflect a highly heterogeneous mantle and possibly unrepresentative sampling of the Martian crust by Martian meteorites. The compositional model of Mars proposed in the current work is the best estimate based on data available today, but it is potentially influenced by these problems.

4 Composition of the bulk silicate Mars

4.1 Refractory lithophile elements

Refractory lithophile elements (RLE; Table 1) remain in the silicate shell during core-mantle differentiation and their relative abundances show limited variation (generally <10%) among chondritic meteorites (e.g., Masuda, 1957; Coryell et al., 1963; Larimer and Wasson, 1988; Wasson and Kallemeyn, 1988; Bouvier et al., 2008b). Thus, if you establish the absolute concentration of one RLE, you can calculate the abundances of all of the others based on chondritic ratios (e.g., Sm/Nd, Lu/Hf, Ca/Al).

As a first step in determining the composition of Mars, we independently tested if Mars has chondritic ratios of the RLE. We used ratio-ratio plots to demonstrate that the trends cross at the intersection of the primitive joint chondritic compositions when using two pairs of refractory lithophile elements with different incompatibilities (Fig. 1). Poikilitic shergottites are interpreted to be olivine-pyroxene cumulates derived from basaltic magma, whereas other shergottites are considered to have formed as lava flows (e.g., McSween and McLennan, 2014). As has been observed for terrestrial komatiites (e.g., Sun, 1982; Arndt and Jenner, 1986), we find that cumulates and their co-existing melts (basaltic shergottites) fall along differentiation trends that project back to residual peridotite compositions (Fig. 1). Thus, these chemical trends see through previous melt-residue differentiation events back to their primordial compositions, which are chondritic RLE ratios, within uncertainties. Given this finding, all RLE are taken to be in chondritic relative proportions in the BSM and, by implication, in bulk Mars too. From this starting point, we can directly determine the BSM abundances of most elements, whose concentrations are correlated with ratios or abundances of refractory lithophile elements in Martian rocks, due to chemical trends resulting from melt-residue differentiation.

The absolute abundance of the RLE are established using variation diagrams involving a single RLE versus an RLE ratio (Fig. 2). The poikilitic shergottite are the best recorders of melt depletion trends, providing an accurate estimate of the primitive BSM composition. Using these melt depletion trends for multiple element combinations, we estimate the absolute abundance of the RLE in the BSM at ~2.26 times that in CI chondrites with ~10% uncertainties (cf. $2.75 \times$ CI in the bulk silicate Earth (BSE); McDonough and Sun, 1995). The uncertainty for the absolute abundances of RLE in the BSM was determined from an analysis of the uncertainties associated with the intercepts of Hf/Sc or Ti/Sc and the heaviest nine REE. The Hf/Sc and Ti/Sc ratios were used because they represented the greatest differences in D-values with Hf and Ti being the most incompatible and Sc being the least incompatible. Doing so provides the greatest leverage in the regression analyses and their uncertainties. The estimated RLE abundance in the BSM is ~20 % higher than that of the Wänke and Dreibus (1994) model.

4.2 Major elements (Mg, Si, Fe)

Magnesia correlates negatively with RLE abundances in shergottites (Fig. 3) and trends for multiple RLE establish the MgO abundance at 31.0 ± 2.0 wt% for the BSM. There is limited variation in silica contents in shergottites (Fig. 4), reflecting silicon's bulk distribution coefficient of ~ 1 during silicate melt production. The SiO₂ content of the Martian surface as measured by GRS (Boynton et al., 2007) overlaps with the range found in basaltic shergottites, confirming the bulk crust of Mars is basaltic (McSween et al., 2009). By averaging the SiO₂ abundances in shergottites, we estimate 45.5 ± 1.8 wt% SiO₂ for the BSM. Assuming no Si or Mg in the Martian core, our BSM and bulk Mars model compositions have a Mg/Si value of 0.88 ± 0.07 , which agrees with an estimate based on Si isotope systematics (0.86 ± 0.05 ; Dauphas et al., 2015). Uncertainty in the Mg/Si value for the BSM does, however, overlap with average values for ordinary (~ 0.82) and carbonaceous chondrites (~ 0.92).

As compared to the Earth's mantle, the Martian mantle is more oxidized and Martian meteorites, including the least evolved samples, have distinctly lower Mg# (atomic ratio of Mg/(Mg + Fe)) relative to basalts from the Earth (e.g., Wadhwa, 2001, 2008; Herd et al., 2002). Estimates of the Mg# of the Martian mantle range between 0.7 and 0.8, and the Wänke and Dreibus model have Mg# = 0.75 (Table 3). The melt-rock partition coefficient for FeO (D_{FeO}) reported by Taylor (2013) is 0.95 ± 0.06 . From this value, the author concluded that the Martian mantle FeO content is 18.1 ± 2.2 wt% ($2\sigma_m$), which leads to Mg# comparable to the estimate of Wänke and Dreibus (1994).

Multiple studies suggest a higher Mg# for the BSM than the Wänke and Dreibus model. Melting experiments by Agee and Draper (2004) showed that the FeO abundance and high CaO/Al₂O₃ ratio of shergottites cannot be reproduced by mantle differentiation from the BSM with Mg# = 0.75, but it can be derived from a more Fe-poor mantle with an Mg# ~ 0.80 . Olivines in primitive depleted shergottites reach Mg# of 0.86 (Usui et al., 2008), which requires extensive (>50%) melting of the Martian primitive mantle if the BSM has Mg# = 0.75, which is unlikely to be achieved when shergottites formed (Musselwhite et al., 2006). On the other hand, with an Fe-poor Martian primitive mantle (Mg# ~ 0.80), much lower degrees of mantle melting can produce the high-Mg olivine (Musselwhite et al., 2006; Collinet et al., 2015; McCoy et al., 2016). Collinet et al. (2015) concluded that the Martian mantle has heterogeneous Mg# ranging between 0.75–0.82. The Fe-poor BSM model is multiply supported by geochemical and geophysical modeling (Borg and Draper, 2003; Draper et al., 2005; Minitti et al., 2006). Given these observations, we prefer to adopt the FeO-poor (Mg# = 0.79 ± 0.02) primitive Martian mantle composition, which gives an FeO content of 14.7 ± 1.0 wt% in the BSM. Collectively, these findings for the RLE (Al, Ca and Ti) oxides, magnesia, silica and ferrous iron sets the BSM composition at a total of 97.8 wt% (Table 4).

4.3 Non-refractory lithophile elements

4.3.1 Manganese, chromium and vanadium

The MnO concentration in the BSM (Wänke and Dreibus, 1994; Taylor, 2013) is established foremost from the nearly constant FeO/MnO ratio in Martian meteorites (shergottite average 39.4 ± 6.7) and the Martian mantle's FeO content, producing a BSM having 0.37 ± 0.07 wt% MnO. An alternative approach uses experimental studies on the partitioning of Mn at 1–2 GPa during melting (Baratoux et al., 2011; Filiberto and Dasgupta, 2011). The measured olivine/melt partition coefficient for MnO (Takahashi and Kushiro, 1983; Herzberg and Zhang, 1996; Walter, 1998; Wasylenki et al., 2003; Le Roux et al., 2011) is 0.93 ± 0.04 (Taylor, 2013). Using this value and a shergottite average MnO content (0.48 ± 0.06 wt%) predicts 0.44 ± 0.06 wt% MnO in the BSM. The MnO content of the BSM obtained using these methods are in agreement within uncertainties.

Chromium correlates with Al ($R^2 = 0.72$) in poikilitic and olivine-phyric shergottites Fig. A1). Where the Cr-Al trend crosses the Al content of the BSM yields 0.88 ± 0.15 wt% Cr₂O₃ in the BSM. The CI-normalized abundances in the BSM for Cr and major elements (Mg, Si and Fe), with similar condensation temperatures (Lodders, 2003), is used to conclude that the Martian inventory of Cr is hosted solely in the mantle.

In the solar nebula, vanadium behaves as a refractory lithophile element (Lodders, 2003). During the formation of the Earth's core, V behaved equally lithophile and siderophile (Ringwood and Hibberson, 1990; Wade and Wood, 2005; Wood et al., 2006, 2008; Corgne et al., 2008; Siebert et al., 2013), consequently half of the Earth's inventory of V is considered to be in the core (McDonough, 2014). Estimates of the V content of the BSM using correlation diagrams yields ~ 130 ppm V, which is an equivalent concentration to that of the other RLE ($\sim 2.26 \times$ CI) (note, here and throughout the paper ppm and ppb will refer to parts per million and billion by weight, respectively). Thus, we conclude that V behaved exclusively as a lithophile element during Mars' core formation and is wholly concentrated in the BSM.

4.3.2 Sodium and potassium

A log-log abundance plot of Na and Al in poikilitic and olivine-phyric shergottites show a well-defined slope ~ 1 correlation ($R^2 = 0.83$; Fig. A2), indicating nearly equal incompatibility of these elements during a partial melting of the Martian mantle. The limited variation in Na/Al ratio in shergottites (0.44 ± 0.10) is consistent with a Na₂O content of 0.59 ± 0.13 wt% in the BSM.

The radioactive elements, K, Th and U, have similar partitioning behavior during mantle melting. Consequently, the Martian surface K/Th value of 5300 ± 220 , measured by GRS aboard Mars Odyssey (Taylor et al., 2006a,b), is taken as the bulk K/Th value. Both Th and U are RLE and this K/Th value gives 0.043 ± 0.005 wt% K₂O (360 ppm K; Table 5) in the BSM. Our BSM model has Na/K of 12 ± 3 , comparable to the Earth's ratio (11) and overlapping within errors of the lower

chondritic value (9.1 ± 1.3 ; Wasson and Kallemeyn, 1988). Importantly, this ratio of elements increases as a function of the relative condensation temperature, such that Na/K increases from CI to CM to CO/CV chondrites as refractory to volatile element ratios increase (Wasson and Kallemeyn, 1988). This trend is consistent with higher Na/K in the Earth and Mars.

4.3.3 Rubidium

Martian meteorites show a negative trend in a plot of initial $\varepsilon^{143}\text{Nd}$ versus $^{87}\text{Sr}/^{86}\text{Sr}$ values, establishing the Martian mantle array (Fig. 5). The Martian mantle array is shifted to higher $^{87}\text{Sr}/^{86}\text{Sr}$ values compared to the Earth's mantle array, consistent with Mars' proportionally higher content of volatile elements. The Martian mantle array yields an initial $^{87}\text{Sr}/^{86}\text{Sr}$ value of $0.709\text{--}0.721$ in the BSM assuming an initial $\varepsilon^{143}\text{Nd} = 0$ for the planet. If Rb/Sr fractionation took place at the earliest stages of accretion, then Mars' initial $^{87}\text{Sr}/^{86}\text{Sr}$ value is consistent with a Rb/Sr of 0.08 ± 0.04 , and thus 1.5 ± 0.8 ppm Rb in the BSM. Analogous to Na/K, K/Rb ratio for Mars is 300, which is higher than the CI value (250) and not as volatile depleted as the Earth's value (400).

Alternatively, a log-log concentration plot of Rb versus La (slope = 1.0 ± 0.1 ; $R^2 = 0.84$; Fig. A3) reveals their similar partition coefficients during mantle melting. Using La (an RLE) abundance in the BSM, we predict 0.9 ± 0.4 ppm Rb in the BSM, comparable to that based on the Nd- and Sr-isotopic systematics. An average of these estimated values yields 1.2 ± 0.4 ppm Rb in the BSM.

4.3.4 Cesium

In a log-log concentration plot, Cs and La show a trend with a slope of 1.0 ± 0.1 ($R^2 = 0.78$; Fig. A4). The Cs/La ratio in shergottites (0.14 ± 0.10) leads to 0.08 ± 0.06 ppm Cs in the BSM. This value is consistent with an average Rb/Cs ratio of shergottites (16.0 ± 3.0) which indicates 0.07 ± 0.03 ppm Cs in the BSM.

4.3.5 Lithium

Lithium correlates with Nb and the LREE in Martian meteorites (Fig. A5). Intercepts of the Li-RLE trends and the BSM abundances of the RLE ($\sim 2.26 \times \text{CI}$) yields Li concentration in the BSM of 1.8 ± 0.4 ppm.

4.3.6 Boron

Boron and Ca are correlated in poikilitic and olivine-phyric shergottites (Fig. A6), except for five high-B (> 10 ppm B) olivine-phyric shergottite samples discussed by Day et al. (2018). We agree that these five high-B samples are possibly affected by terrestrial weathering (Curtis et al., 1980;

Yang et al., 2015; Day et al., 2018) and exclude them from consideration. The average B/Ca (0.41 ± 0.25) in poikilitic and olivine-phyric shergottites leads to 0.84 ± 0.53 ppm B in the BSM.

4.3.7 Gallium

Gallium and Al are positively correlated in shergottites ($R^2 = 0.84$; Fig. A7). An average Ga/Al ratio for shergottites (4.6 ± 0.9) yields 8.7 ± 1.9 ppm Ga in the BSM. Similarly, the Earth's average Ga/Al ratio for basalts and mantle rocks is 4.3 (McDonough, 1990), the same as that for Mars. The abundance of Ga in the BSM and BSE points to its lithophile behavior during core–mantle differentiation and these cores having negligible quantities of Ga.

4.3.8 Halogens

Efforts to estimate the abundances of the halogens (Cl, F, Br, I) are fraught with challenges, because halogens are fluid-mobile and thus readily lost during magma degassing and by alteration processes (e.g., Filiberto et al., 2019 and references therein). Many have attempted to filter Martian meteorite data affected by such secondary processes (Dreibus and Wänke, 1985, 1987; Treiman, 2003; Filiberto and Treiman, 2009; Filiberto et al., 2016, 2019).

Filiberto and Treiman (2009) and Filiberto et al. (2016) constrained Cl/La value for Martian basalt to be 51 ± 17 , which is higher than the terrestrial Cl/La ratio (21 ± 6). This Cl/La ratio and the BSM abundance of La (0.55 ± 0.05 ppm) yields 28 ± 10 ppm Cl in the BSM, which is our preferred value. We also observed a well-defined correlation between Cl and Sr in Martian meteorites ($R^2 = 0.79$; Fig. A8), which corresponds to 32 ± 21 ppm of Cl in the BSM. Although errors in the Cl abundance estimated by these two methods are large, these values are consistent in general. Taylor et al. (2010) used GRS data to establish the Cl/K ratio of 1.3 ± 0.2 , which is a factor of six higher than the CI value (Table 2). Chlorine abundance in the Martian surface reflects secondary deposition and thus high Cl/K ratios are not an indicator of the primitive Cl content of the BSM (Keller et al., 2006; Filiberto et al., 2019).

There are limited F data for Martian meteorites. The few shergottites samples with coupled F and B data show a correlation ($R^2 = 0.80$; Fig. A9), indicating 16 ± 12 ppm F in the BSM. Filiberto et al. (2016) reported shergottites and terrestrial basalts with a mean Cl/F of 0.8 ± 0.4 . Given terrestrial and Martian basalts are modified by magma degassing, which decreases the initial value, whereas alteration increases the ratio, Filiberto et al. (2016) suggested $\text{Cl}/\text{F} \sim 1$ in the Martian mantle. Using our estimate of the BSM abundance for Cl, we obtained the BSM abundance for F of ~ 30 ppm, our preferred value.

An average Cl/Br ratio in Martian meteorites (224 ± 140 ; Filiberto et al., 2016) would suggest 0.12 ± 0.09 ppm Br in the BSM. In contrast, the chondritic Cl/Br ratio is 600, which is comparable to the BSE value (e.g., McDonough and Sun, 1995; Palme and O'Neill, 2014; Clay et al., 2017

and references therein). If we assume \sim 0.12 ppm Br in the BSM, it would result in a marked spike in the volatility curve singularly for Br. This raises our suspicion and leads us to question the resiliency of the Martian meteoritic record for Br. Thus we conclude Br content of \sim 0.05 ppm in the BSM based on the chondritic Cl/Br ratio.

There is limited data for I in Martian meteorites, the most volatile of the lithophile elements (Table 1). We do not observe any clear correlation of the halides with other elements. Chondritic meteorites show limited variation of I/Cl ratios (Clay et al., 2017) comparable to that observed for the BSE composition (e.g., McDonough and Sun, 1995; Palme and O’Neill, 2014; Clay et al., 2017 and references therein). Assuming the BSM has CI-like I/Cl ratio ($(5.0 \pm 1.7) \times 10^{-4}$; Clay et al., 2017), we estimate 14 ± 7 ppb I in the BSM.

4.4 Siderophile and chalcophile elements in the BSM

4.4.1 Refractory and major siderophile elements in the BSM

These elements include W and Mo along with Fe, Ni, and Co (Table 1). Nickel in poikilitic and olivine-phyric shergottites correlate with Mg (Fig. A10) and their average Ni/Mg ratio is 19.4 ± 5.0 , consistent with 0.046 ± 0.012 wt% NiO in the BSM. Likewise these rocks have an average Co/Ni ratio of 0.27 ± 0.10 , consistent with 96 ± 44 ppm Co in the BSM.

Molybdenum abundance in shergottites is highly variable between 0.05–0.7, and is not well correlated with lithophile elements. The origin of the wide variation in Mo contents in shergottites is not constrained. Yang et al. (2015) attributes this variation to hydrothermal processes, whereas Noll et al. (1996) argues that Mo is not fluid-mobile. Based on a broad Mo-Ce co-variation, Righter and Chabot (2011) and Yang et al. (2015) estimated the BSM abundance of Mo is 0.08–0.6 ppm. We estimate the BSM to have between 0.1–0.8 ppm Mo.

In a log-log plot for all shergottites, W and Th shows a linear trend with a slope 1.1 ± 0.2 (Fig. A11), indicating their similar incompatibilities. Using an average W/Th ratio in shergottites (1.0 ± 0.5), W concentration in the BSM is estimated to be 0.07 ± 0.04 ppm. Our BSM model has Hf/W of (3.47 ± 1.90) , which is consistent with an estimate by Dauphas and Pourmand (2011).

4.4.2 Highly siderophile elements

Highly siderophile elements (HSE) include Re, Os, Ir, Pt, Ru, Rh, Pd and Au. Brandon et al. (2012) and Tait and Day (2018) estimated the BSM abundances of the HSE based on co-variation between the HSE and MgO in shergottites. Although Re, Pd and Pt are poorly correlated with Mg, Tait and Day (2018) assumed MgO \sim 35 wt% in the BSM and obtained flat, chondrite-like HSE patterns in the BSM, with absolute abundances at $(0.010 \pm 0.003) \times$ CI. The MgO composition of the BSM used by Tait and Day (2018) is slightly higher than our estimate (MgO \sim 31.0 wt%). However, this

difference is negligible for the predicted abundances of the HSE in the BSM and so we adopt the Tait and Day (2018) estimate.

Similarly, Au abundances show a broad correlation with MgO in shergottites (Fig. A12). This correlation indicates ~ 2 ppb Au in the BSM, which corresponds to the BSM abundance of $\sim 0.01 \times \text{CI}$ (Fig. 6). Thus it is likely that the bulk of the BSM budget of Au originated in the late accretion of materials with a chondritic HSE composition.

There are limited data for Rh in Martian meteorites with a wide variation, and Rh is not correlated with other elements in Martian meteorites. If we take the mean Rh concentration in the Martian meteorites (~ 2 ppb) as the BSM abundance of Rh, this value corresponds to $\sim 0.02 \times \text{CI}$ in the BSM, which is close to that of other HSE (Fig. 6; Tait and Day, 2018).

4.4.3 Moderately volatile siderophile elements

Moderately-volatile, siderophile elements include P, Cu, Ge, As, Ag, Sb, Sn, Pb and Bi. A well-defined positive correlation for P versus Y ($R^2 = 0.88$), with a slope of 1.1 ± 0.1 , is seen for shergottites (Fig. A13). Their average P/Y value in shergottites (0.021 ± 0.005) is used to estimate the P_2O_5 at 0.17 ± 0.05 wt% in the BSM.

Wang and Becker (2017) estimated Cu in the BSM abundance at 2.0 ± 0.4 ppm, based on Cu and MgO correlations in shergottites. Similarly, we find positive Cu versus Ti correlations in shergottites (Fig. A14), except for some anomalously high Cu/Ti samples ($\text{Cu}/\text{Ti} > 0.005$), and their average Cu/Ti value (0.0026 ± 0.0005) yields 2.6 ± 0.6 ppm Cu in the BSM, which is comparable to the estimate by Wang and Becker (2017).

Germanium does not correlate with lithophile elements in Martian meteorites, as mantle melting produces little variation in Ge content in the melt and residue (Ringwood, 1966). Germanium contents in shergottites ranges from 0.8 ± 0.4 ppm in poikilitic shergottites to 1.5 ± 0.3 ppm in olivine-phyric shergottites and $0.7\text{--}2.0$ ppm basaltic shergottites. From a weak negative correlation between Ge and MgO in poikilitic and olivine-phyric shergottites (Fig. A15), we estimate Ge abundance in the BSM is 0.6 ± 0.4 ppm.

In terrestrial rocks, As correlates with Ce (Noll et al., 1996). In contrast, As in shergottites does not correlate with tested lithophile elements (Yang et al., 2015). Arsenic is a fluid-mobile element (Noll et al., 1996); thus, the lack of any As-Ce correlation in shergottites might be due to hydrothermal processes (Yang et al., 2015). By attributing elevated As abundance in some Martian meteorites to the hydrothermal modification and ignoring such data, Yang et al. (2015) derived 30 ± 25 ppb As in the BSM.

We do not observe any correlation of Sb and Ag with lithophile elements. Yang et al. (2015) estimated the BSM abundance of Sb to be $0.01\text{--}0.03$ ppm using a roughly constrained Sb/Pr ratio

of Martian meteorites and the BSM abundance of Pr of 0.17 ppm from Lodders and Fegley (1997). We accept their estimate given that 0.21 ppm Pr in our model does not make significant changes in the estimation of the BSM abundance of Sb. A log-log plot of Sb versus Ag concentrations in shergottites (slope ~ 1 ; Fig. A16) indicates their similar compatibility during differentiation. The average Sb/Ag ratio of 1.4 ± 1.0 , with Ag being 0.02 ppm in the BSM with $\sim 90\%$ uncertainty.

Yang et al. (2015) estimated the BSM abundance of Sn, Cd and In based on their broad correlation with lithophile elements in Martian meteorites and a model of BSM abundances for lithophile elements by Lodders and Fegley (1997). The observed correlation resulted in more than a factor of two uncertainties in their estimates. Although abundances of lithophile elements in our model are different from that of Lodders and Fegley (1997), this difference does not produce any significant decrease in the estimated BSM abundances of Cd, In and Sn in Yang et al. (2015). Thus, we accept the BSM abundances of these elements given by Yang et al. (2015).

The BSM abundance of Pb is constrained from U-Pb isotopic systematics of Martian meteorites. Martian meteorites have a wide ranges of μ ($= {}^{238}\text{U}/{}^{204}\text{Pb}$) values and Pb isotopic heterogeneity (Nakamura et al., 1982; Misawa et al., 1997; Borg et al., 2005; Bouvier et al., 2005, 2008a, 2009; Chen and Wasserburg, 1986; Gaffney et al., 2007; Moriwaki et al., 2017; Bellucci et al., 2018). The recent review of the Martian μ value (~ 3.6), the average ${}^{208}\text{Pb}/{}^{204}\text{Pb}$, ${}^{207}\text{Pb}/{}^{204}\text{Pb}$ and ${}^{206}\text{Pb}/{}^{204}\text{Pb}$ in Martian meteorites of 33, 12.6 and 13, respectively, and 18 ppb U (Table 5) yields 0.26 ± 0.05 ppm Pb in the BSM.

Bismuth is correlated with Th in shergottites (except for high-Bi samples EETA 79001, Tissint and NWA 5990; Fig. A17) (Yang et al., 2015), which yields 2 ± 1 ppb Bi in the BSM.

4.4.4 Moderately volatile chalcophile elements

Moderately-volatile, chalcophile elements include Zn, Te, Se, S and Cd. As mentioned in Section 4.4.3, we adopt the BSM abundances of Cd estimated by Yang et al. (2015).

Zinc and Lu positively correlate in shergottites ($R^2 = 0.63$) as do Zn and Ti ($R^2 = 0.56$), which yield 45 ± 15 ppm and 40 ± 15 ppm Zn, respectively, in the BSM (Fig. A18). These two estimates agree within errors.

Taylor (2013) estimated Zn in the BSM at 18.9 ± 1.5 ppm, whereas as Yang et al. (2015) proposed 50–70 ppm. Taylor (2013) estimate was based on a Zn–Sc correlation, which is poorly correlated in our dataset ($R^2 = 0.27$). The relatively flat Zn–Sc trend observed by Taylor (2013) leads to a poor control on an accuracy estimate. Yang et al. (2015) assumed an olivine-rich Martian mantle and bulk mineral-melt partition coefficients for Zn of ~ 1 during mantle melting (Le Roux et al., 2011; Davis et al., 2013). The positive Zn–Lu correlation in shergottites (Fig. A18) reflects

the slightly incompatible nature of Zn in the Martian mantle. Thus, Yang et al. (2015) overestimates the Zn abundance in the BSM.

There is a wide range of estimates for the abundances of S-Se-Te in the BSM (Franz et al., 2019; Wang and Becker, 2017 and references therein). The limited variation in S/Se/Te ratios indicates little degassing loss of S, Se and Te, which led Wang and Becker (2017) to derive the BSM abundance of these elements at 360 ± 120 ppm, 100 ± 27 ppb and 0.50 ± 0.25 ppb, respectively. Here we adopt their estimates.

4.4.5 Volatile chalcophile elements

Volatile siderophile and chalcophile elements include In, Tl and Hg. As described in Section 4.4.3, we adopt the BSM abundances of In estimated by Yang et al. (2015) in our BSM model. Thallium is positively correlated with Sm ($R^2 = 0.73$; Fig. A19) in shergottites with a slope of 1.29 ± 0.38 in a log-log slope, indicating 4 ± 2 ppb Tl in the BSM.

Limited data exist for Hg (≤ 0.7 ppm) in Martian meteorites (Ehmann and Lovering, 1967; Weinke, 1978; Treiman and Lindstrom, 1997). It is readily contaminated by terrestrial sources, it is a highly volatile element, and it is lost during magma transport (e.g., Treiman and Lindstrom, 1997). Therefore it is very difficult to constrain the BSM abundance of Hg. Estimates of the solar abundance of Hg (few hundred ppb) are poorly constrained and Hg is undetectable in the solar photosphere (Lauretta et al., 1999; Grevesse et al., 2015; Meier et al., 2016). The BSM abundance of Hg is estimated to be ~ 7 ppb, with uncertainty ranging from ≤ 1 to a few tens of ppb.

4.5 Atmophile elements

The Mars' volatility trend (Fig. 6) cannot provide strong constraints on the planetary abundances of atmophile elements (H, C, N, O, noble gases; Table 1), given their distinctive behaviors compared with less volatile elements that are retained in rocks. However, approximate estimates of these elements in the BSM were predicted from the Martian volatility trend, following the practice used in McDonough (2014). An extrapolation of the Martian volatility trend to the lower temperature indicates their abundances to be $0.001\text{--}0.01 \times \text{CI}$.

Based on the water contents of Martian meteorites and their constituting hydrous phases (e.g., apatite, amphibole, glass), the BSM is estimated to have ~ 140 ppm H₂O (e.g., McCubbin et al., 2016a,b; Filiberto et al., 2019). This H₂O content corresponds to ~ 16 ppm H in the BSM, which is lower than that is expected based on the volatility trend. The low H abundance in the BSM might reflect H incorporation into the core (see Section 5.1) and/or loss of H from the mantle by degassing. Estimates for the water content of the Martian mantle range between 14–250 ppm, which likely reflects a heterogeneous water distribution in the mantle (e.g., McCubbin et al., 2010, 2016a,b).

The BSM might have contained \sim 1000 ppm H₂O if volatile-rich chondritic materials were added during a late accretion (i.e., 0.6–0.7% by mass of Mars), as indicated by highly siderophile element abundances and Os isotope systematics in shergottites (Tait and Day, 2018).

Filiberto et al. (2019) estimated the BSM abundances of C and N, based on mean C/H and N/H ratios in CI and CM carbonaceous chondrites (2.1 and 0.11, respectively; Alexander et al., 2012) and a BSM estimate for its H₂O content. This method assumes the BSM inventory of these atmophile elements is dominantly by a late addition component (e.g., Tait and Day, 2018) with CI- and CM-chondritic chemical composition (Filiberto et al., 2019). These assumptions lead to a BSM with \sim 140 ppm H₂O, \sim 32 ppm C and \sim 1.6 ppm N. These estimates have large uncertainties, given the degree of mantle degassing is essentially unconstrained.

Martian meteorites contain several noble gas components of distinct origins (Bogard et al., 2001; Ott et al., 2019). It is likely that significant fractions of Martian noble gas budgets are located in the Martian interior (Dauphas and Morbidelli, 2014), but their abundances are poorly constrained. Chassigny meteorite shows high abundance of noble gases with low Ar/Xe and Kr/Xe ratios, which is considered to reflect mixing of a composition of the Martian interior component (Ott, 1988; Bogard et al., 2001; Mathew and Marti, 2001). Further studies are needed to understand noble gas budgets and composition in the Martian interior.

5 Composition of the Martian core

5.1 Compositional model of the Martian core

To constrain the present-day Martian core composition, we modeled geophysical properties of Mars. Mineralogy, radial density distribution and seismic velocity profiles in the Martian mantle were computed using the Gibbs free energy minimization method that is employed in the thermodynamic modeling code *Perple_X* version 6.8.6 (Connolly, 2009). Calculations for the BSM composition (i.e., primitive Martian mantle composition; Table 4) were performed using thermodynamic parameters of Stixrude and Lithgow-Bertelloni (2011) within a chemical system Na₂O–MgO–Al₂O₃–SiO₂–CaO–FeO. Temperature profile in the Martian mantle (areotherm) is estimated assuming an Earth-like profile (Katsura et al., 2010), mantle potential temperature of \sim 1,500 K (Baratoux et al., 2011, 2013; Putirka, 2016; Filiberto, 2017), a lithosphere thickness of 200 km (Grott et al., 2013) and conductive and adiabatic thermal gradients of 2.7 K/km and 0.12 K/km, respectively (Verhoeven et al., 2005), which are consistent with the surface heat flux estimates (Parro et al., 2017). Fig. 7 shows a result of the thermodynamic modeling.

We also estimated mineralogy and physical properties of the present-day Martian mantle (not the BSM), which is calculated using compositional models for the BSM (Table 4) and the Martian crust (Taylor and McLennan, 2009), and a crustal mass fraction of \sim 5 % in the BSM. We observed small changes in the modal abundances of mineral species, but the density profiles are similar in

the present-day and primitive mantle models. Thus, the use of the density profile obtained using the composition of primitive mantle or present-day mantle makes negligible changes in our discussion.

Using the obtained radial density profile in the Martian mantle, we computed the Martian interior structure. Here we consider Mars as a spherically symmetric body divided into three layers (crust, mantle and core). The average crustal thickness of 50 km, which is consistent with geo-physical and geochemical constraints (Zuber et al., 2000; McGovern et al., 2002, 2004; Wieczorek and Zuber, 2004; Ruiz et al., 2009), is adopted in the modeling. We consider a crust of basaltic composition (e.g., Taylor and McLennan, 2009; McSween and McLennan, 2014 and references therein) with a density of 3010 kg/m^3 , which is in agreement with gravity and topography studies (McKenzie et al., 2002; McGovern et al., 2002, 2004; Phillips et al., 2008). The mass and moment of inertia (MOI) in Mars are expressed as a function of radial density distribution as:

$$M = 4\pi \int_0^a \rho(r)r^2 dr \quad (1)$$

$$C = \frac{8\pi}{3} \int_0^a \rho(r)r^4 dr, \quad (2)$$

where M is mass, C is MOI, a is Mars' equatorial radius (3389.5 km; Seidelmann et al., 2002), $\rho(r)$ is density and r is distance from the center of the planet.

Sulfur abundance in the Martian core has been of particular interests. Previous estimates vary between 3.5–25 wt% S (Table 6; also see Franz et al., 2019). With the Martian mantle having 360 ppm S (Wang and Becker, 2017), the Martian volatility curve restricts the core to having ≤ 7 wt% S (Fig. 8) if its core mass fraction is 18 wt% (see below). The low S composition for the Martian core is supported by metal-silicate partition coefficients for S (Rose-Weston et al., 2009; Boujibar et al., 2014; Wang and Becker, 2017) and an experimental study of Fe isotopic fractionation under high pressure and temperature (Shahar et al., 2015). If we adopt a higher S content for the BSM (up to 2000 ppm; Gaillard et al., 2013; Ding et al., 2015), the S content of the Martian core decreases. Thus, we conclude that the Martian core has ≤ 7 wt% S.

This estimate stands in contrast to widely adopted Martian core models that argue for >10 wt% S (Wänke and Dreibus, 1994; Taylor, 2013). Such a high sulfur content for the bulk Mars would, in principle, treat S differently with respect to other moderately volatile elements. We find no justification for such a S enrichment (Fig. 8).

For the Earth's core, C, H, S, Si and O are proposed as candidate light elements that decrease its density (Birch, 1952, 1964). Given the P-T-fO₂ condition of the Martian interior, we do not expect Si in the Martian core (Wade and Wood, 2005; Corgne et al., 2008), which is supported by a lack of Si isotopic fractionation in Martian meteorites resulted from a metal-silicate segregation (Zambardi et al., 2013; Dauphas et al., 2015). We also exclude C as a candidate light element in

the Martian core since the Martian meteorites lack C isotope fractionation unlike terrestrial rocks (Grady et al., 2004; Wood et al., 2013) and addition of C does not efficiently decrease the core density (Wood, 1993; Bertka and Fei, 1998b). In contrast, experimental studies indicate that O and H can be incorporated into the Martian core (Okuchi, 1997; Shibasaki et al., 2009; Tsuno et al., 2011) and their addition can decrease the core density (Badding et al., 1992; Bertka and Fei, 1998b; Zharkov, 1996; Zharkov and Gudkova, 2005). Moreover, having the Martian core-mantle boundary in contact with ringwoodite can contribute to the incorporation of H and O into the Martian core (Shibasaki et al., 2009; Tsuno et al., 2011; O'Rourke and Shim, 2018). Thus, we consider O and H, in addition to S, as candidates for light elements in the Martian core.

We calculated density of the Martian core using elastic properties of liquid Fe (Anderson and Ahrens, 1994), FeS (Nagamori, 1969; Kaiura and Toguri, 1979; Antonangeli et al., 2015; Nishida et al., 2016) and FeO (Lee and Gaskell, 1974; Komabayashi, 2014) and solid FeH (Umemoto and Hirose, 2015) at core pressures and temperatures and a third-order finite strain Birch-Murnaghan or Vinet equation of state (Stixrude and Lithgow-Bertelloni, 2005), following previous studies (Longhi et al., 1992; Sohl and Spohn, 1997; Bertka and Fei, 1998b; Verhoeven et al., 2005; Zharkov and Gudkova, 2005; Rivoldini et al., 2011; Khan et al., 2018). Given a lack of elastic properties of liquid FeH, we assumed that the properties of liquid FeH is similar to that of solid FeH. Temperature profile in the core is calculated based on the temperature of core-mantle boundary (Fig. 7) and a convection in the score.

By fitting mass, density and MOI in the three layers and the bulk planet to geodetically constrained values (Table 7), the density and composition of the metallic core is estimated. Finally we obtained a core composition with 6.6 wt% S, 5.2 wt% O and 0.9 wt% H, and a mass fraction of 18% as our best estimate. This core model yields a bulk planetary Fe/Si ratio of 1.36, which is lower than the CI value (1.74) but within the range of chondritic meteorite compositions (1.0–1.8; Wasson and Kallemeyn, 1988). With a mass fraction of 18%, the Martian core radius is 1580 km (i.e., 1810 km deep) and its mean density is $\sim 6910 \text{ kg/m}^3$ (Fig. 9).

Siderophile element abundances in the bulk Mars and its core were constrained by the BSM and a core model (Table 8). This yields the Fe content in the core and bulk Mars to be 79.5 wt% and 23.7 wt%, respectively. Given chondritic meteorites (aside from the few examples of iron rich chondrites (e.g., CB)) show limited variation in Fe/Ni (~ 17.4) and Ni/Co (~ 20) values (McDonough, 2016), we set the bulk Mars composition to these values.

Abundances of moderately volatile, lithophile elements in the BSM, which can be directly converted to the bulk Mars composition after correcting for the core mass fraction, define a robust depletion trend (Fig. 6). The volatility trend provides a method to determine the rest of the element abundances, except for the atmophile elements, in the bulk Mars and its core (Tables 8 to 10). For the refractory siderophile and chalcophile elements (Table 1), the bulk Mars abundances are set at ~ 1.85 times CI abundance.

The possible conditions of Mars core formation (e.g., 10–17 GPa, 1900–2300 K, $f\text{O}_2 = \text{IW} - 2$ to -1) are considered to be markedly different than that for the Earth’s core (Righter and Chabot, 2011; Rai and van Westrenen, 2013). These findings (i.e., wholly lithophile character of Mn, Cr and V) are also in harmony with the relatively oxidized conditions for Mars’ core formation as compared to the Earth (e.g., Wadhwa, 2001, 2008; Herd et al., 2002).

5.2 Comparison of the core models

Although cosmochemical and geodetic insights constrain the composition and interior structure of Mars, we cannot determine a unique core model composition, given the available data. Thus, other Martian core models, distinct from that proposed in this study (Table 8), are viable. The non-uniqueness can be readily viewed in Fig. A20, where we show trade-offs between core mass fraction, density and core radius, in order to constrain MOI, planetary density and mean mass. We tested three (end-member like) core compositions with (1) no H and O, (2) 9.5 wt% O, and (3) 1.4 wt% H, in addition to our preferred one (Table 11). There is a non-uniqueness in core mass fraction – core radius – core density, with limits being ~ 15 to 26% , ~ 1500 to 2000 km, and ~ 5500 to 7500 kg/m³, respectively. Composition and physical properties of core models were constrained by a combination of our BSM model, volatility trend, and geodetic properties of the planet. Importantly, as discussed in Section 5.1, the Martian volatility trend puts strong constraint on the S content in the Martian core (Fig. 8).

Core models assuming H- and O-free have the highest density (~ 7460 kg/m³), given only S as the light element. A dense core forces down its mass fraction (~ 17 wt%) and low bulk Fe/Si (1.29) and Fe/Al (14.5) ratios, as compared to most chondritic meteorites (1.0–1.8 and 15–25, respectively; Wasson and Kallemeyn, 1988). An exception, CV chondrite, has low Fe/Al ratio (13.4) due to its high abundance of refractory inclusions (i.e., high Al concentration). In contrast, however, the Fe/Si ratio in CV chondrites (1.36) is higher than that of Mars containing a core that is H- and O-free. Thus, to explain such a Mars’ bulk composition requires a chemical fractionation process not recorded in chondritic meteorites. Similar arguments can be applied for the H-bearing, O-free core model.

Physical properties of an O-rich, H-free core model is similar to that of the O- and H-bearing model proposed as the best core model. However, solubility of oxygen in liquid iron does not support such a high O concentration in the Martian core (Rubie et al., 2004; Tsuno et al., 2011).

6 Heat production in Mars

Abundance of heat-producing elements (HPE: K, Th and U), which is constrained by the compositional modeling of the planets, is an important factor that influences thermal history of terrestrial planets. Our model predicts that the present-day HPE in the BSM produce 2.5 ± 0.2 TW

heat (Table 3). In Mars, K is a dominant radiogenic heat source during its first 3.5 Gyr history (Fig. 10). Based on the BSM abundances of ^{40}K , ^{232}Th , ^{235}U , ^{238}U and ^{87}Rb , we estimate the Martian antineutrino (or areoneutrino) luminosity is $(7.7 \pm 0.8) \times 10^{24} \bar{\nu}_e/\text{s}$ (i.e., $(4.9 \pm 0.5) \times 10^6 \bar{\nu}_e/\text{cm}^2/\text{s}$).

7 Conclusions and implications for future works

Compositional modeling of Mars reveals that the bulk silicate Mars (BSM) is enriched in refractory lithophile elements at 2.26 times higher than that in CI carbonaceous chondrites. Moderately volatile elements are systematically depleted in Mars as a function of their volatility compared to the chondritic composition, but less so than in the Earth. The Martian core contains S, O and H as light elements, which is consistent with the volatility trend and occurrence of ringwoodite at the Martian core-mantle boundary.

The chemical compositions of Solar System bodies record accretion of solar nebular materials, core-mantle and mantle-crust differentiation and subsequent surface processes. The physico-chemical similarities and differences between Mars and Earth provide insights into the origin and evolution of terrestrial planets, which are discussed elsewhere.

To constrain further the interior structure and composition of Mars direct evidence from the planet is needed. The best constraints would be provided by seismic determination of the depth of Martian core-mantle boundary, which would immediately define the core's mass fraction and density. NASA's ongoing Interior Exploration using Investigations, Geodesy and Heat Transport (InSight) mission will provide significant constraints on the Martian core composition (Smrekar et al., 2019). In turn, our model for composition and interior structure of Mars can be tested by seismic and surface heat flux data from the InSight mission. In addition, rock samples which will be returned from Phobos in JAXA's planned Martian Moons eXploration (MMX) mission (Kuramoto et al., 2018) are keys to constrain further not only the origin of the Martian moons (Murchie et al., 2014), but also the composition of the Martian mantle, if Phobos has formed via giant impacts (Craddock, 2011; Citron et al., 2015; Hyodo et al., 2017; Canup and Salmon, 2018).

Acknowledgments

TY acknowledges supports from the Japanese Society for the Promotion of Science (JP18J20708), GP-EES Research Grant and DIARE Research Grant. WFM gratefully acknowledges NSF support (EAR1650365). We acknowledge Eiji Ohtani and Attilio Rivoldini for their comments on early versions of this manuscript. We gratefully acknowledge Jeff Taylor and two anonymous referees for their constructive reviews that greatly improved this manuscript. We thank the Associate Editor James Day for his thoughtful comments and editorial effort.

Author contributions

TY and WFM proposed and conceived various portions of this study and together calculated the compositional model of Mars. The manuscript was jointly written by TY and WFM and they read and approved the final manuscript.

Competing interests

The authors declare no competing interests.

Data and materials availability

Materials used in this study are provided as supplementary materials.

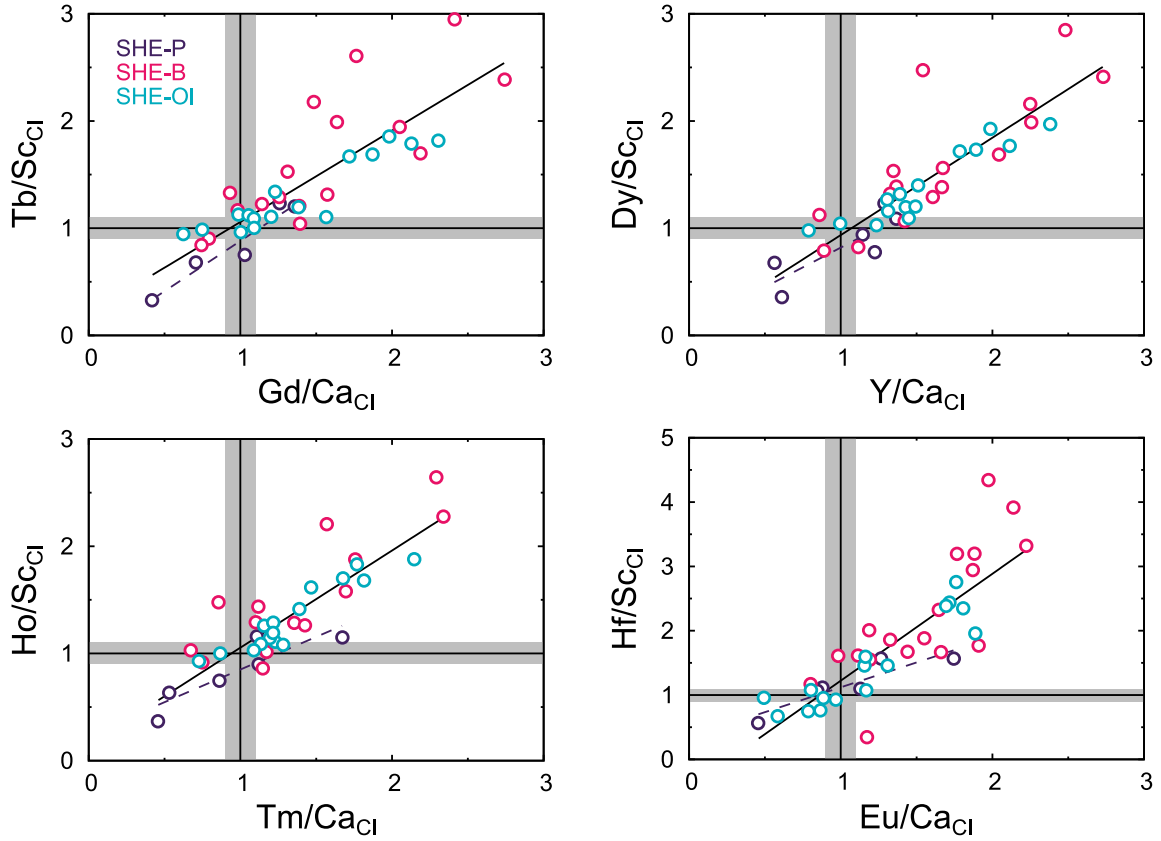


Fig. 1: Ratios versus ratios of refractory lithophile elements in shergottites. The values are normalized to CI chondrite abundance (Table 2). Horizontal and vertical gray bands show CI ratio $\pm 10\%$. Trend lines for all shergottites and poikilitic shergottites, shown in solid black and broken purple lines, respectively, cross CI chondritic compositions, showing that these chemical trends reflect melt-residue differentiation in the Martian silicate mantle. SHE-P, SHE-B and SHE-OI are poikilitic, basaltic and olivine-phyric shergottites, respectively.

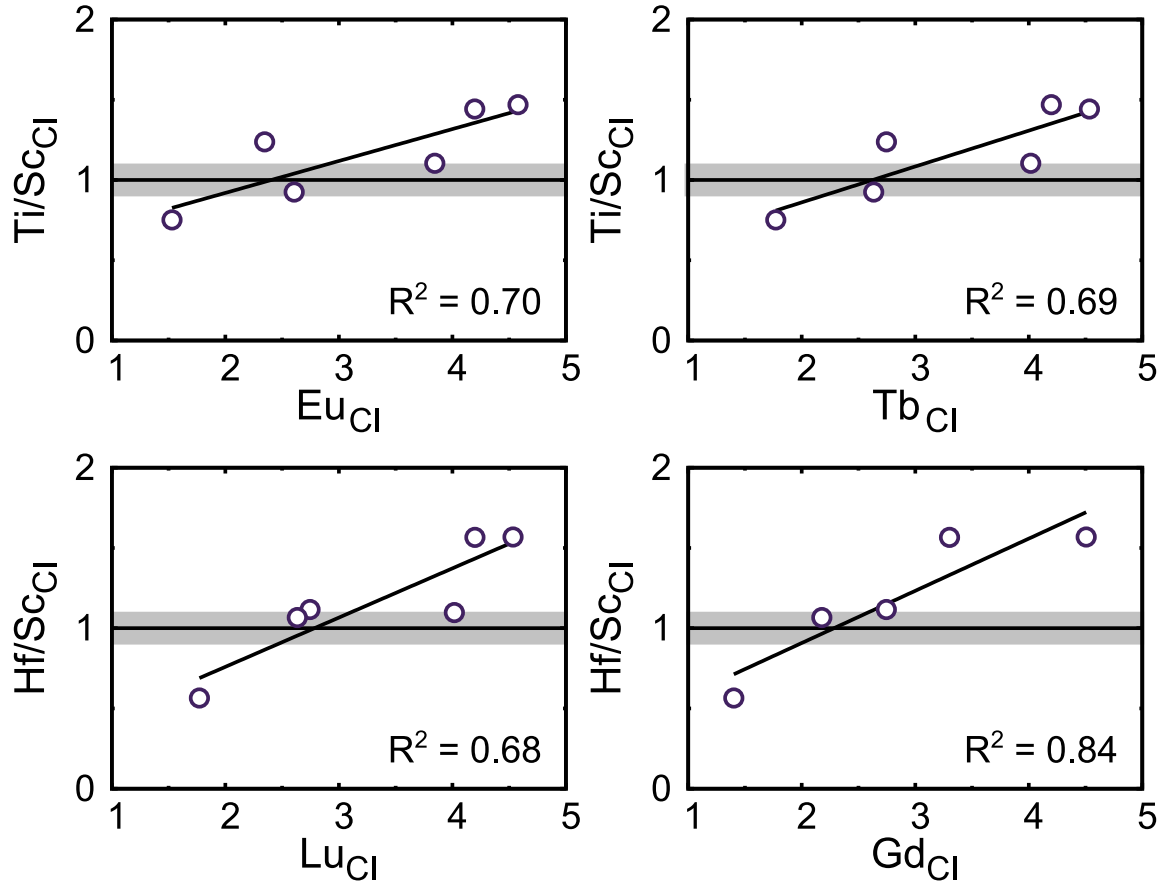


Fig. 2: Ratios versus abundances of refractory lithophile elements in poikilitic shergottites. The values are normalized to CI chondrite ratios/abundance (Table 2). Horizontal gray bands show CI ratio $\pm 10\%$. The correlations among multiple element combinations indicate that refractory lithophile element abundance in the BSM is 2.26 times higher than in the CI chondrites (cf. $2.75 \times$ CI in the BSE (McDonough and Sun, 1995)).

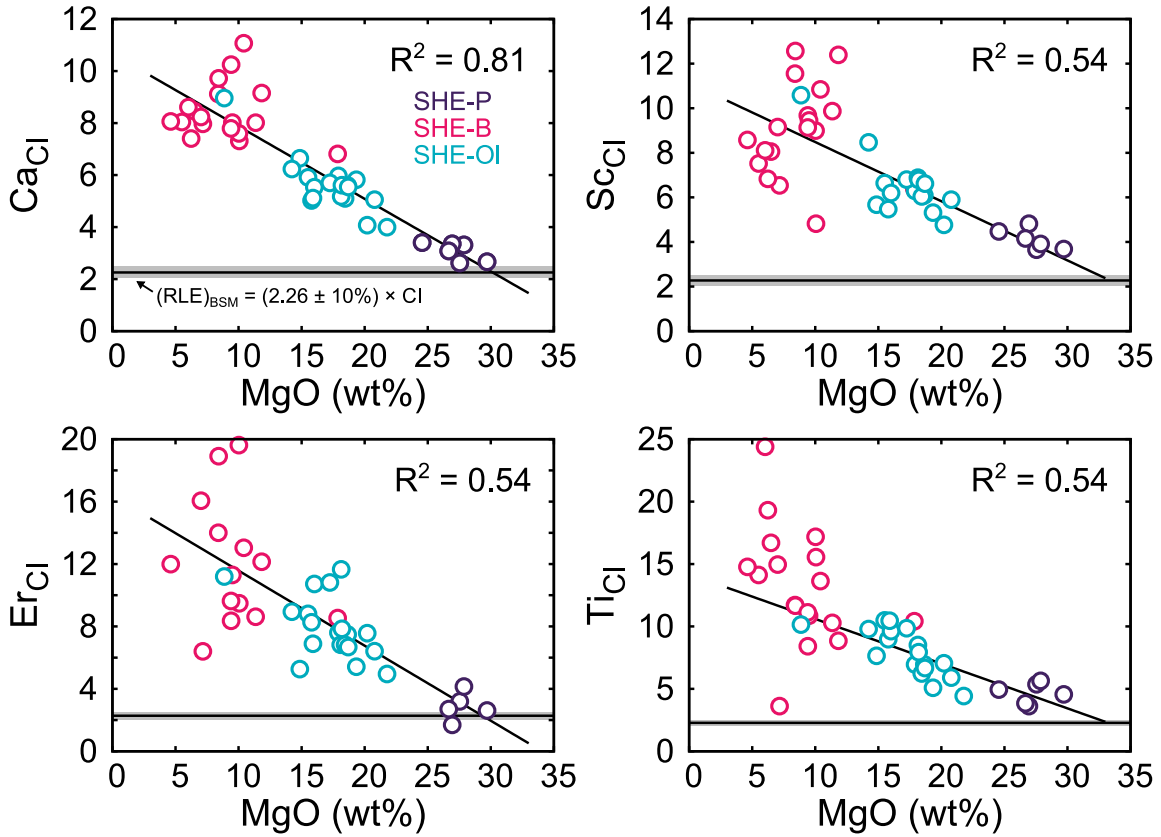


Fig. 3: Magnesium oxide contents versus CI-normalized abundances of refractory lithophile elements in shergottites. Horizontal gray bands show the CI-normalized abundance of refractory lithophile elements in the BSM with 10% uncertainties. Intercepts of the correlation lines and the BSM composition suggest 31.0 ± 2.0 wt% MgO in the BSM. SHE-P, SHE-B and SHE-OI are poikilitic, basaltic and olivine-phyric shergottites, respectively.

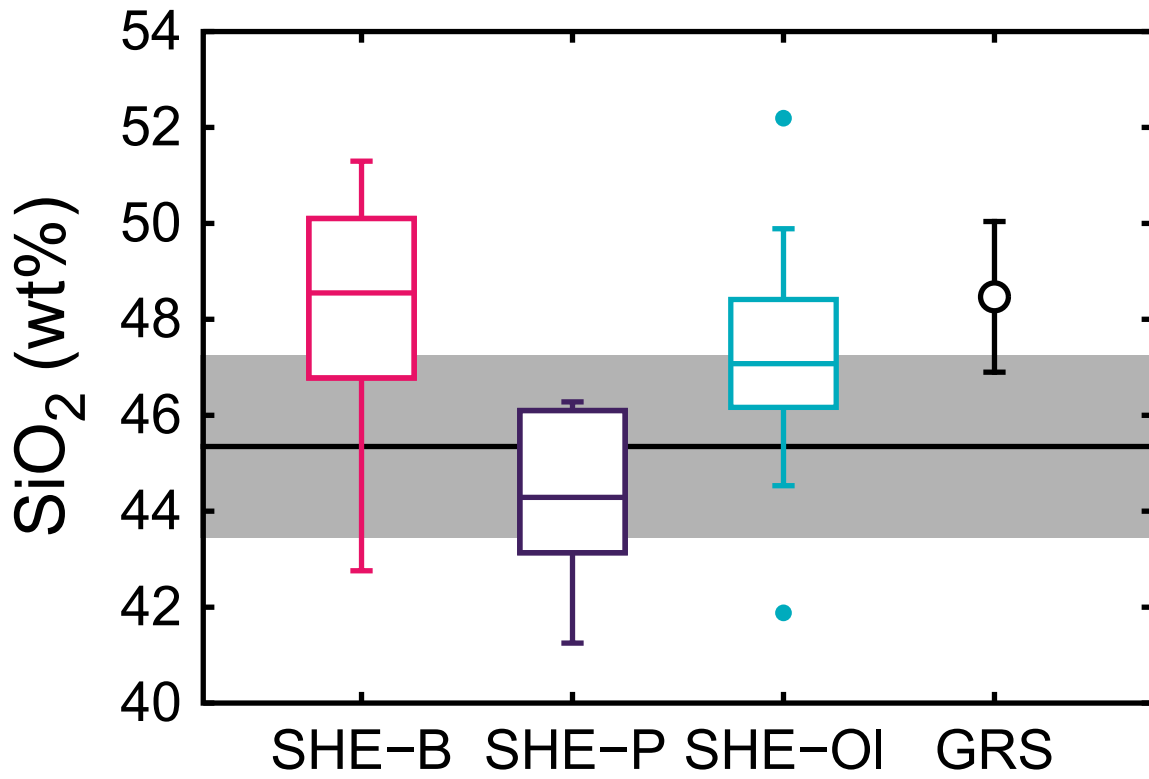


Fig. 4: Silicon oxide data from shergottites and GRS survey of Martian surface. The box plots show median, minimum, maximum, first and last quartile of SiO₂ contents in shergottites. Outliers which are more than 1.5 times the interquartile range from the end of boxes are shown in dots. The Martian surface composition is determined by gamma-ray spectroscopy (GRS) (Boynton et al., 2007), whose error is in 1 standard deviation. Horizontal line and gray bands show BSM abundance of SiO₂ of 45.5 ± 1.8 wt%. SHE-P, SHE-B and SHE-OI are poikilitic, basaltic and olivine-phyric shergottites, respectively.

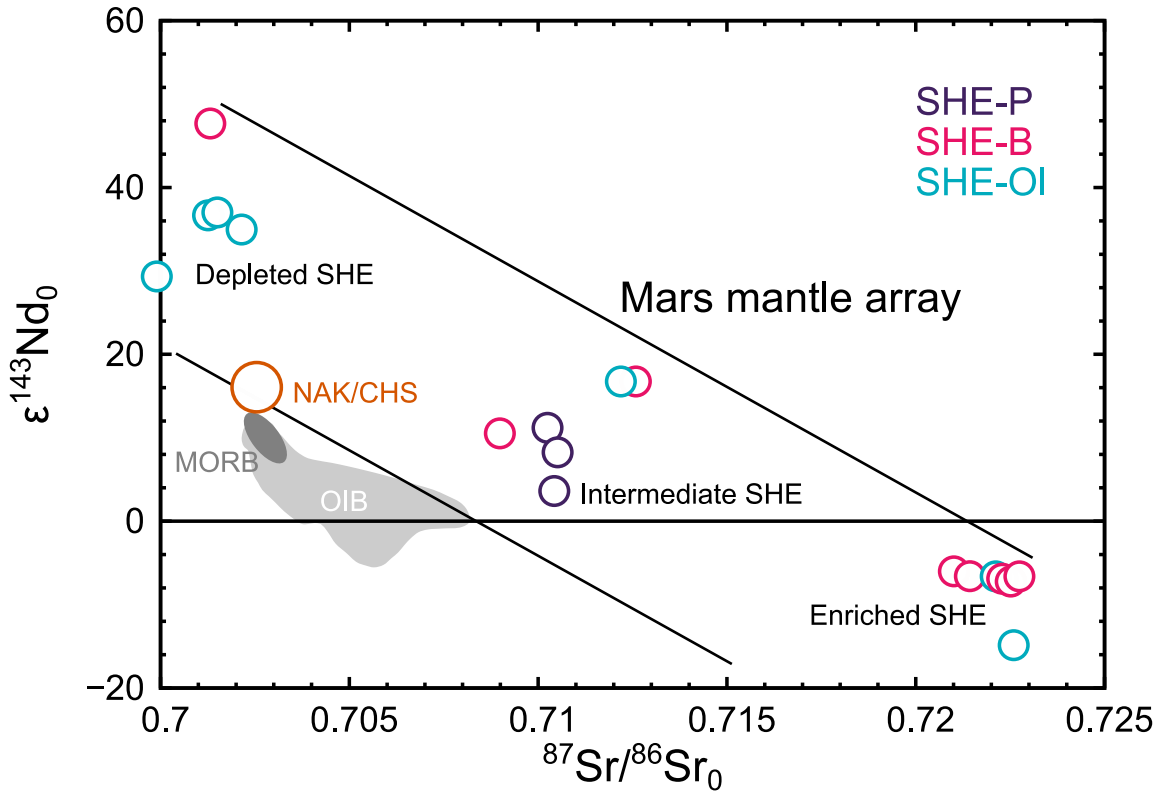


Fig. 5: Initial $^{87}\text{Sr}/^{86}\text{Sr}$ versus $\varepsilon^{143}\text{Nd}_0$ of Martian meteorites. Modified after Day et al. (2018). Compositions of individual shergottite samples and a compositional range for nakhrites and chassignites are shown. Isotopic compositions of terrestrial basalts (mid-ocean ridge basalt (MORB) and ocean island basalts (OIB) are also shown. Assuming that Martian meteorites represent isotopic composition of the Martian mantle and Rb/Sr fractionation at 4.56 Ga, the BSM abundance of Rb is estimated to be 1.6 ± 0.8 ppm Rb. $\varepsilon^{143}\text{Nd} = [({^{143}\text{Nd}}/{^{144}\text{Nd}_0})_{\text{sample}} / ({^{143}\text{Nd}}/{^{144}\text{Nd}_0})_{\text{chondritic}} - 1] \times 10^4$. Data are from Day et al. (2018) and references therein.

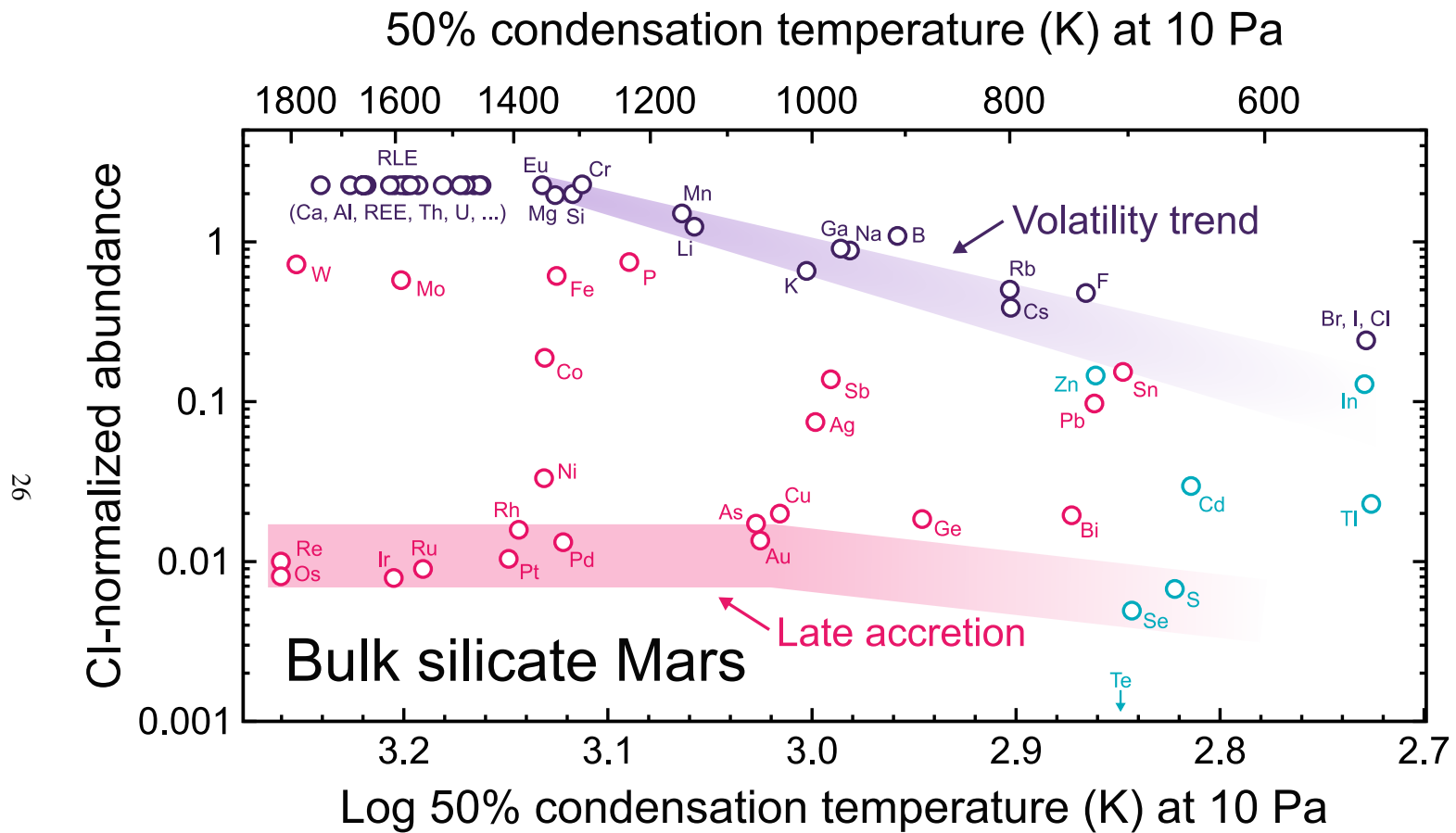


Fig. 6: Abundance of lithophile (purple), siderophile (pink) and chalcophile (blue) elements in the bulk silicate Mars (Table 5) are normalized to CI chondrites (Table 2) and plotted against log of the 50% condensation temperature (K) at 10 Pa (see Table 1 for updates to condensation temperatures of elements).

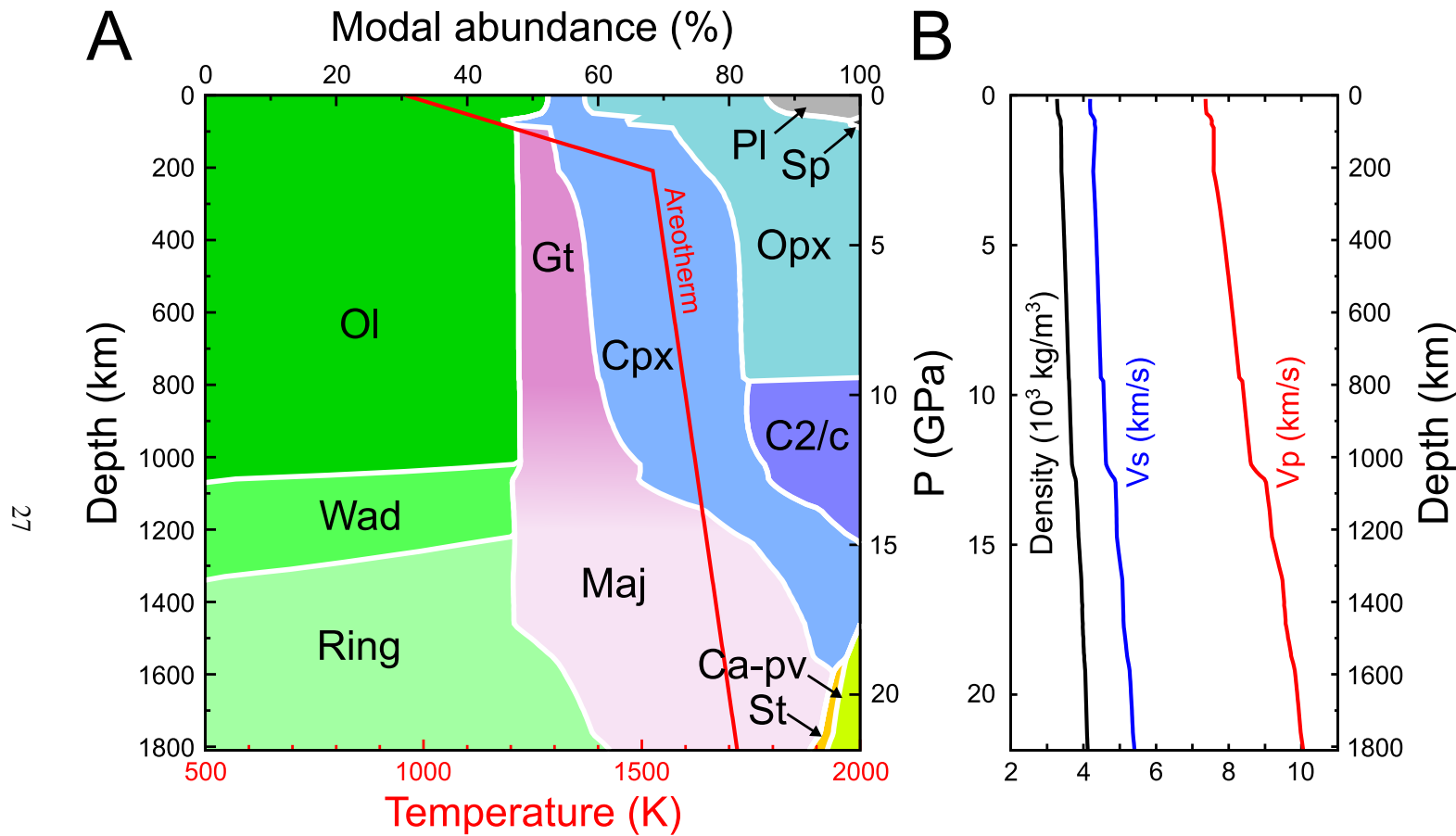


Fig. 7: Mineralogy and physical properties of the Martian mantle. (A) Phase transitions in the Martian mantle. A red line shows an areotherm (Martian geotherm). (B) Depth versus P- and S-wave velocities and density from surface to the core-mantle boundary of Mars. Abbreviations: Ol—olivine; Wad—wadsleyite; Ring—ringwoodite; Gt—garnet; Maj—majorite; Cpx—clinopyroxene; Opx—orthopyroxene; C2/c—high-pressure clinopyroxene; Pl—plagioclase; Sp—spinel; Ca-pv—Ca-perovskite; St—stishovite.

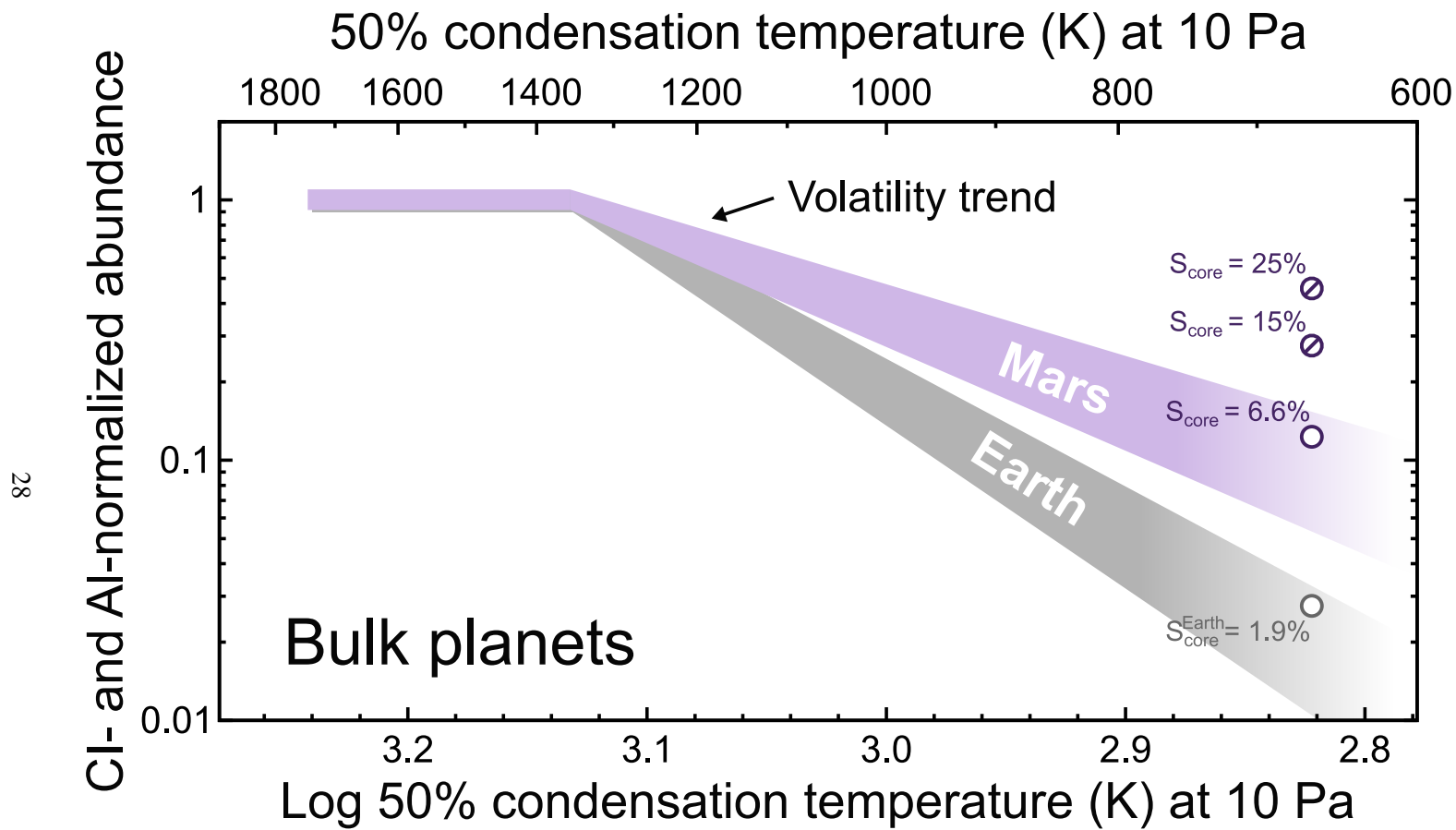


Fig. 8: Volatility trends for Mars (this study) and Earth (McDonough and Sun, 1995) constrain S contents in the metallic cores. The S-rich Martian core models (>15 wt%; e.g., Wänke and Dreibus, 1994; Taylor, 2013; Table 6) are not consistent with the Martian volatility trend.

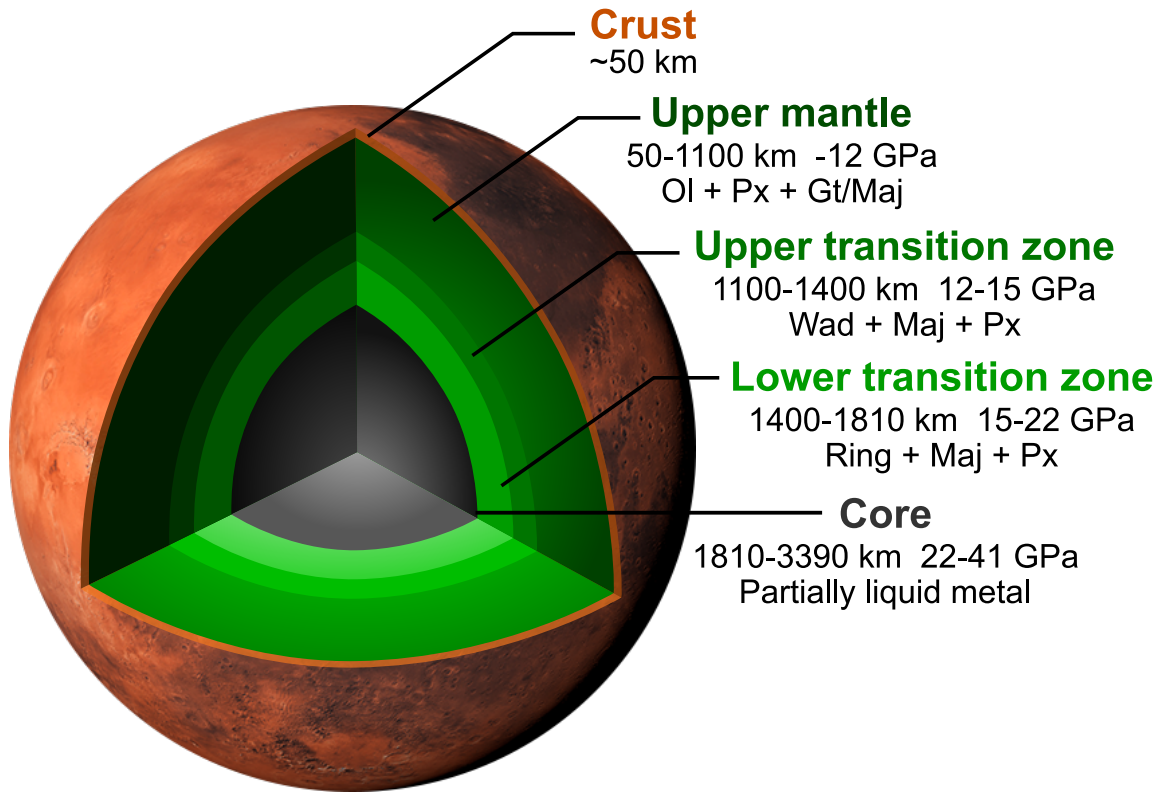


Fig. 9: Interior structure of Mars. Abbreviations: Ol—olivine; Px—pyroxene; Gt—garnet; Wad—wadsleyite; Ring—ringwoodite; Maj—majorite.

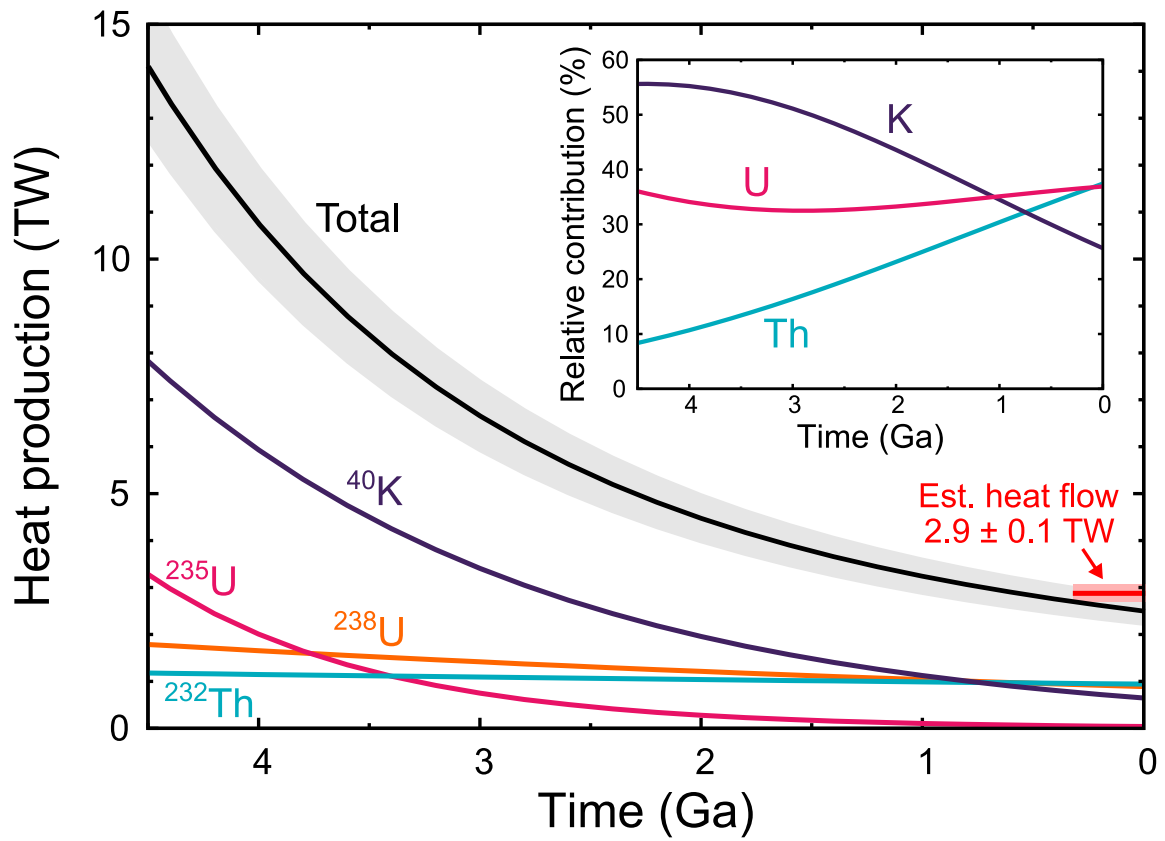


Fig. 10: Radiogenic heat production in the Martian mantle through time. Grey band shows an uncertainty of the total radiogenic heat production. Present-day surface heat flow estimate ($2.9 \pm 0.1 \text{ TW}$) is from Parro et al. (2017). The inset shows relative contributions of heat-producing elements as a function of time.

Table 1: Cosmochemical (refractory and volatile) and geochemical (lithophile, siderophile, chalcophile and atmophile) classification of elements. Elements are in the order of their 50% condensation temperature (50% Tc) in a gas of solar composition at 10 Pa (Lodders, 2003). Elements with multiple geochemical affinity (e.g., lithophile and chalcophile behavior of Zn) are shown in both classifications.

	50% Tc (K)	Lithophile	Siderophile	Chalcophile
Refractory	1821–1355	Zr, Hf, Sc, Y, Gd, Tb, Dy, Ho, Er, Tm, Lu, Th, Al, U, Nd, Sm, Ti, Pr, La, Ta, Nb, Ca, Yb, Ce, Sr, Ba, Be, Eu	Re, Os, W, Ir, Mo, Ru, Pt, Rh	
Major component	1355–1250	Mg, Fe, Si, Cr	Ni, Co, Fe, Pd, Cr	Fe
Moderately volatile	1250–600	Mn, Li, K, Na, Ga, B, Rb, Cs, F, Zn	P, Mn, As, Au, Cu, Ag, Sb, Ga, Ge, Bi, Pb, Te, Sn	Zn, Te, Se, S, Cd
Volatile	600–252	Cl ^a , Br, I, Tl		In ^b , Tl, Hg
	50% Tc (K)	Atmophile		
Highly volatile	<252	O, N, Xe, Kr, Ar, C, Ne, He, H		

^a Condensation temperature of Cl, Br and I may be similar (Clay et al., 2017; Wood et al., 2019).

^b Condensation temperature of In might be ~800 K (Righter et al., 2017).

Table 2: Composition of CI chondrites adopted in this study.

Element	Unit ^a	Value	Reference ^b	Element	Unit ^a	Value	Reference ^b
H	%	1.97	P14	Rh	ppm	0.132	P14
Li	ppm	1.45	P14	Pd	ppm	0.56	P14
Be	ppm	0.0219	P14	Ag	ppm	0.201	P14
B	ppm	0.775	P14	Cd	ppm	0.674	P14
C	ppm	34800	P14	In	ppm	0.0778	P14
N	ppm	2950	P14	Sn	ppm	1.63	P14
O	%	45.9	P14	Sb	ppm	0.145	P14
F	ppm	58.2	P14	Te	ppm	2.28	P14
Na	ppm	4962	P14	I	ppm	0.057	C17
Mg	%	9.54	P14	Cs	ppm	0.188	P14
Al	%	0.840	P14	Ba	ppm	2.42	P14
Si	%	10.7	P14	La	ppm	0.241	P14
P	ppm	985	P14	Ce	ppm	0.619	P14
S	ppm	53500	P14	Pr	ppm	0.0939	P14
Cl	ppm	115	C17	Nd	ppm	0.474	P14
K	ppm	546	P14	Sm	ppm	0.154	P14
Ca	%	0.911	P14	Eu	ppm	0.0588	P14
Sc	ppm	5.81	P14	Gd	ppm	0.207	P14
Ti	ppm	447	P14	Tb	ppm	0.0380	P14
V	ppm	54.6	P14	Dy	ppm	0.256	P14
Cr	ppm	2623	P14	Ho	ppm	0.0564	P14
Mn	ppm	1916	P14	Er	ppm	0.166	P14
Fe	%	18.66	P14	Tm	ppm	0.0261	P14
Co	ppm	513	P14	Yb	ppm	0.169	P14
Ni	ppm	10910	P14	Lu	ppm	0.0250	P14
Cu	ppm	133	P14	Hf	ppm	0.107	P14
Zn	ppm	309	P14	Ta	ppm	0.0150	P14
Ga	ppm	9.62	P14	W	ppm	0.0960	P14
Ge	ppm	32.6	P14	Re	ppm	0.0381	D16
As	ppm	1.74	P14	Os	ppm	0.461	D16
Se	ppm	20.3	P14	Ir	ppm	0.431	D16
Br	ppm	0.189	C17	Pt	ppm	0.874	D16
Rb	ppm	2.32	P14	Au	ppm	0.175	D16
Sr	ppm	7.79	P14	Hg	ppm	0.35	P14
Y	ppm	1.46	P14	Tl	ppm	0.169	W15
Zr	ppm	3.63	P14	Pb	ppm	2.62	P14
Nb	ppm	0.283	P14	Bi	ppm	0.087	W15
Mo	ppm	0.87	W15	Th	ppm	0.0300	P14
Ru	ppm	0.69	P14	U	ppm	0.00796	W18

^a ppm– $\mu\text{g/g}$. ^b C17–Clay et al. (2017); D16–Day et al. (2016); P14–Palme et al. (2014); W15–Wang et al. (2015); W18–Wipperfurth et al. (2018).

Table 3: Comparison of compositional models of the bulk silicate Mars.

wt%	This study	WD94 ^a	T13 ^b	MA79 ^c	OK92 ^d	LF97 ^e	S99 ^f	KC08 ^g
SiO ₂	45.5	44.4	43.7	41.6	43.0	45.4	47.5	44
TiO ₂	0.17	0.14	0.14	0.33	0.24	0.14	0.1	-
Al ₂ O ₃	3.59	3.02	3.04	6.39	3.48	2.89	2.5	2.5
MnO	0.37	0.46	0.44	0.15	0.22	0.37	0.4	-
FeO	14.7	17.9	18.1	15.9	15.1	17.2	17.7	17
MgO	31.0	30.2	30.5	29.8	34.3	29.7	27.3	33
CaO	2.88	2.45	2.43	5.16	2.81	2.36	2.0	2.2
Na ₂ O	0.59	0.5	0.53	0.10	0.46	0.98	1.2	-
K ₂ O	0.043	0.037	0.037	0.009	-	0.11	-	-
P ₂ O ₅	0.17	0.16	0.19	-	-	0.18	-	-
NiO	0.046	-	0.03	-	-	-	-	-
Cr ₂ O ₃	0.88	0.76	0.73	0.65	0.40	0.68	0.7	-
K (ppm)	360	305	309	76.5	-	920	-	-
Th (ppb)	68	56	58	125	-	55	-	-
U (ppb)	18	16	16	35	-	16	-	-
Total	99.9	100	99.8	100	100	100	100	98.7
Mg#	0.79	0.75	0.75	0.77	0.75	0.76	0.72	0.77
Mg/Si	0.88	0.88	0.90	0.92	1.03	0.84	0.74	0.97
Al/Si	0.09	0.08	0.08	0.17	0.09	0.07	0.06	0.06
RLE/CI ^h	2.3	2.1	2.1	4.4	2.4	2.0	1.7	1.9
Fe/Si	0.54	0.67	0.69	0.63	0.58	0.63	0.62	0.64
Fe/Al	6.0	8.7	8.7	3.6	6.4	8.8	10.4	10.0
H _{BSM} ⁱ (TW)	2.5	2.0	2.0	3.4	-	3.0	-	-
H _{BSM} (pW/kg)	4.8	4.1	4.2	7.0	-	6.2	-	-

^a Wänke and Dreibus (1994).

^b Taylor (2013).

^c Morgan and Anders (1979).

^d Ohtani and Kamaya (1992).

^e Lodders and Fegley (1997).

^f Sanloup et al. (1999)

^g (EH45:H55 model). ^h Khan and Connolly (2008). ^h An average enrichment factor of major refractory lithophile elements (Ca, Al and Ti) compared to CI abundance (Table 2).

ⁱ Heat production in the bulk silicate Mars (BSM: mantle + crust).

Table 4: Major element composition of the bulk silicate Mars (BSM). See text for the details of methods used to determine the BSM abundance of elements.

	wt%	1sd	rsd%	Method ^a
SiO ₂	45.5	1.8	4	Mean SHE
TiO ₂	0.17	0.02	10	RLE
Al ₂ O ₃	3.59	0.36	10	RLE
MnO	0.37	0.07	18	FeO/MnO in SNC
FeO	14.7	1.0	7	Mg# = 0.79 ± 0.02 ^b
MgO	31.0	2.0	6	vs RLE in SHE
CaO	2.88	0.29	10	RLE
Na ₂ O	0.59	0.13	22	Na/Al in SHE
K ₂ O	0.043	0.005	11	K/Th (GRS) ^c
P ₂ O ₅	0.17	0.05	28	P/Y in SHE
NiO	0.046	0.01	26	Ni/Mg in SHE-P and SHE-OI
Cr ₂ O ₃	0.88	0.15	17	vs Al in SHE-P and SHE-OI
Total	99.9			
Mg#	0.79			
Mg/Si	0.88			
Al/Si	0.09			
RLE/CI	2.26			
Fe/Si	0.54			
Fe/Al	6.0			

^a GRS—gamma-ray spectroscopy; RLE—refractory lithophile elements; SHE-P—poikilitic shergottites; SHE-OI—olivine shergottites; SNC—shergottite, nakhlite and chassignite.

^b Borg and Draper (2003); Agee and Draper (2004); Draper et al. (2005); Minitti et al. (2006); Musselwhite et al. (2006); Collinet et al. (2015); McCoy et al. (2016).

^c Taylor et al. (2006a,b).

Table 5: Composition of the bulk silicate Mars. Concentrations are in ppm ($\mu\text{g/g}$), otherwise noted. See text for the details of methods used to determine the BSM abundances of elements.

Element	BSM	rsd% ^a	Method ^b	Element	BSM	rsd%	Method
H	16	U	See text ^c	Rh	0.0021	4	Mean SNC
Li	1.8	22	vs RLE in SNC	Pd	0.0074	70	vs MgO ⁱ
Be	0.05	10	RLE	Ag	0.02	U	Sb/Ag in SHE
B	0.84	63	B/Ca in SHE-P and SHE-OI	Cd	0.020	50	Cd/Yb in SHE ⁱ
C	32	U	Chondritic C/H	In	0.010	50	In/Y in SHE ⁱ
N	1.6	U	Chondritic N/H	Sn	0.25	40	Sn/Sni in SHE ⁱ
O (%)	43.2	8	Major oxide stoichiometry, $\text{Fe}^{3+}/\text{Fe}^{\text{tot}} = 0.1^d$	Sb	0.02	50	Sb/Pr in SHE ⁱ
F	30	U	Cl/F in SNC ^e	Te	0.0005	50	Cu/Te and Se/Te in SHE ^f
Na	4380	22	Na/Al in SHE	I	0.014	50	Chondritic I/Cl ^j
Mg (%)	18.7	6	vs RLE in SHE	Cs	0.07	41	Cs/La in SHE
Al (%)	1.90	10	RLE	Ba	5.47	10	RLE
Si (%)	21.3	4	Mean SHE	La	0.546	10	RLE
P	740	28	P/Y in SHE	Ce	1.40	10	RLE
S	360	33	S/Cu and S/Se in SHE ^f	Pr	0.212	10	RLE
Cl	28	35	Cl/La in SHE ^e	Nd	1.07	10	RLE
K	360	11	K/Th (GRS) ^g	Sm	0.347	10	RLE
Ca (%)	2.06	10	RLE	Eu	0.133	10	RLE
Sc	13.1	10	RLE	Gd	0.468	10	RLE
Ti	1010	10	RLE	Tb	0.0858	10	RLE
V	123	10	RLE	Dy	0.578	10	RLE
Cr	6000	17	vs Al in SHE-P and SHE-OI	Ho	0.128	10	RLE
Mn	2880	18	FeO/MnO in SNC	Er	0.374	10	RLE
Fe (%)	11.4	7	Mg# = 0.79 \pm 0.02 ^h	Tm	0.0590	10	RLE
Co	96	46	Co/Ni in SHE-P and SHE-OI	Yb	0.381	10	RLE
Ni	360	26	Ni/Mg in SHE-P and SHE-OI	Lu	0.0566	10	RLE
Cu	2.6	23	Cu/Ti in SHE	Hf	0.241	10	RLE
Zn	45	33	vs Lu in SHE	Ta	0.0339	14	RLE
Ga	8.7	22	Ga/Al in SHE	W	0.069	54	W/Th in SHE
Ge	0.6	67	vs MgO in SHE-P and SHE-OI	Re	0.0004	75	vs MgO ⁱ
As	0.03	76	As/Ce in SHE ⁱ	Os	0.004	50	vs MgO ⁱ
Se	0.10	27	Cu/Se in SHE ^f	Ir	0.0037	60	vs MgO ⁱ
Br	0.05	U	Chondritic Cl/Br ^j	Pt	0.0096	80	vs MgO ⁱ
Rb	1.2	36	Initial $^{87}\text{Sr}/^{86}\text{Sr}$ in SNC, vs La in SHE	Au	0.002	80	vs MgO
Sr	17.6	10	RLE	Hg	0.007	U	Hg/Se in NAK and the BSE
Y	3.30	10	RLE	Tl	0.004	50	Tl/Sm in SHE
Zr	8.20	10	RLE	Pb	0.255	18	U-Pb isotope systematics in SNC ^m
Nb	0.640	10	RLE	Bi	0.002	60	Bi/Th in SHE
Mo	0.5	80	Mo/Ce in SHE ^k	Th	0.0678	10	RLE
Ru	0.0062	60	vs MgO ^l	U	0.0180	10	RLE

^a U- \geq 2 factors of uncertainties. ^b BSE-bulk silicate Earth; GRS-gamma-ray spectroscopy; NAK-nakhlite; SNC-shergottite, nakhelite and chassignite. RLE-refractory lithophile elements; SHE-P-poikilitic shergottites; SHE-OI-olivine shergottites. ^c McCubbin et al. (2016a,b); Filiberto et al. (2019).

^d Schmidt et al. (2013); Medard et al. (2014). ^e Filiberto et al. (2016); this study. ^f Wang and Becker (2017).

^g Taylor et al. (2006a,b); this study. ^h Borg and Draper (2003); Agee and Draper (2004); Draper et al. (2005); Miniti et al. (2006); Musselwhite et al. (2006);

Collinet et al. (2015); McCoy et al. (2016). ⁱ Yang et al. (2015). ^j Clay et al. (2017). ^k Righter and Chabot (2011). ^l Tait and Day (2018).

^m μ (= $^{238}\text{U}/^{204}\text{Pb}$) = 3.6; $^{208}\text{Pb}/^{204}\text{Pb}$ = 33; $^{207}\text{Pb}/^{204}\text{Pb}$ = 13; $^{206}\text{Pb}/^{204}\text{Pb}$ = 14.

Table 6: Comparison of compositional models of the Martian core.

wt%	This study	WD94 ^a	T13 ^b	MA79 ^c	OK92 ^d	LF97 ^e	S99 ^f	KC08 ^g
Fe	79.5	77.8	78.6 ^h	88.1	78.4	81.1	76.6	75–78 ^h
Ni	7.4	7.6	-	8.0	7.6	7.7	7.2	-
Co	0.33	0.36	-	0.37	-	0.4	-	-
S	6.6	14.24	21.4	3.5	14.0	10.6	16.2	22–25
P	0.33	-	-	-	-	0.2	-	-
O	5.2	-	-	-	-	-	-	-
H	0.9	-	-	-	-	-	-	-
Total	100	100	100	100	100	100	100	-

^a Wänke and Dreibus (1994).

^b Taylor (2013).

^c Morgan and Anders (1979).

^d Ohtani and Kamaya (1992).

^e Lodders and Fegley (1997).

^f Sanloup et al. (1999) (EH45:H55 model).

^g Khan and Connolly (2008).

^h Sum of Fe and Ni.

Table 7: Physical properties of Mars. Modeled values are in a normal font and reference values are in italic.

Observation	Unit	Crust	Mantle	Core	Bulk planet	Reference value
Mass	kg	2.56×10^{22}	5.01×10^{23}	1.17×10^{23}	6.419×10^{23}	$6.417(3) \times 10^{23}$ ^a
Mean density	kg/m ³	3010	3640	6910	3936	$3935(1)$ ^b
Moment of inertia	–	7%	89%	4%	0.3638	$0.3639(1)$ ^a
Heat production (K, Th, U)	TW pW/kg	1.3 ^d	1.3 ^e	0 0	2.5 ^f	$2.9(1)$ ^c –

^a Konopliv et al. (2016); Khan et al. (2018). ^b Rivoldini et al. (2011). ^c Surface heat loss estimated based on an average surface heat flux of 20 ± 1 mW/m² (Parro et al., 2017). ^d Abundances of heat-producing elements (HPE) in the crust: 3740 ppm K, 700 ppb Th and 180 ppb U (Taylor and McLennan, 2009).

^e HPE abundance in the mantle is calculated from mass-balance considerations: 190 ppm K, 36 ppb Th and 10 ppb U.

^f BSM abundances of HPE are 360 ppm K, 68 ppb Th and 18 ppb U (this study).

Table 8: Composition of the Martian core. Concentrations are in ppm ($\mu\text{g/g}$), otherwise noted.

Element	Martian core	Element	Martian core
Fe (%)	79.5	Os	5
Ni (%)	7.4	Pd	5
O (%)	5.2	Ir	5
S (%)	6.6	Te	3
H (%)	0.9	Pb	3.1
Co	3300	Rh	1.3
P	3300	Sn	1.3
Cu	560	W	0.7
Zn	290	Ag	0.7
Ge	90	Au	0.7
Se	30	Cd	0.7
Pt	9	Re	0.4
As	8	Sb	0.4
Mo	7	Bi	0.1
Ru	7	Tl	0.1

Table 9: Composition of the bulk Mars.
 Concentrations are in ppm ($\mu\text{g/g}$), otherwise noted.

Element	Bulk Mars	Element	Bulk Mars
H	1600	Rh	0.24
Li	1.5	Pd	0.84
Be	0.041	Ag	0.14
B	0.69	Cd	0.15
C	26	In	0.01
N	1.4	Sn	0.43
O (%)	36.3	Sb	0.1
F	23	Te	0.6
Na	3600	I	0.01
Mg (%)	15.3	Cs	0.06
Al (%)	1.56	Ba	4.5
Si (%)	17.4	La	0.45
P	1200	Ce	1.1
S	12100	Pr	0.17
Cl	23	Nd	0.88
K	300	Sm	0.28
Ca (%)	1.69	Eu	0.11
Sc	10.8	Gd	0.38
Ti	830	Tb	0.070
V	100	Dy	0.47
Cr	4900	Ho	0.10
Mn	2400	Er	0.31
Fe (%)	23.7	Tm	0.048
Co	680	Yb	0.31
Ni	13600	Lu	0.046
Cu	100	Hf	0.20
Zn	89	Ta	0.028
Ga	7.2	W	0.18
Ge	16	Re	0.07
As	1.4	Os	0.9
Se	5.2	Ir	0.9
Br	0.1	Pt	1.7
Rb	0.96	Au	0.1
Sr	14	Hg	0.006
Y	2.7	Tl	0.02
Zr	6.7	Pb	0.8
Nb	0.52	Bi	0.03
Mo	1.6	Th	0.056
Ru	1.3	U	0.015

Table 10: Compositional models for the bulk Mars, bulk silicate Mars (BSM) and core and atomic proportions for major elements.

	wt%	Bulk	BSM	Core		atomic%	Bulk	BSM	Core
O	36.3	43.2	5.2		O	53	59	11	
Mg	15.3	18.7	0		Mg	15	17	0	
Si	17.4	21.3	0		Si	14	16	0	
Fe	23.7	11.4	79.5		Fe	10	4.4	48	
Al	1.56	1.90	0		Al	1.3	1.5	0	
S	1.2	0.04	6.6		S	0.9	0.02	6.9	
Ca	1.69	2.06	0		Ca	1.0	1.1	0	
Ni	1.4	0.04	7.4		Ni	0.5	0.01	4.2	
H	0.2	0.00	0.9		H	3.8	0.03	30	

Table 11: Comparison of chemical and physical properties of Martian core models.

	H ₂ O-bearing	H ₂ O-free	H-free	O-free	Reference value
Chemical composition					
Core wt%					
Fe	79.5	81.6	76.5	83.3	
Ni	7.4	7.8	7.1	7.8	
Co	0.33	0.35	0.32	0.35	
S	6.6	10	6.10	7.04	
P	0.33	0.37	0.32	0.36	
O	5.2	0.0	9.5	0	
H	0.9	0.0	0.0	1.4	
Total	100.2	100.1	99.9	100.3	
Bulk Mars					
Fe/Si	1.36	1.29	1.35	1.34	1.0–1.6 ^a
Fe/Al	15.2	14.5	15.1	15.0	15.5–24.3 ^a
Modeled physical properties ^b					
M' _{core}	18%	17%	18%	17%	
ρ _{core} (kg/m ³)	6910	7460	6910	7180	
r _{core} (km)	1580	1510	1600	1540	
P _{CMB} (GPa)	22	24	22	23	

^a Compositional range of ordinary chondrites (Wasson and Kallemeyn, 1988).

^b M'—mass fraction; ρ_{core}—density of the core; r_{core}—radius of the core; P_{CMB}—pressure at the core–mantle boundary.

References

- Agee, C.B., Draper, D.S., 2004. Experimental constraints on the origin of Martian meteorites and the composition of the Martian mantle. *Earth and Planetary Science Letters* 224, 415–429. doi:10.1016/j.epsl.2004.05.022.
- Agostini, M., Altenmüller, K., Appel, S., Atroshchenko, V., Bagdasarian, Z., Basilico, D., Bellini, G., Benziger, J., Bick, D., Bonfini, G., Bravo, D., Caccianiga, B., Calaprice, F., Caminata, A., Caprioli, S., Carlini, M., Cavalcante, P., Chepurnov, A., Choi, K., Collica, L., D'Angelo, D., Davini, S., Derbin, A., Ding, X.F., Di Ludovico, A., Di Noto, L., Drachnev, I., Fomenko, K., Formozov, A., Franco, D., Gabriele, F., Galbiati, C., Ghiano, C., Giammarchi, M., Goretti, A., Gromov, M., Guffanti, D., Hagner, C., Houdy, T., Hungerford, E., Ianni, A., Ianni, A., Jany, A., Jeschke, D., Kobychev, V., Korablev, D., Korga, G., Kryn, D., Laubenstein, M., Litvinovich, E., Lombardi, F., Lombardi, P., Ludhova, L., Lukyanchenko, G., Lukyanchenko, L., Machulin, I., Manuzio, G., Marcocci, S., Martyn, J., Meroni, E., Meyer, M., Miramonti, L., Misiaszek, M., Muratova, V., Neumair, B., Oberauer, L., Opitz, B., Orekhov, V., Ortica, F., Pallavicini, M., Papp, L., Penek, Ö., Pilipenko, N., Pocar, A., Porcelli, A., Raikov, G., Ranucci, G., Razeto, A., Re, A., Redchuk, M., Romani, A., Roncin, R., Rossi, N., Schönert, S., Semenov, D., Skorokhvatov, M., Smirnov, O., Sotnikov, A., Stokes, L.F.F., Suvorov, Y., Tartaglia, R., Testera, G., Thurn, J., Toropova, M., Unzhakov, E., Villante, F.L., Vishneva, A., Vogelaar, R.B., von Feilitzsch, F., Wang, H., Weinz, S., Wojcik, M., Wurm, M., Yokley, Z., Zaimidoroga, O., Zavatarelli, S., Zuber, K., Zuzel, G., 2018. Comprehensive measurement of *pp*-chain solar neutrinos. *Nature* 562, 505–510. doi:10.1038/s41586-018-0624-y.
- Alexander, C.M.O'D., Bowden, R., Fogel, M.L., Howard, K.T., Herd, C.D.K., Nittler, L.R., 2012. The provenances of asteroids, and their contributions to the volatile inventories of the terrestrial planets. *Science* 337, 721–723. doi:10.1126/science.1223474.
- Anderson, W.W., Ahrens, T.J., 1994. An equation of state for liquid iron and implications for the Earth's core. *Journal of Geophysical Research: Solid Earth* 99, 4273–4284. doi:10.1029/93JB03158.
- Antonangeli, D., Morard, G., Schmerr, N.C., Komabayashi, T., Krisch, M., Fiquet, G., Fei, Y., 2015. Toward a mineral physics reference model for the Moon's core. *Proceedings of the National Academy of Sciences* 112, 3916–3919. doi:10.1073/pnas.1417490112.
- Arndt, N.T., Jenner, G.A., 1986. Crustally contaminated komatiites and basalts from Kam-balda, Western Australia. *Chemical Geology* 56, 229–255. doi:10.1016/0009-2541(86)90006-9.
- Asplund, M., Grevesse, N., Sauval, A.J., Scott, P., 2009. The chemical composition of the Sun. *Annual Review of Astronomy and Astrophysics* 47, 481–522. doi:10.1146/annurev.astro.46.060407.145222.

- Badding, J.V., Mao, H.K., Hemley, R.J., 1992. High-pressure crystal structure and equation of state of iron hydride: Implications for the Earth's core, in: Syono, Y., Manghnani, M.H. (Eds.), High Pressure Research: Application to Earth and Planetary Sciences. American Geophysical Union. volume 67. chapter 5, pp. 363–371. doi:10.1029/GM067p0363.
- Bailey, J.E., Nagayama, T., Loisel, G.P., Rochau, G.A., Blancard, C., Colgan, J., Cosse, P., Faus-surier, G., Fontes, C.J., Gilleron, F., Golovkin, I., Hansen, S.B., Iglesias, C.A., Kilcrease, D.P., MacFarlane, J.J., Mancini, R.C., Nahar, S.N., Orban, C., Pain, J.C., Pradhan, A.K., Sherrill, M., Wilson, B.G., 2015. A higher-than-predicted measurement of iron opacity at solar interior temperatures. *Nature* 517, 56–59. doi:10.1038/nature14048.
- Baratoux, D., Toplis, M., Monnereau, M., Sautter, V., 2013. The petrological expression of early Mars volcanism. *Journal of Geophysical Research: Planets* 118, 59–64. doi:10.1029/2012JE004234.
- Baratoux, D., Toplis, M.J., Monnereau, M., Gasnault, O., 2011. Thermal history of Mars inferred from orbital geochemistry of volcanic provinces. *Nature* 472, 338–341. doi:10.1038/nature09903.
- Barrat, J.A., Greenwood, R.C., Keil, K., Rouget, M.L., Boesenberg, J.S., Zanda, B., Franchi, I.A., 2016. The origin of aubrites: Evidence from lithophile trace element abundances and oxygen isotope compositions. *Geochimica et Cosmochimica Acta* 192, 29–48. doi:10.1016/j.gca.2016.07.025.
- Basu, S., Antia, H.M., 2008. Helioseismology and solar abundances. *Physics Reports* 457, 217–283. doi:10.1016/j.physrep.2007.12.002.
- Bellucci, J.J., Nemchin, A.A., Whitehouse, M.J., Snape, J.F., Bland, P., Benedix, G.K., Roszjar, J., 2018. Pb evolution in the Martian mantle. *Earth and Planetary Science Letters* 485, 79–87. doi:10.1016/j.epsl.2017.12.039.
- Bergemann, M., Serenelli, A., 2014. Solar abundance problem, in: Niemczura, E., Smalley, B., Pych, W. (Eds.), *Determination of Atmospheric Parameters of B-, A-, F-and G-Type Stars*. Springer, Cham, pp. 245–258. doi:10.1007/978-3-319-06956-2_21.
- Bertka, C.M., Fei, Y., 1997. Mineralogy of the Martian interior up to core-mantle boundary pressures. *Journal of Geophysical Research: Solid Earth* 102, 5251–5264. doi:10.1029/96JB03270.
- Bertka, C.M., Fei, Y., 1998a. Density profile of an SNC model Martian interior and the moment-of-inertia factor of Mars. *Earth and Planetary Science Letters* 157, 79–88. doi:10.1016/S0012-821X(98)00030-2.
- Bertka, C.M., Fei, Y., 1998b. Implications of Mars Pathfinder data for the accretion history of the terrestrial planets. *Science* 281, 1838–1840. doi:10.1126/science.281.5384.1838.

- Birch, F., 1952. Elasticity and constitution of the Earth's interior. *Journal of Geophysical Research* 57, 227–286. doi:10.1029/JZ057i002p00227.
- Birch, F., 1964. Density and composition of mantle and core. *Journal of Geophysical Research* 69, 4377–4388. doi:10.1029/JZ069i020p04377.
- Blichert-Toft, J., Gleason, J.D., Télouk, P., Albarède, F., 1999. The Lu–Hf isotope geochemistry of shergottites and the evolution of the Martian mantle–crust system. *Earth and Planetary Science Letters* 173, 25–39. doi:10.1016/S0012-821X(99)00222-8.
- Bogard, D.D., Clayton, R.N., Marti, K., Owen, T., Turner, G., 2001. Martian volatiles: isotopic composition, origin, and evolution. *Space Science Reviews* 96, 425–458. doi:10.1023/A:1011974028370.
- Borg, L.E., Draper, D.S., 2003. A petrogenetic model for the origin and compositional variation of the Martian basaltic meteorites. *Meteoritics & Planetary Science* 38, 1713–1731. doi:10.1111/j.1945-5100.2003.tb00011.x.
- Borg, L.E., Edmunson, J.E., Asmerom, Y., 2005. Constraints on the U-Pb isotopic systematics of Mars inferred from a combined U-Pb, Rb-Sr, and Sm-Nd isotopic study of the Martian meteorite Zagami. *Geochimica et Cosmochimica Acta* 69, 5819–5830. doi:10.1016/j.gca.2005.08.007.
- Boujibar, A., Andrault, D., Bouhifd, M.A., Bolfan-Casanova, N., Devidal, J.L., Trcera, N., 2014. Metal–silicate partitioning of sulphur, new experimental and thermodynamic constraints on planetary accretion. *Earth and Planetary Science Letters* 391, 42–54. doi:10.1016/j.epsl.2014.01.021.
- Bouvier, A., Blichert-Toft, J., Albarede, F., 2009. Martian meteorite chronology and the evolution of the interior of Mars. *Earth and Planetary Science Letters* 280, 285–295. doi:10.1016/j.epsl.2009.01.042.
- Bouvier, A., Blichert-Toft, J., Vervoort, J.D., Albarede, F., 2005. The age of SNC meteorites and the antiquity of the Martian surface. *Earth and Planetary Science Letters* 240, 221–233. doi:10.1016/j.epsl.2005.09.007.
- Bouvier, A., Blichert-Toft, J., Vervoort, J.D., Gillet, P., Albarède, F., 2008a. The case for old basaltic shergottites. *Earth and Planetary Science Letters* 266, 105–124. doi:10.1016/j.epsl.2007.11.006.
- Bouvier, A., Vervoort, J.D., Patchett, P.J., 2008b. The Lu–Hf and Sm–Nd isotopic composition of CHUR: Constraints from unequilibrated chondrites and implications for the bulk composition of terrestrial planets. *Earth and Planetary Science Letters* 273, 48–57. doi:10.1016/j.epsl.2008.06.010.

- Bouvier, L.C., Costa, M.M., Connelly, J.N., Jensen, N.K., Wielandt, D., Storey, M., Nemchin, A.A., Whitehouse, M.J., Snape, J.F., Bellucci, J.J., Moynier, F., Agranier, A., Gueguen, B., Schönbächler, M., Bizzarro, M., 2018. Evidence for extremely rapid magma ocean crystallization and crust formation on Mars. *Nature* 558, 586–589. doi:10.1038/s41586-018-0222-z.
- Boynton, W.V., Taylor, G.J., Evans, L.G., Reedy, R.C., Starr, R., Janes, D.M., Kerry, K.E., Drake, D.M., Kim, K.J., Williams, R.M.S., Crombie, M.K., Dohm, J.M., Baker, V., Metzger, A.E., Karunatillake, S., Keller, J.M., Newsom, H.E., Arnold, J.R., Brckner, J., Englert, P.A.J., Gasnault, O., Sprague, A.L., Mitrofanov, I., Squyres, S.W., Trombka, J.I., d'Uston, L., Wnke, H., Hamara, D.K., 2007. Concentration of H, Si, Cl, K, Fe, and Th in the low- and mid-latitude regions of Mars. *Journal of Geophysical Research: Planets* 112, E12S99. doi:10.1029/2007JE002887.
- Boynton, W.V., Taylor, G.J., Karunatillake, S., Reedy, R.C., Keller, J.M., 2008. Elemental abundances determined via the Mars Odyssey GRS, in: Bell III, J. (Ed.), *The Martian Surface: Composition, Mineralogy, and Physical Properties*. Cambridge University Press, Cambridge, pp. 105–124. doi:10.1017/CBO9780511536076.006.
- Brandon, A.D., Puchtel, I.S., Walker, R.J., Day, J.M.D., Irving, A.J., Taylor, L.A., 2012. Evolution of the martian mantle inferred from the ^{187}Re – ^{187}Os isotope and highly siderophile element abundance systematics of shergottite meteorites. *Geochimica et Cosmochimica Acta* 76, 206–235. doi:10.1016/j.gca.2011.09.047.
- Burbine, T.H., O'Brien, K.M., 2004. Determining the possible building blocks of the Earth and Mars. *Meteoritics & Planetary Science* 39, 667–681. doi:10.1111/j.1945-5100.2004.tb00110.x.
- Canup, R., Salmon, J., 2018. Origin of Phobos and Deimos by the impact of a Vesta-to-Ceres sized body with Mars. *Science Advances* 4, eaar6887. doi:10.1126/sciadv.aar6887.
- Chen, J.H., Wasserburg, G.J., 1986. Formation ages and evolution of Shergotty and its parent planet from U-Th-Pb systematics. *Geochimica et Cosmochimica Acta* 50, 955–968. doi:10.1016/0016-7037(86)90376-5.
- Citron, R.I., Genda, H., Ida, S., 2015. Formation of Phobos and Deimos via a giant impact. *Icarus* 252, 334–338. doi:10.1016/j.icarus.2015.02.011.
- Clay, P.L., Burgess, R., Busemann, H., Ruzié-Hamilton, L., Joachim, B., Day, J.M.D., Ballentine, C.J., 2017. Halogens in chondritic meteorites and terrestrial accretion. *Nature* 551, 614–618. doi:10.1038/nature24625.
- Collinet, M., Médard, E., Charlier, B., Vander Auwera, J., Grove, T.L., 2015. Melting of the primitive Martian mantle at 0.5–2.2 GPa and the origin of basalts and alkaline rocks on Mars. *Earth and Planetary Science Letters* 427, 83–94. doi:10.1016/j.epsl.2015.06.056.

- Connolly, J.A.D., 2009. The geodynamic equation of state: what and how. *Geochemistry, Geophysics, Geosystems* 10, Q10014. doi:10.1029/2009GC002540.
- Corgne, A., Keshav, S., Wood, B.J., McDonough, W.F., Fei, Y., 2008. Metal–silicate partitioning and constraints on core composition and oxygen fugacity during Earth accretion. *Geochimica et Cosmochimica Acta* 72, 574–589. doi:10.1016/j.gca.2007.10.006.
- Coryell, C.D., Chase, J.W., Winchester, J.W., 1963. A procedure for geochemical interpretation of terrestrial rare-earth abundance patterns. *Journal of Geophysical Research* 68, 559–566. doi:10.1029/JZ068i002p00559.
- Craddock, R.A., 2011. Are Phobos and Deimos the result of a giant impact? *Icarus* 211, 1150–1161. doi:10.1016/j.icarus.2010.10.023.
- Curtis, D., Gladney, E., Jurney, E., 1980. A revision of the meteorite based cosmic abundance of boron. *Geochimica et Cosmochimica Acta* 44, 1945–1953. doi:10.1016/0016-7037(80)90194-5.
- Dauphas, N., Morbidelli, A., 2014. Geochemical and Planetary Dynamical Views on the Origin of Earth's Atmosphere and Oceans, in: Holland, H.D., Turekian, K.K. (Eds.), *Treatise on Geochemistry (Second Edition)*. Elsevier, Oxford. volume 6, pp. 1–35. doi:10.1016/B978-0-08-095975-7.01301-2.
- Dauphas, N., Poitrasson, F., Burkhardt, C., Kobayashi, H., Kurosawa, K., 2015. Planetary and meteoritic Mg/Si and $\delta^{30}\text{Si}$ variations inherited from solar nebula chemistry. *Earth and Planetary Science Letters* 427, 236–248. doi:10.1016/j.epsl.2015.07.008.
- Dauphas, N., Pourmand, A., 2011. Hf–W–Th evidence for rapid growth of Mars and its status as a planetary embryo. *Nature* 473, 489–492. doi:10.1038/nature10077.
- Dauphas, N., Pourmand, A., 2015. Thulium anomalies and rare earth element patterns in meteorites and Earth: Nebular fractionation and the nugget effect. *Geochimica et Cosmochimica Acta* 163, 234–261. doi:10.1016/j.gca.2015.03.037.
- Dauphas, N., Schauble, E.A., 2016. Mass fractionation laws, mass-independent effects, and isotopic anomalies. *Annual Review of Earth and Planetary Sciences* 44, 709–783. doi:10.1146/annurev-earth-060115-012157.
- Davis, F.A., Humayun, M., Hirschmann, M.M., Cooper, R.S., 2013. Experimentally determined mineral/melt partitioning of first-row transition elements (FRTE) during partial melting of peridotite at 3 GPa. *Geochimica et Cosmochimica Acta* 104, 232–260. doi:10.1016/j.gca.2012.11.009.
- Day, J.M.D., Brandon, A.D., Walker, R.J., 2016. Highly siderophile elements in Earth, Mars, the Moon, and asteroids. *Reviews in Mineralogy and Geochemistry* 81, 161–238. doi:10.2138/rmg.2016.81.04.

- Day, J.M.D., Tait, K.T., Udry, A., Moynier, F., Liu, Y., Neal, C.R., 2018. Martian magmatism from plume metasomatized mantle. *Nature Communications* 9, 4799. doi:10.1038/s41467-018-07191-0.
- Desch, S.J., Kalyaan, A., Alexander, C.M.O'D., 2018. The effect of Jupiter's formation on the distribution of refractory elements and inclusions in meteorites. *The Astrophysical Journal Supplement Series* 238, 11. doi:10.3847/1538-4365/aad95f.
- Ding, S., Dasgupta, R., Lee, C.T.A., Wadhwa, M., 2015. New bulk sulfur measurements of Martian meteorites and modeling the fate of sulfur during melting and crystallization—Implications for sulfur transfer from Martian mantle to crust–atmosphere system. *Earth and Planetary Science Letters* 409, 157–167. doi:10.1016/j.epsl.2014.10.046.
- Draper, D.S., Borg, L.E., Agee, C.B., 2005. Crystallization of a martian magma ocean and the formation of Shergottite source regions: A less Fe-rich Mars?, in: *Lunar and Planetary Science Conference*, p. 1429.
- Dreibus, G., Wänke, H., 1984. Accretion of the Earth and the inner planets, in: *Proceedings of the 27th International Geological Congress*, VNU Science Press. pp. 1–20.
- Dreibus, G., Wänke, H., 1985. Mars, a volatile-rich planet. *Meteoritics* 20, 367–381.
- Dreibus, G., Wänke, H., 1987. Volatiles on Earth and Mars: A comparison. *Icarus* 71, 225–240. doi:10.1016/0019-1035(87)90148-5.
- Ehmann, W.D., Lovering, J.F., 1967. The abundance of mercury in meteorites and rocks by neutron activation analysis. *Geochimica et Cosmochimica Acta* 31, 357–376. doi:10.1016/0016-7037(67)90047-6.
- Filiberto, J., 2017. Geochemistry of Martian basalts with constraints on magma genesis. *Chemical Geology* 466, 1–14. doi:10.1016/j.chemgeo.2017.06.009.
- Filiberto, J., Dasgupta, R., 2011. Fe²⁺–Mg partitioning between olivine and basaltic melts: Applications to genesis of olivine-phyric shergottites and conditions of melting in the Martian interior. *Earth and Planetary Science Letters* 304, 527–537. doi:10.1016/j.epsl.2011.02.029.
- Filiberto, J., Gross, J., McCubbin, F.M., 2016. Constraints on the water, chlorine, and fluorine content of the Martian mantle. *Meteoritics & Planetary Science* 51, 2023–2035. doi:10.1111/maps.12624.
- Filiberto, J., McCubbin, F.M., Taylor, G.J., 2019. Volatiles in Martian Magmas and the Interior: Inputs of Volatiles Into the Crust and Atmosphere, in: Filiberto, J., Schwenzer, S.P. (Eds.), *Volatile in the Martian Crust*. Elsevier, pp. 13–33. doi:10.1016/B978-0-12-804191-8.00002-7.

- Filiberto, J., Treiman, A.H., 2009. Martian magmas contained abundant chlorine, but little water. *Geology* 37, 1087–1090. doi:10.1130/G30488A.1.
- Foley, C.N., Wadhwa, M., Borg, L., Janney, P., Hines, R., Grove, T., 2005. The early differentiation history of Mars from ^{182}W - ^{142}Nd isotope systematics in the SNC meteorites. *Geochimica et Cosmochimica Acta* 69, 4557–4571. doi:10.1016/j.gca.2005.05.009.
- Franz, H.B., King, P.L., Gaillard, F., 2019. Sulfur on Mars from the Atmosphere to the Core, in: Filiberto, J., Schwenzer, S.P. (Eds.), *Volatiles in the Martian Crust*. Elsevier, pp. 119–183. doi:10.1016/B978-0-12-804191-8.00006-4.
- Gaffney, A.M., Borg, L.E., Connelly, J.N., 2007. Uranium–lead isotope systematics of Mars inferred from the basaltic shergottite QUE 94201. *Geochimica et Cosmochimica Acta* 71, 5016–5031. doi:10.1016/j.gca.2007.08.009.
- Gaillard, F., Michalski, J., Berger, G., McLennan, S.M., Scaillet, B., 2013. Geochemical reservoirs and timing of sulfur cycling on Mars. *Space Science Reviews* 174, 251–300. doi:10.1007/s11214-012-9947-4.
- Grady, M.M., Verchovsky, A.B., Wright, I., 2004. Magmatic carbon in Martian meteorites: attempts to constrain the carbon cycle on Mars. *International Journal of Astrobiology* 3, 117–124. doi:10.1017/S1473550404002071.
- Grevesse, N., Scott, P., Asplund, M., Sauval, A.J., 2015. The elemental composition of the Sun-III. The heavy elements Cu to Th. *Astronomy & Astrophysics* 573, A27. doi:10.1051/0004-6361/201424111.
- Grott, M., Baratoux, D., Hauber, E., Sautter, V., Mustard, J., Gasnault, O., Ruff, S.W., Karato, S.I., Debaille, V., Knapmeyer, M., Sohl, F., Van Hoolst, T., Breuer, D., Morschhauser, A., Toplis, M.J., 2013. Long-term evolution of the Martian crust-mantle system. *Space Science Reviews* 174, 49–111. doi:10.1007/s11214-012-9948-3.
- Halliday, A.N., Wänke, H., Birck, J.L., Clayton, R.N., 2001. The accretion, composition and early differentiation of Mars. *Space Science Reviews* 96, 197–230. doi:10.1023/A:1011997206080.
- Haxton, W.C., Hamish Robertson, R.G., Serenelli, A.M., 2013. Solar neutrinos: status and prospects. *Annual Review of Astronomy and Astrophysics* 51, 21–61. doi:10.1146/annurev-astro-081811-125539.
- Herd, C.D.K., Borg, L.E., Jones, J.H., Papike, J.J., 2002. Oxygen fugacity and geochemical variations in the martian basalts: Implications for martian basalt petrogenesis and the oxidation state of the upper mantle of Mars. *Geochimica et Cosmochimica Acta* 66, 2025–2036. doi:10.1016/S0016-7037(02)00828-1.

- Herzberg, C., Zhang, J., 1996. Melting experiments on anhydrous peridotite KLB-1: Compositions of magmas in the upper mantle and transition zone. *Journal of Geophysical Research: Solid Earth* 101, 8271–8295. doi:10.1029/96JB00170.
- Hui, H., Peslier, A.H., Lapen, T.J., Shafer, J.T., Brandon, A.D., Irving, A.J., 2011. Petrogenesis of basaltic shergottite Northwest Africa 5298: Closed-system crystallization of an oxidized mafic melt. *Meteoritics & Planetary Science* 46, 1313–1328. doi:10.1111/j.1945-5100.2011.01231.x.
- Hyodo, R., Genda, H., Charnoz, S., Rosenblatt, P., 2017. On the impact origin of Phobos and Deimos. I. Thermodynamic and physical aspects. *The Astrophysical Journal* 845, 125. doi:10.3847/1538-4357/aa81c4.
- Johansen, A., Mac Low, M.M., Lacerda, P., Bizzarro, M., 2015. Growth of asteroids, planetary embryos, and Kuiper belt objects by chondrule accretion. *Science Advances* 1, e1500109. doi:10.1126/sciadv.1500109.
- Jones, J.H., 2003. Constraints on the structure of the martian interior determined from the chemical and isotopic systematics of SNC meteorites. *Meteoritics & Planetary Science* 38, 1807–1814. doi:10.1111/j.1945-5100.2003.tb00016.x.
- Kaiura, G.H., Toguri, J.M., 1979. Densities of the molten FeS, FeS–Cu₂S and Fe–S–O systems—utilizing a bottom-balance Archimedean technique. *Canadian Metallurgical Quarterly* 18, 155–164. doi:10.1179/cmq.1979.18.2.155.
- Katsura, T., Yoneda, A., Yamazaki, D., Yoshino, T., Ito, E., 2010. Adiabatic temperature profile in the mantle. *Physics of the Earth and Planetary Interiors* 183, 212–218. doi:10.1016/j.pepi.2010.07.001.
- Keller, J.M., Boynton, W.V., Karunatillake, S., Baker, V.R., Dohm, J.M., Evans, L.G., Finch, M.J., Hahn, B.C., Hamara, D.K., Janes, D.M., Kerry, K.E., Newsom, H.E., Reedy, R.C., Sprague, A.L., Squyres, S.W., Starr, R.D., Taylor, G.J., Williams, R.M., 2006. Equatorial and midlatitude distribution of chlorine measured by Mars Odyssey GRS. *Journal of Geophysical Research: Planets* 111, E03S08. doi:10.1029/2006JE002679.
- Khan, A., Connolly, J.A.D., 2008. Constraining the composition and thermal state of Mars from inversion of geophysical data. *Journal of Geophysical Research: Planets* 113, E07003. doi:10.1029/2007JE002996.
- Khan, A., Liebske, C., Rozel, A., Rivoldini, A., Nimmo, F., Connolly, J.A.D., Plesa, A.C., Giardini, D., 2018. A geophysical perspective on the bulk composition of Mars. *Journal of Geophysical Research: Planets* 123, 575–611. doi:10.1002/2017JE005371.

- Komabayashi, T., 2014. Thermodynamics of melting relations in the system Fe-FeO at high pressure: Implications for oxygen in the Earth's core. *Journal of Geophysical Research: Solid Earth* 119, 4164–4177. doi:10.1002/2014JB010980.
- Konopliv, A.S., Park, R.S., Folkner, W.M., 2016. An improved JPL Mars gravity field and orientation from Mars orbiter and lander tracking data. *Icarus* 274, 253–260. doi:10.1016/j.icarus.2016.02.052.
- Kruijer, T.S., Burkhardt, C., Budde, G., Kleine, T., 2017a. Age of Jupiter inferred from the distinct genetics and formation times of meteorites. *Proceedings of the National Academy of Sciences* 114, 6712–6716. doi:10.1073/pnas.1704461114.
- Kruijer, T.S., Kleine, T., Borg, L.E., Brennecke, G.A., Irving, A.J., Bischoff, A., Agee, C.B., 2017b. The early differentiation of Mars inferred from Hf–W chronometry. *Earth and Planetary Science Letters* 474, 345–354. doi:10.1016/j.epsl.2017.06.047.
- Kuramoto, K., Kawakatsu, Y., Fujimoto, M., Bibring, J.P., Genda, H., Imamura, T., Kameda, S., Lawrence, D., Matsumoto, K., Miyamoto, H., Morota, T., Nagaoka, H., Nakamura, T., Ogawa, K., Otake, H., Ozaki, M., Sasaki, S., Senshu, H., Tachibana, S., Terada, N., Usui, T., J, W., Watanabe, S., MMX study team, 2018. Martian Moons eXploration (MMX): an overview of its science, in: European Planetary Science Congress, pp. EPSC2018–1036.
- Larimer, J.W., Wasson, J.T., 1988. Refractory lithophile elements, in: Kerridge, J.F., Matthews, M.S. (Eds.), *Meteorites and the Early Solar System*. The University of Arizona Press, Tucson, pp. 394–415.
- Lauretta, D.S., Devouard, B., Buseck, P.R., 1999. The cosmochemical behavior of mercury. *Earth and Planetary Science Letters* 171, 35–47. doi:10.1016/S0012-821X(99)00129-6.
- Le Roux, V., Dasgupta, R., Lee, C.T.A., 2011. Mineralogical heterogeneities in the Earth's mantle: constraints from Mn, Co, Ni and Zn partitioning during partial melting. *Earth and Planetary Science Letters* 307, 395–408. doi:10.1016/j.epsl.2011.05.014.
- Lee, Y.E., Gaskell, D.R., 1974. The densities and structures of melts in the system CaO-FeO-SiO₂. *Metallurgical Transactions* 5, 853–860. doi:10.1007/BF02643138.
- Levison, H.F., Kretke, K.A., Walsh, K.J., Bottke, W.F., 2015. Growing the terrestrial planets from the gradual accumulation of submeter-sized objects. *Proceedings of the National Academy of Sciences* 112, 14180–14185. doi:10.1073/pnas.1513364112.
- Lodders, K., 2003. Solar system abundances and condensation temperatures of the elements. *Astrophysical Journal* 591, 1220–1247. doi:10.1086/375492.
- Lodders, K., Fegley, Jr., B., 1997. An oxygen isotope model for the composition of Mars. *Icarus* 126, 373–394. doi:10.1006/icar.1996.5653.

- Longhi, J., Knittle, E., Holloway, J.R., Wänke, H., 1992. The bulk composition, mineralogy and internal structure of Mars, in: Kieffer, H.H., Jakosky, B.M., Snyder, C.W., Matthews, M.S. (Eds.), Mars. University of Arizona Press, Tuscon, pp. 184–208.
- Masuda, A., 1957. Simple regularity in the variation of relative abundances of rare earth elements. *The Journal of Earth Sciences, Nagoya University* 5, 125–134.
- Mathew, K.J., Marti, K., 2001. Early evolution of Martian volatiles: Nitrogen and noble gas components in ALH84001 and Chassigny. *Journal of Geophysical Research: Planets* 106, 1401–1422. doi:10.1029/2000JE001255.
- McCoy, C.L., Chartrand, Z., Caroebter, P.K., Gross, J., Filiberto, J., 2016. Experimentally melting a Mg#80 Martian mantle at 0.5 to 1.5 GPa: Implications for basalt genesis, in: The Geological Society of America Annual Meeting, p. 7. doi:10.1130/abs/2016AM-282245.
- McCubbin, F.M., Boyce, J.W., Novák-Szabó, T., Santos, A.R., Tartèse, R., Muttik, N., Domokos, G., Vazquez, J., Keller, L.P., Moser, D.E., Jerolmack, D.J., Shearer, C.K., Steele, A., Elardo, S.M., Rahman, Z., Anand, M., Delhayé, T., Agee, C.B., 2016a. Geologic history of Martian regolith breccia Northwest Africa 7034: Evidence for hydrothermal activity and lithologic diversity in the Martian crust. *Journal of Geophysical Research: Planets* 121, 2120–2149. doi:10.1002/2016JE005143.
- McCubbin, F.M., Boyce, J.W., Srinivasan, P., Santos, A.R., Elardo, S.M., Filiberto, J., Steele, A., Shearer, C.K., 2016b. Heterogeneous distribution of H₂O in the Martian interior: Implications for the abundance of H₂O in depleted and enriched mantle sources. *Meteoritics & Planetary Science* 51, 2036–2060. doi:10.1111/maps.12639.
- McCubbin, F.M., Elardo, S.M., Shearer, Jr., C.K., Smirnov, A., Hauri, E.H., Draper, D.S., 2013. A petrogenetic model for the comagmatic origin of chassignites and nakhlites: Inferences from chlorine-rich minerals, petrology, and geochemistry. *Meteoritics & Planetary Science* 48, 819–853. doi:10.1111/maps.12095.
- McCubbin, F.M., Smirnov, A., Nekvasil, H., Wang, J., Hauri, E., Lindsley, D.H., 2010. Hydrous magmatism on Mars: A source of water for the surface and subsurface during the Amazonian. *Earth and Planetary Science Letters* 292, 132–138. doi:10.1016/j.epsl.2010.01.028.
- McDonough, W.F., 1990. Comment on Abundance and distribution of gallium in some spinel and garnet lherzolites by D.B. McKay and R.H. Mitchell. *Geochimica et Cosmochimica Acta* 54, 471–473. doi:10.1016/0016-7037(90)90335-I.
- McDonough, W.F., 2014. Compositional model for the Earth's core, in: Holland, H.D., Turekian, K.K. (Eds.), *Treatise on Geochemistry* (Second Edition). Elsevier, Oxford. volume 3, pp. 559–577. doi:10.1016/B978-0-08-095975-7.00215-1.

- McDonough, W.F., 2016. The composition of the lower mantle and core, in: Terasaki, H., Fischer, R.A. (Eds.), Deep Earth. American Geophysical Union (AGU). chapter 12, pp. 145–159. doi:10.1002/9781118992487.ch12.
- McDonough, W.F., Sun, S.s., 1995. The composition of the Earth. *Chemical Geology* 120, 223–253. doi:10.1016/0009-2541(94)00140-4.
- McGovern, P.J., Solomon, S.C., Smith, D.E., Zuber, M.T., Simons, M., Wieczorek, M.A., Phillips, R.J., Neumann, G.A., Aharonson, O., Head, J.W., 2002. Localized gravity/topography admittance and correlation spectra on Mars: Implications for regional and global evolution. *Journal of Geophysical Research: Planets* 107, 19–1–19–25. doi:10.1029/2002JE001854.
- McGovern, P.J., Solomon, S.C., Smith, D.E., Zuber, M.T., Simons, M., Wieczorek, M.A., Phillips, R.J., Neumann, G.A., Aharonson, O., Head, J.W., 2004. Correction to Localized gravity/topography admittance and correlation spectra on Mars: Implications for regional and global evolution. *Journal of Geophysical Research: Planets* 109, E07007. doi:10.1029/2004JE002286.
- McKenzie, D., Barnett, D.N., Yuan, D.N., 2002. The relationship between Martian gravity and topography. *Earth and Planetary Science Letters* 195, 1–16. doi:10.1016/S0012-821X(01)00555-6.
- McLennan, S.M., 2003. Large-ion lithophile element fractionation during the early differentiation of Mars and the composition of the Martian primitive mantle. *Meteoritics & Planetary Science* 38, 895–904. doi:10.1111/j.1945-5100.2003.tb00286.x.
- McSween, Jr., H.Y., 2008. Martian meteorites as crustal samples, in: Bell III, J. (Ed.), *The Martian Surface: Composition, Mineralogy, and Physical Properties*. Cambridge University Press, pp. 383–395. doi:10.1017/CBO9780511536076.018.
- McSween, Jr., H.Y., 2015. Petrology on Mars. *American Mineralogist* 100, 2380–2395. doi:10.2138/am-2015-5257.
- McSween, Jr., H.Y., McLennan, S.M., 2014. Mars, in: Holland, H.D., Turekian, K.K. (Eds.), *Treatise on Geochemistry (Second Edition)*. Elsevier, Oxford. volume 2, pp. 251–300. doi:10.1016/B978-0-08-095975-7.00125-X.
- McSween, Jr., H.Y., Taylor, G.J., Wyatt, M.B., 2009. Elemental composition of the Martian crust. *Science* 324, 736–739. doi:10.1126/science.1165871.
- Medard, E., Martin, A.M., Collinet, M., Righter, K., Grove, T.L., Newville, M., Lanzotti, A., 2014. Fe³⁺ partitioning during basalt differentiation on Mars: insights into the oxygen fugacity of the shergottite mantle source(s), in: AGU Fall Meeting Abstracts, pp. V52B–03.

- Meier, M.M., Cloquet, C., Marty, B., 2016. Mercury (Hg) in meteorites: Variations in abundance, thermal release profile, mass-dependent and mass-independent isotopic fractionation. *Geochimica et Cosmochimica Acta* 182, 55–72. doi:10.1016/j.gca.2016.03.007.
- Minniti, M.E., Fei, Y., Bertka, C.M., 2006. New, geophysically-constrained martian mantle compositions, in: Workshop on Early Planetary Differentiation, pp. 72–73.
- Misawa, K., Nakamura, N., Premo, W.R., Tatsumoto, M., 1997. U-Th-Pb isotopic systematics of lherzolitic shergottite Yamato-793605. *Antarctic Meteorite Research* 10, 95–108.
- Morgan, J.W., Anders, E., 1979. Chemical composition of Mars. *Geochimica et Cosmochimica Acta* 43, 1601–1610. doi:10.1016/0016-7037(79)90180-7.
- Moriwaki, R., Usui, T., Simon, J.I., Jones, J.H., Yokoyama, T., Tobita, M., 2017. Coupled Pb isotopic and trace element systematics of the Tissint meteorite: Geochemical signatures of the depleted shergottite source mantle. *Earth and Planetary Science Letters* 474, 180–189. doi:10.1016/j.epsl.2017.06.044.
- Murchie, S.L., Britt, D.T., Pieters, C.M., 2014. The value of Phobos sample return. *Planetary and Space Science* 102, 176–182. doi:10.1016/j.pss.2014.04.014.
- Musselwhite, D.S., Dalton, H.A., Kiefer, W.S., Treiman, A.H., 2006. Experimental petrology of the basaltic shergottite Yamato-980459: Implications for the thermal structure of the Martian mantle. *Meteoritics & Planetary Science* 41, 1271–1290. doi:10.1111/j.1945-5100.2006.tb00521.x.
- Nagamori, M., 1969. Density of molten Ag-S, Cu-S, Fe-S, and Ni-S systems. *Transactions of the Metallurgical Society of the American Institute of Mechanical Engineers* 245, 1897–1902.
- Nagayama, T., Bailey, J.E., Loisel, G.P., Dunham, G.S., Rochau, G.A., Blancard, C., Colgan, J., Cossé, P., Faussurier, G., Fontes, C.J., Gilleron, F., Hansen, S.B., Iglesias, C.A., Golovkin, I.E., Kilcrease, D.P., MacFarlane, J.J., Mancini, R.C., More, R.M., Orban, C., Pain, J.C., Sherrill, M.E., Wilson, B.G., 2019. Systematic study of *L*-shell opacity at stellar interior temperatures. *Physical Review Letters* 122, 235001. doi:10.1103/PhysRevLett.122.235001.
- Nakamura, N., Unruh, D.M., Tatsumoto, M., Hutchison, R., 1982. Origin and evolution of the Nakhla meteorite inferred from the Sm-Nd and U-Pb systematics and REE, Ba, Sr, Rb and K abundances. *Geochimica et Cosmochimica Acta* 46, 1555–1573. doi:10.1016/0016-7037(82)90314-3.
- Nishida, K., Suzuki, A., Terasaki, H., Shibasaki, Y., Higo, Y., Kuwabara, S., Shimoyama, Y., Sakurai, M., Ushioda, M., Takahashi, E., Kikegawa, T., Wakabayashi, D., Funamori, N., 2016. Towards a consensus on the pressure and composition dependence of sound velocity in the liquid Fe-S system. *Physics of the Earth and Planetary Interiors* 257, 230–239. doi:10.1016/j.pepi.2016.06.009.

- Noll, Jr., P.D., Newsom, H.E., Leeman, W.P., Ryan, J.G., 1996. The role of hydrothermal fluids in the production of subduction zone magmas: evidence from siderophile and chalcophile trace elements and boron. *Geochimica et Cosmochimica Acta* 60, 587–611. doi:10.1016/0016-7037(95)00405-X.
- Norman, M.D., 1999. The composition and thickness of the crust of Mars estimated from rare earth elements and neodymium-isotopic compositions of Martian meteorites. *Meteoritics & Planetary Science* 34, 439–449. doi:10.1111/j.1945-5100.1999.tb01352.x.
- Ohtani, E., Kamaya, N., 1992. The geochemical model of Mars: An estimation from the high pressure experiments. *Geophysical Research Letters* 19, 2239–2242. doi:10.1029/92GL02369.
- Okuchi, T., 1997. Hydrogen partitioning into molten iron at high pressure: implications for Earth's core. *Science* 278, 1781–1784. doi:10.1126/science.278.5344.1781.
- O'Rourke, J.G., Shim, S.H., 2018. Suppressing the Martian dynamo with ongoing hydrogenation of the core by hydrated mantle minerals, in: *Lunar and Planetary Science Conference*, p. 2390.
- Ott, U., 1988. Noble gases in SNC meteorites: Shergotty, Nakhla, Chassigny. *Geochimica et Cosmochimica Acta* 52, 1937–1948. doi:10.1016/0016-7037(88)90017-8.
- Ott, U., Swindle, T.D., Schwenzer, S.P., 2019. Noble Gases in Martian Meteorites: Budget, Sources, Sinks, and Processes, in: Filiberto, J., Schwenzer, S.P. (Eds.), *Volatiles in the Martian Crust*. Elsevier, pp. 35–70. doi:10.1016/B978-0-12-804191-8.00003-9.
- Palme, H., Lodders, K., Jones, A., 2014. Solar system abundances of the elements, in: Holland, H.D., Turekian, K.K. (Eds.), *Treatise on Geochemistry (Second Edition)*. Elsevier, Oxford. volume 2, pp. 15–36. doi:10.1016/B978-0-08-095975-7.00118-2.
- Palme, H., O'Neill, H.S.C., 2014. Cosmochemical estimates of mantle composition, in: Holland, H.D., Turekian, K.K. (Eds.), *Treatise on Geochemistry (Second Edition)*. Elsevier, Oxford. volume 3, pp. 1–39. doi:10.1016/B978-0-08-095975-7.00201-1.
- Parro, L.M., Jiménez-Díaz, A., Mansilla, F., Ruiz, J., 2017. Present-day heat flow model of Mars. *Scientific Reports* 7, 45629. doi:10.1038/srep45629.
- Peplowski, P.N., Evans, L.G., Hauck, S.A., McCoy, T.J., Boynton, W.V., Gillis-Davis, J.J., Ebel, D.S., Goldsten, J.O., Hamara, D.K., Lawrence, D.J., McNutt, R.L., Nittler, L.R., Solomon, S.C., Rhodes, E.A., Sprague, A.L., Starr, R.D., Stockstill-Cahill, K.R., 2011. Radioactive elements on Mercurys surface from MESSENGER: Implications for the planets formation and evolution. *Science* 333, 1850–1852. doi:10.1126/science.1211576.
- Phillips, R.J., Zuber, M.T., Smrekar, S.E., Mellon, M.T., Head, J.W., Tanaka, K.L., Putzig, N.E., Milkovich, S.M., Campbell, B.A., Plaut, J.J., Safaeinili, A., Seu, R., Biccari, D., Carter, L.M., Picardi, G., Orosei, R., Surdas Mohit, P., Heggy, E., Zurek, R.W., Egan, A.F., Giacomoni, E.,

- Russo, F., Cutigni, M., Pettinelli, E., Holt, J.W., Leuschen, C.J., Marinangeli, L., 2008. Mars north polar deposits: Stratigraphy, age, and geodynamical response. *Science* 320, 1182–1185. doi:10.1126/science.1157546.
- Prettyman, T.H., Yamashita, N., Reedy, R.C., McSween, Jr., H.Y., Mittlefehldt, D.W., Hendricks, J.S., Toplis, M.J., 2015. Concentrations of potassium and thorium within Vesta's regolith. *Icarus* 259, 39–52. doi:10.1016/j.icarus.2015.05.035.
- Putirka, K., 2016. Rates and styles of planetary cooling on Earth, Moon, Mars, and Vesta, using new models for oxygen fugacity, ferric-ferrous ratios, olivine-liquid Fe-Mg exchange, and mantle potential temperature. *American Mineralogist* 101, 819–840. doi:10.2138/am-2016-5402.
- Rai, N., van Westrenen, W., 2013. Core-mantle differentiation in Mars. *Journal of Geophysical Research: Planets* 118, 1195–1203. doi:10.1002/jgre.20093.
- Raymond, S.N., Izidoro, A., 2017. Origin of water in the inner Solar System: Planetesimals scattered inward during Jupiter and Saturn's rapid gas accretion. *Icarus* 297, 134–148. doi:10.1016/j.icarus.2017.06.030.
- Righter, K., 2017. The Martian Meteorite Compendium. URL: <https://curator.jsc.nasa.gov/antmet/mmc/>.
- Righter, K., Chabot, N.L., 2011. Moderately and slightly siderophile element constraints on the depth and extent of melting in early Mars. *Meteoritics & Planetary Science* 46, 157–176. doi:10.1111/j.1945-5100.2010.01140.x.
- Righter, K., Nickodem, K., Pando, K., Danielson, L., Boujibar, A., Righter, M., Lapen, T.J., 2017. Distribution of Sb, As, Ge, and In between metal and silicate during accretion and core formation in the Earth. *Geochimica et Cosmochimica Acta* 198, 1–16. doi:10.1016/j.gca.2016.10.045.
- Ringwood, A.E., 1966. Chemical evolution of the terrestrial planets. *Geochimica et Cosmochimica Acta* 30, 41–104. doi:10.1016/0016-7037(66)90090-1.
- Ringwood, A.E., Hibberson, W., 1990. The system Fe-FeO revisited. *Physics and Chemistry of Minerals* 17, 313–319. doi:10.1007/BF00200126.
- Rivoldini, A., Van Hoolst, T., Verhoeven, O., Mocquet, A., Dehant, V., 2011. Geodesy constraints on the interior structure and composition of Mars. *Icarus* 213, 451–472. doi:10.1016/j.icarus.2011.03.024.
- Rose-Weston, L., Brenan, J.M., Fei, Y., Secco, R.A., Frost, D.J., 2009. Effect of pressure, temperature, and oxygen fugacity on the metal-silicate partitioning of Te, Se, and S: Implications for Earth differentiation. *Geochimica et Cosmochimica Acta* 73, 4598–4615. doi:10.1016/j.gca.2009.04.028.

- Rubie, D.C., Gessmann, C.K., Frost, D.J., 2004. Partitioning of oxygen during core formation on the Earth and Mars. *Nature* 429, 58–61. doi:10.1038/nature02473.
- Ruiz, J., Williams, J.P., Dohm, J.M., Fernández, C., López, V., 2009. Ancient heat flow and crustal thickness at Warrego rise, Thaumasia highlands, Mars: Implications for a stratified crust. *Icarus* 203, 47–57. doi:10.1016/j.icarus.2009.05.008.
- Sanloup, C., Jambon, A., Gillet, P., 1999. A simple chondritic model of Mars. *Physics of the Earth and Planetary Interiors* 112, 43–54. doi:10.1016/S0031-9201(98)00175-7.
- Schmelz, J.T., Reames, D.V., Von Steiger, R., Basu, S., 2012. Composition of the solar corona, solar wind, and solar energetic particles. *The Astrophysical Journal* 755, 33. doi:10.1088/0004-637X/755/1/33.
- Schmidt, M.E., Schrader, C.M., McCoy, T.J., 2013. The primary fO_2 of basalts examined by the Spirit rover in Gusev Crater, Mars: Evidence for multiple redox states in the Martian interior. *Earth and Planetary Science Letters* 384, 198–208. doi:10.1016/j.epsl.2013.10.005.
- Scott, E.R.D., Krot, A.N., 2014. Chondrites and their Components, in: Holland, H.D., Turekian, K.K. (Eds.), *Treatise on Geochemistry* (Second Edition). Elsevier, Oxford. volume 1, pp. 65–137. doi:10.1016/B978-0-08-095975-7.00104-2.
- Seidelmann, P.K., Abalakin, V.K., Bursa, M., Davies, M.E., De Bergh, C., Lieske, J.H., Oberst, J., Simon, J.L., Standish, E.M., Stooke, P., Thomas, P.C., 2002. Report of the IAU/IAG working group on cartographic coordinates and rotational elements of the planets and satellites: 2000. *Celestial Mechanics and Dynamical Astronomy* 82, 83–111. doi:10.1023/A:1013939327465.
- Shahar, A., Hillgren, V.J., Horan, M.F., Mesa-Garcia, J., Kaufman, L.A., Mock, T.D., 2015. Sulfur-controlled iron isotope fractionation experiments of core formation in planetary bodies. *Geochimica et Cosmochimica Acta* 150, 253–264. doi:10.1016/j.gca.2014.08.011.
- Shibasaki, Y., Ohtani, E., Terasaki, H., Suzuki, A., Funakoshi, K.i., 2009. Hydrogen partitioning between iron and ringwoodite: Implications for water transport into the Martian core. *Earth and Planetary Science Letters* 287, 463–470. doi:10.1016/j.epsl.2009.08.034.
- Siebert, J., Badro, J., Antonangeli, D., Ryerson, F.J., 2013. Terrestrial accretion under oxidizing conditions. *Science* 339, 1194–1197. doi:10.1126/science.122792.
- Smrekar, S.E., Lognonné, P., Spohn, T., Banerdt, W.B., Breuer, D., Christensen, U., Dehant, V., Drilleau, M., Folkner, W., Fuji, N., Garcia, R.F., Giardini, D., Golombek, M., Grott, M., Gudkova, T., Johnson, C., Khan, A., Langlais, B., Mittelholz, A., Mocquet, A., Myhill, R., Panning, M., Perrin, C., Pike, T., Plesa, A.C., Rivoldini, A., Samuel, H., Stähler, S.C., van Driel, M., Van Hoolst, T., Verhoeven, O., Weber, R., Wieczorek, M., 2019. Pre-mission InSights on the interior of Mars. *Space Science Reviews* 215, 3. doi:10.1007/s11214-018-0563-9.

- Sohl, F., Spohn, T., 1997. The interior structure of Mars: Implications from SNC meteorites. *Journal of Geophysical Research: Planets* 102, 1613–1635. doi:10.1029/96JE03419.
- Stixrude, L., Lithgow-Bertelloni, C., 2005. Thermodynamics of mantle minerals—I. Physical properties. *Geophysical Journal International* 162, 610–632. doi:10.1111/j.1365-246X.2005.02642.x.
- Stixrude, L., Lithgow-Bertelloni, C., 2011. Thermodynamics of mantle minerals-II. Phase equilibria. *Geophysical Journal International* 184, 1180–1213. doi:10.1111/j.1365-246X.2010.04890.x.
- Sun, S.s., 1982. Chemical composition and origin of the Earth's primitive mantle. *Geochimica et Cosmochimica Acta* 46, 179–192. doi:10.1016/0016-7037(82)90245-9.
- Surkov, Y.A., 1977. Gamma-Spectrometry in Cosmic Investigations. Atomizdat, Moscow.
- Surkov, Y.A., Kirnozov, F.F., Glazov, V.N., Dunchenko, A.G., Tatsy, L.P., Sobornov, O.P., 1987. Uranium, thorium, and potassium in the Venusian rocks at the landing sites of Vega 1 and 2. *Journal of Geophysical Research: Solid Earth* 92, E537–E540. doi:10.1029/JB092iB04p0E537.
- Surkov, Y.A., Moskalyova, L.P., Kharyukova, V.P., Dudin, A.D., Smirnov, G.G., Zaitseva, S.Y., 1986. Venus rock composition at the Vega 2 landing site. *Journal of Geophysical Research: Solid Earth* 91, E215–E218. doi:10.1029/JB091iB13p0E215.
- Symes, S.J.K., Borg, L.E., Shearer, C.K., Irving, A.J., 2008. The age of the Martian meteorite Northwest Africa 1195 and the differentiation history of the shergottites. *Geochimica et Cosmochimica Acta* 72, 1696–1710. doi:10.1016/j.gca.2007.12.022.
- Tait, K.T., Day, J.M.D., 2018. Chondritic late accretion to Mars and the nature of shergottite reservoirs. *Earth and Planetary Science Letters* 494, 99–108. doi:10.1016/j.epsl.2018.04.040.
- Takahashi, E., Kushiro, I., 1983. Melting of a dry peridotite at high pressures and basalt magma genesis. *American Mineralogist* 68, 859–879.
- Taylor, G.J., 2013. The bulk composition of Mars. *Chemie der Erde-Geochemistry* 73, 401–420. doi:10.1016/j.chemer.2013.09.006.
- Taylor, G.J., Boynton, W., Brckner, J., Wnke, H., Dreibus, G., Kerry, K., Keller, J., Reedy, R., Evans, L., Starr, R., Squyres, S., Karunatillake, S., Gasnault, O., Maurice, S., d'Uston, C., Englert, P., Dohm, J., Baker, V., Hamara, D., Janes, D., Sprague, A., Kim, K., Drake, D., 2006a. Bulk composition and early differentiation of Mars. *Journal of Geophysical Research: Planets* 111, E03S10. doi:10.1029/2005JE002645.

- Taylor, G.J., Boynton, W.V., McLennan, S.M., Martel, L.M.V., 2010. K and Cl concentrations on the Martian surface determined by the Mars Odyssey Gamma Ray Spectrometer: Implications for bulk halogen abundances in Mars. *Geophysical Research Letters* 37, L12204. doi:10.1029/2010GL043528.
- Taylor, G.J., Stopar, J.D., Boynton, W.V., Karunatillake, S., Keller, J.M., Brckner, J., Wnke, H., Dreibus, G., Kerry, K.E., Reedy, R.C., Evans, L.G., Starr, R.D., Martel, L.M.V., Squyres, S.W., Gasnault, O., Maurice, S., d'Uston, C., Englert, P., Dohm, J.M., Baker, V.R., Hamara, D., Janes, D., Sprague, A.L., Kim, K.J., Drake, D.M., McLennan, S.M., Hahn, B.C., 2006b. Variations in K/Th on Mars. *Journal of Geophysical Research: Planets* 111, E03S06. doi:10.1029/2006JE002676.
- Taylor, S.R., McLennan, S., 2009. *Planetary Crusts: Their Composition, Origin and Evolution*. volume 10. Cambridge University Press.
- Treiman, A.H., 2003. Chemical compositions of martian basalts (shergottites): Some inferences on basalt formation, mantle metasomatism, and differentiation in Mars. *Meteoritics & Planetary Science* 38, 1849–1864. doi:10.1111/j.1945-5100.2003.tb00019.x.
- Treiman, A.H., 2005. The nakhlite meteorites: Augite-rich igneous rocks from Mars. *Chemie der Erde-Geochemistry* 65, 203–270. doi:10.1016/j.chemer.2005.01.004.
- Treiman, A.H., Lindstrom, D.J., 1997. Trace element geochemistry of Martian iddingsite in the Lafayette meteorite. *Journal of Geophysical Research: Planets* 102, 9153–9163. doi:10.1029/96JE03884.
- Tsuno, K., Frost, D.J., Rubie, D.C., 2011. The effects of nickel and sulphur on the core–mantle partitioning of oxygen in Earth and Mars. *Physics of the Earth and Planetary Interiors* 185, 1–12. doi:10.1016/j.pepi.2010.11.009.
- Udry, A., Day, J.M.D., 2018. 1.34 billion-year-old magmatism on Mars evaluated from the co-genetic nakhlite and chassignite meteorites. *Geochimica et Cosmochimica Acta* 238, 292–315. doi:10.1016/j.gca.2018.07.006.
- Umemoto, K., Hirose, K., 2015. Liquid iron-hydrogen alloys at outer core conditions by first-principles calculations. *Geophysical Research Letters* 42, 7513–7520. doi:10.1002/2015GL065899.
- Usui, T., McSween, Jr., H.Y., Floss, C., 2008. Petrogenesis of olivine-phyric shergottite Yamato 980459, revisited. *Geochimica et Cosmochimica Acta* 72, 1711–1730. doi:10.1016/j.gca.2008.01.011.
- Verhoeven, O., Rivoldini, A., Vacher, P., Mocquet, A., Choblet, G., Menvielle, M., Dehant, V., Van Hoolst, T., Sleewaegen, J., Barriot, J.P., Lognonné, P., 2005. Interior structure of terrestrial plan-

- ets: Modeling Mars' mantle and its electromagnetic, geodetic, and seismic properties. *Journal of Geophysical Research: Planets* 110, E04009. doi:10.1029/2004JE002271.
- Wade, J., Wood, B.J., 2005. Core formation and the oxidation state of the Earth. *Earth and Planetary Science Letters* 236, 78–95. doi:10.1016/j.epsl.2005.05.017.
- Wadhwa, M., 2001. Redox state of Mars' upper mantle and crust from Eu anomalies in shergottite pyroxenes. *Science* 291, 1527–1530. doi:10.1126/science.1057594.
- Wadhwa, M., 2008. Redox conditions on small bodies, the Moon and Mars, in: MacPherson, G.J. (Ed.), *Reviews in Mineralogy and Geochemistry*. Mineralogical Society of America. volume 68, pp. 493–510. doi:10.2138/rmg.2008.68.17.
- Walsh, K.J., Morbidelli, A., Raymond, S.N., O'Brien, D.P., Mandell, A.M., 2011. A low mass for Mars from Jupiter's early gas-driven migration. *Nature* 475, 206–209. doi:10.1038/nature10201.
- Walter, M.J., 1998. Melting of garnet peridotite and the origin of komatiite and depleted lithosphere. *Journal of Petrology* 39, 29–60. doi:10.1093/petroj/39.1.29.
- Wang, Z., Becker, H., 2017. Chalcophile elements in Martian meteorites indicate low sulfur content in the Martian interior and a volatile element-depleted late veneer. *Earth and Planetary Science Letters* 463, 56–68. doi:10.1016/j.epsl.2017.01.023.
- Wang, Z., Becker, H., Wombacher, F., 2015. Mass fractions of S, Cu, Se, Mo, Ag, Cd, In, Te, Ba, Sm, W, Tl and Bi in geological reference materials and selected carbonaceous chondrites determined by isotope dilution ICP-MS. *Geostandards and Geoanalytical Research* 39, 185–208. doi:10.1111/j.1751-908X.2014.00312.x.
- Wänke, H., 1981. Constitution of terrestrial planets. *Philosophical Transactions of the Royal Society of London. Series A: Mathematical and Physical Sciences* 303, 287–302. doi:10.1098/rsta.1981.0203.
- Wänke, H., 1987. Chemistry and accretion of Earth and Mars. *Bulletin de la Société Géologique de France* 3, 13–19.
- Wänke, H., Dreibus, G., 1988. Chemical composition and accretion history of terrestrial planets. *Philosophical Transactions of the Royal Society of London. Series A, Mathematical and Physical Sciences* 325, 545–557. doi:10.1098/rsta.1988.0067.
- Wänke, H., Dreibus, G., 1994. Chemistry and accretion history of Mars. *Philosophical Transactions of the Royal Society of London. Series A, Mathematical and Physical Sciences* 349, 285–293. doi:10.1098/rsta.1994.0132.

- Warren, P.H., 2011. Stable-isotopic anomalies and the accretionary assemblage of the Earth and Mars: A subordinate role for carbonaceous chondrites. *Earth and Planetary Science Letters* 311, 93–100. doi:10.1016/j.epsl.2011.08.047.
- Wasson, J.T., Kallemeyn, G.W., 1988. Compositions of chondrites. *Philosophical Transactions of the Royal Society of London A: Mathematical, Physical and Engineering Sciences* 325, 535–544. doi:10.1098/rsta.1988.0066.
- Wasylewski, L.E., Baker, M.B., Kent, A.J., Stolper, E.M., 2003. Near-solidus melting of the shallow upper mantle: partial melting experiments on depleted peridotite. *Journal of Petrology* 44, 1163–1191. doi:10.1093/petrology/44.7.1163.
- Weinke, H.H., 1978. Chemical and mineralogical examination of the Nakhla achondrite. *Meteoritics* 13, 660–664.
- Wieczorek, M.A., Zuber, M.T., 2004. Thickness of the Martian crust: Improved constraints from geoid-to-topography ratios. *Journal of Geophysical Research: Planets* 109. doi:10.1029/2003JE002153.
- Wipperfurth, S.A., Guo, M., Šrámek, O., McDonough, W.F., 2018. Earth's chondritic Th/U: Negligible fractionation during accretion, core formation, and crust-mantle differentiation. *Earth and Planetary Science Letters* 498, 196–202. doi:10.1016/j.epsl.2018.06.029.
- Wood, B.J., 1993. Carbon in the core. *Earth and Planetary Science Letters* 117, 593–607. doi:10.1016/0012-821X(93)90105-I.
- Wood, B.J., Li, J., Shahar, A., 2013. Carbon in the core: its influence on the properties of core and mantle. *Reviews in Mineralogy and Geochemistry* 75, 231–250. doi:10.2138/rmg.2013.75.8.
- Wood, B.J., Smythe, D.J., Harrison, T., 2019. The condensation temperatures of the elements: A reappraisal. *American Mineralogist* 104, 844–856. doi:10.2138/am-2019-6852CCBY.
- Wood, B.J., Wade, J., Kilburn, M.R., 2008. Core formation and the oxidation state of the Earth: Additional constraints from Nb, V and Cr partitioning. *Geochimica et Cosmochimica Acta* 72, 1415–1426. doi:10.1016/j.gca.2007.11.036.
- Wood, B.J., Walter, M.J., Wade, J., 2006. Accretion of the Earth and segregation of its core. *Nature* 441, 825–833. doi:10.1038/nature04763.
- Yang, S., Humayun, M., Righter, K., Jefferson, G., Fields, D., Irving, A.J., 2015. Siderophile and chalcophile element abundances in shergottites: Implications for Martian core formation. *Meteoritics & Planetary Science* 50, 691–714. doi:10.1111/maps.12384.

- Zambardi, T., Poitrasson, F., Corgne, A., Méheut, M., Quitté, G., Anand, M., 2013. Silicon isotope variations in the inner solar system: Implications for planetary formation, differentiation and composition. *Geochimica et Cosmochimica Acta* 121, 67–83. doi:10.1016/j.gca.2013.06.040.
- Zharkov, V.N., 1996. The internal structure of Mars: a key to understanding the origin of terrestrial planets. *Solar System Research* 30, 456–466.
- Zharkov, V.N., Gudkova, T.V., 2005. Construction of Martian interior model. *Solar System Research* 39, 343–373. doi:10.1007/s11208-005-0049-7.
- Zuber, M.T., Solomon, S.C., Phillips, R.J., Smith, D.E., Tyler, G.L., Aharonson, O., Balmino, G., Banerdt, W.B., Head, J.W., Johnson, C.L., Lemoine, F.G., McGovern, P.J., Neumann, G.A., Rowlands, D.D., Zhong, S., 2000. Internal structure and early thermal evolution of Mars from Mars Global Surveyor topography and gravity. *Science* 287, 1788–1793. doi:10.1126/science.287.5459.1788.

Appendix A: Supplementary data

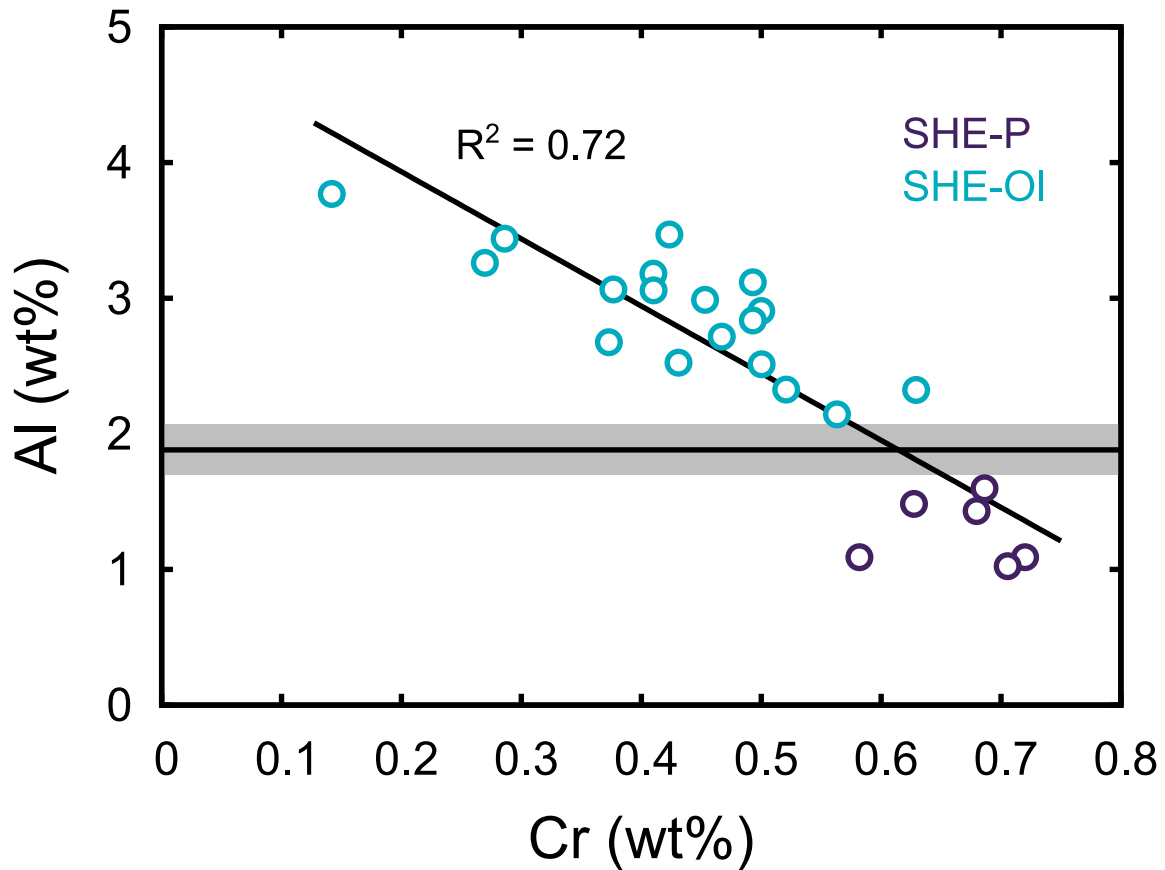


Fig. A1: Chromium versus Al contents in poikilitic (SHE-P) and olivine-phyric (SHE-OI) shergottites. Horizontal line and gray band show the BSM abundance of Al and its uncertainty, respectively (Table 5).

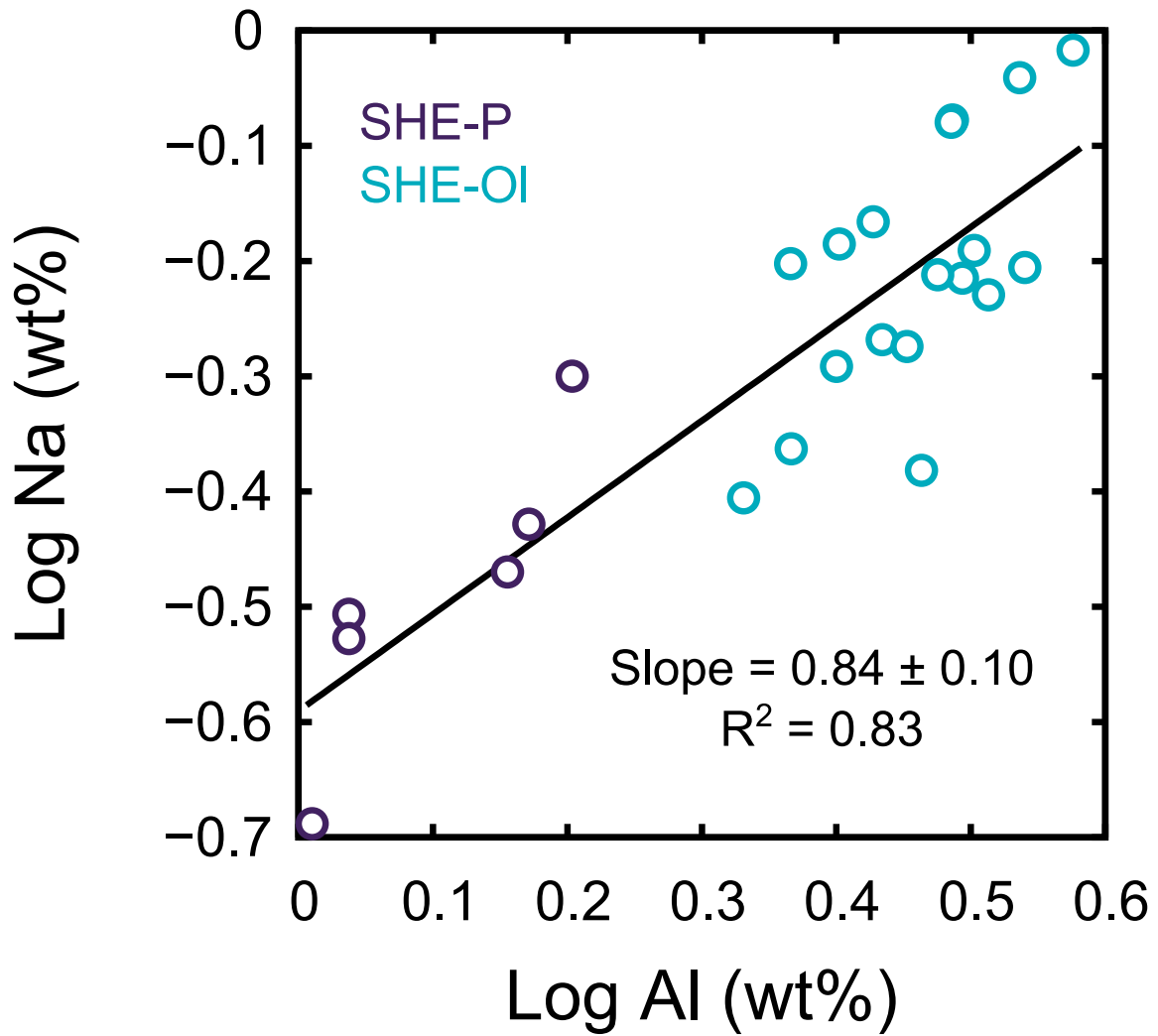


Fig. A2: Log-log plot of Na and Al in poikilitic and olivine-phyric shergottites.

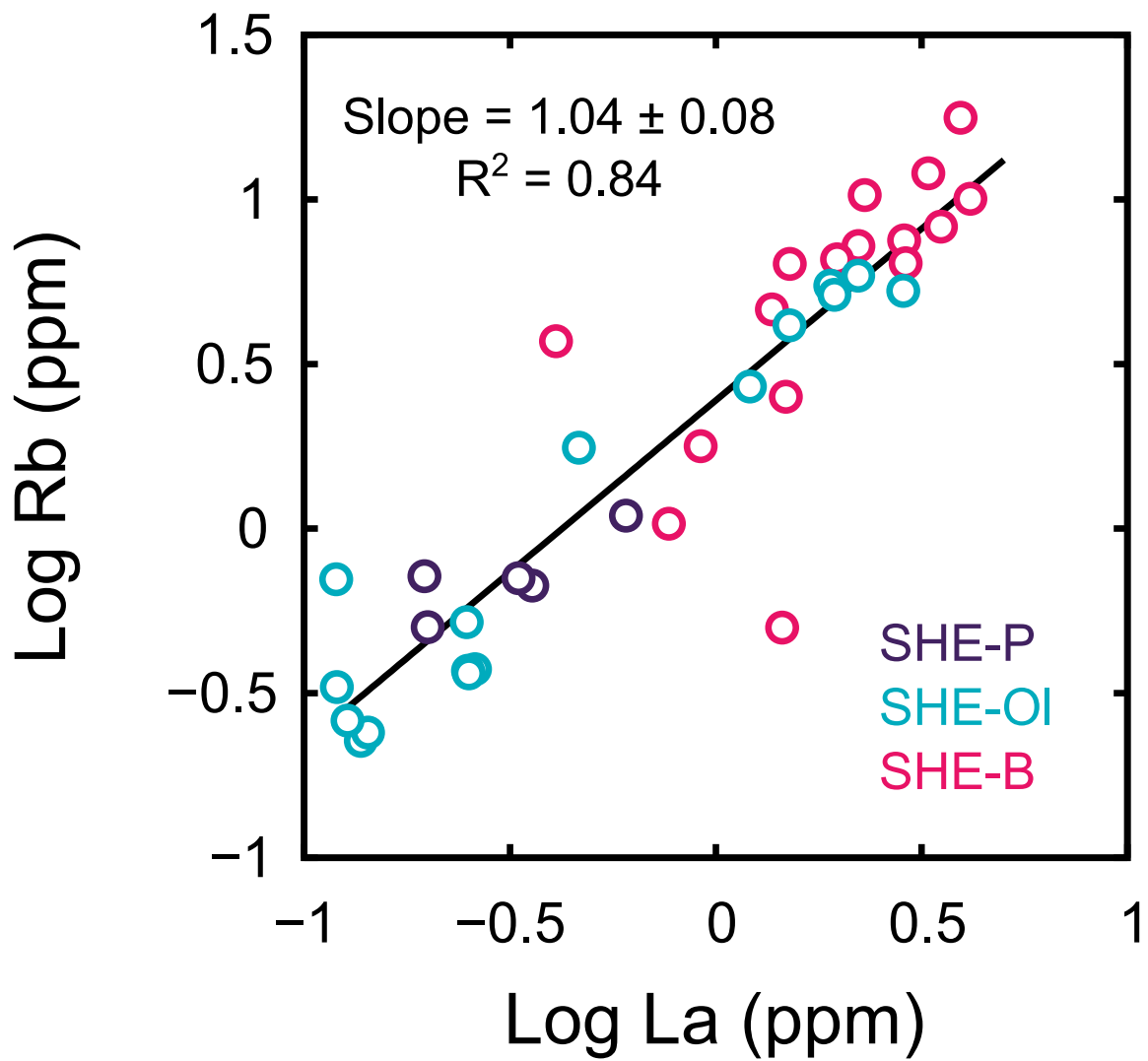


Fig. A3: Log-log plot of Rb and La in poikilitic, olivine-phyric and basaltic (SHE-B) shergottites.

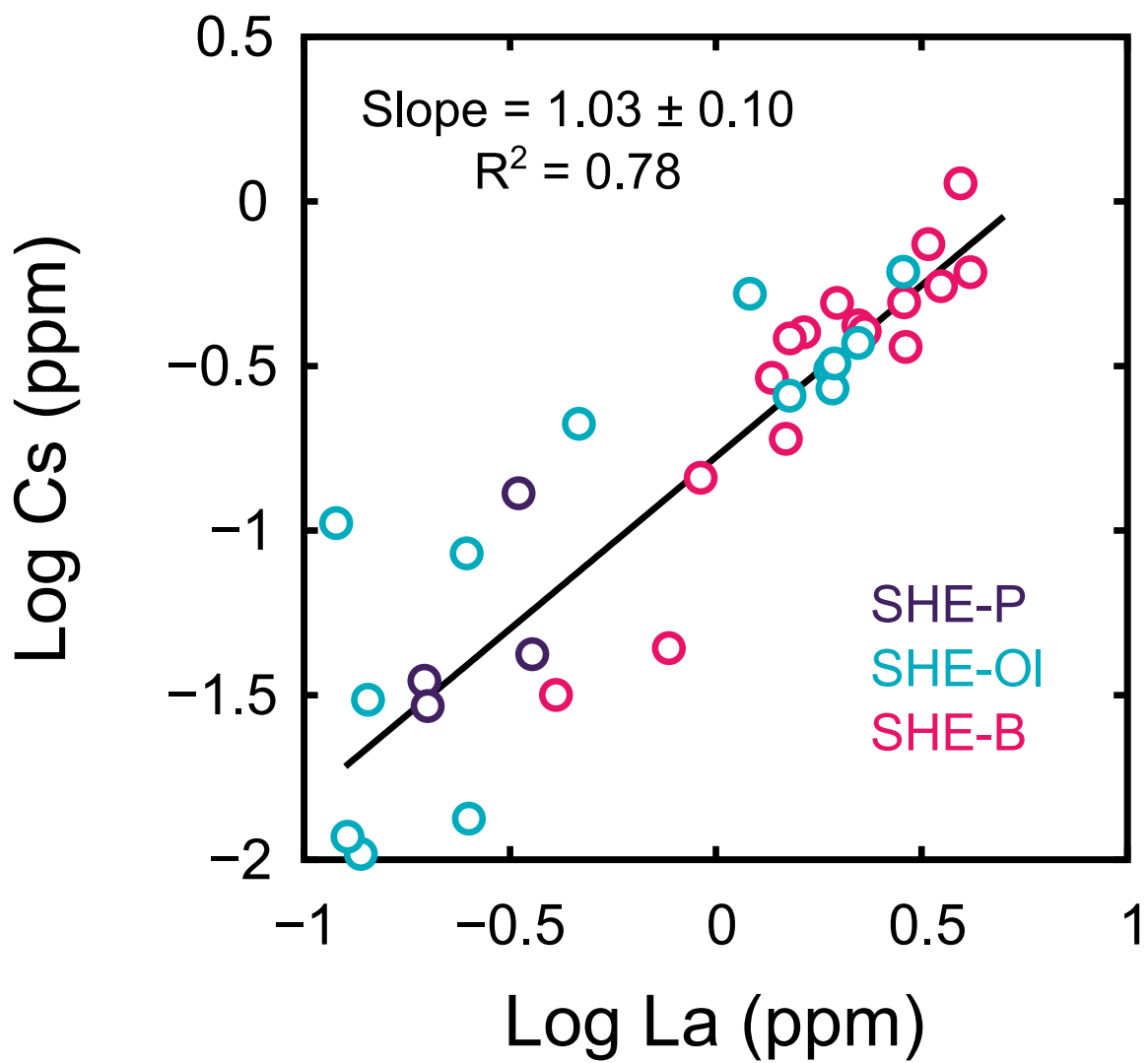


Fig. A4: Log-log plot of Cs and La in poikilitic, olivine-phyric and basaltic shergottites.

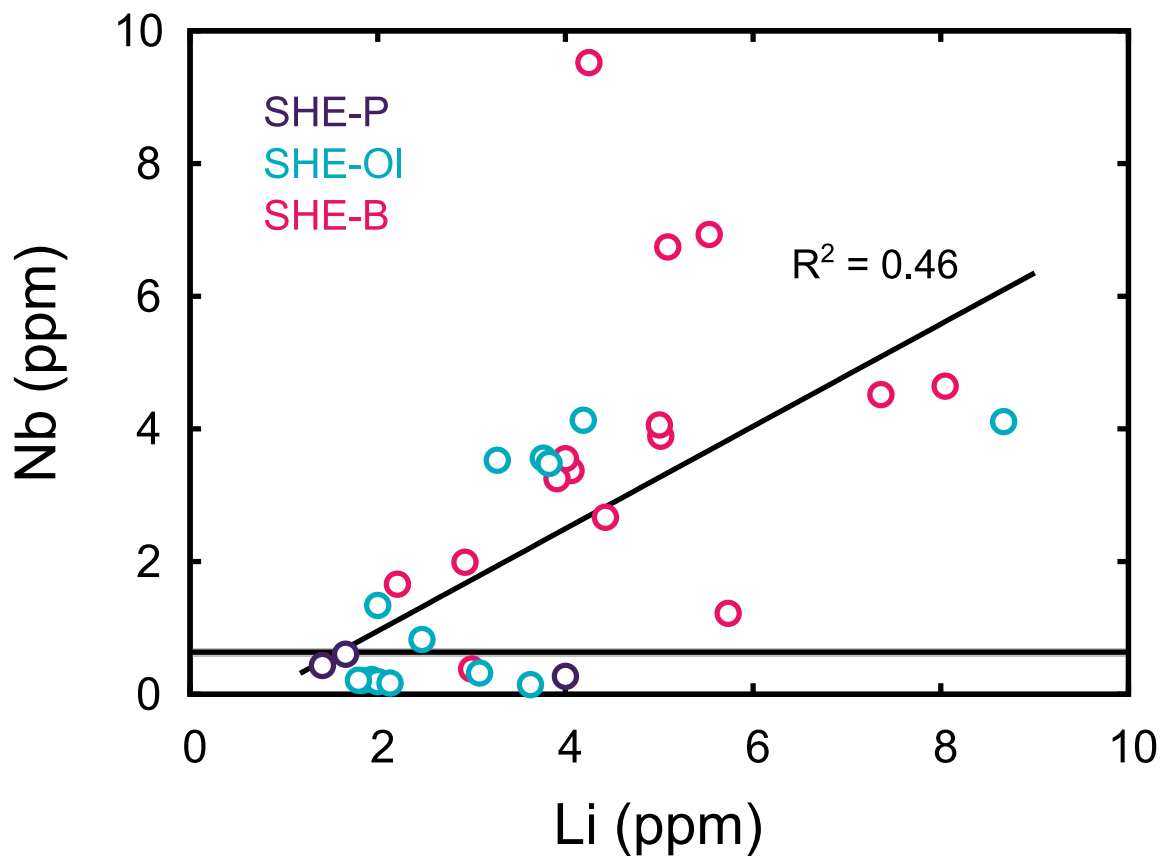


Fig. A5: Lithium versus Nb contents in poikilitic, olivine-phyric and basaltic shergottites. Horizontal line and gray band show the BSM abundance of Nb and its uncertainty, respectively (Table 5).

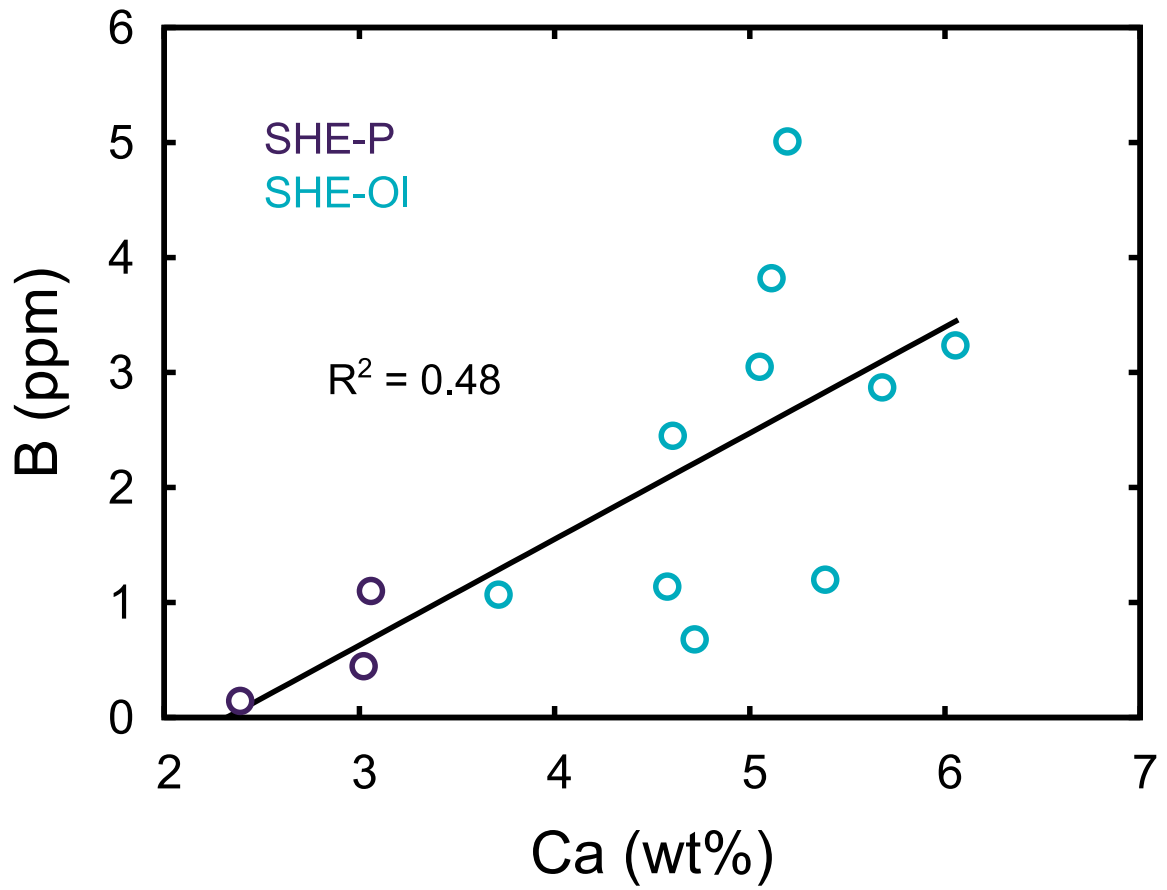


Fig. A6: Boron versus Ca contents in poikilitic and olivine-phyric shergottites.

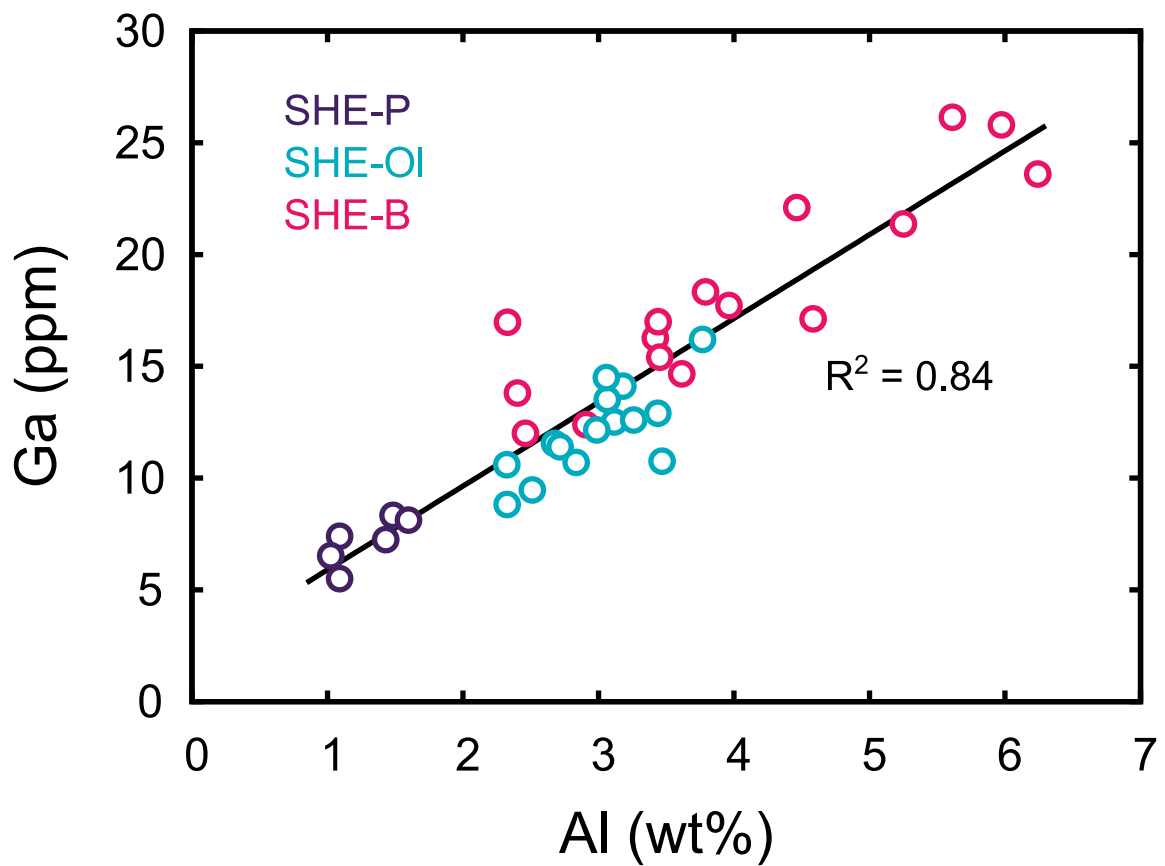


Fig. A7: Gallium versus Al contents in poikilitic, olivine-phyric and basaltic shergottites.

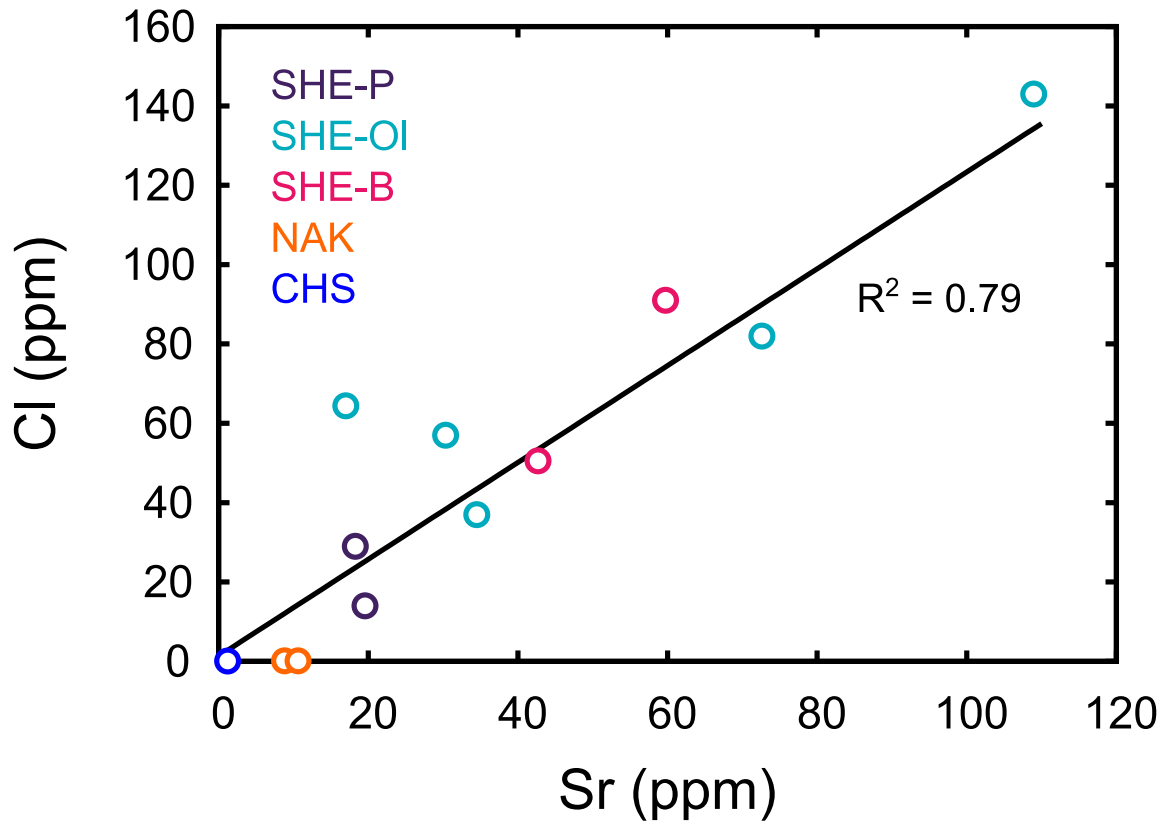


Fig. A8: Chlorine versus Sr contents in Martian meteorites.

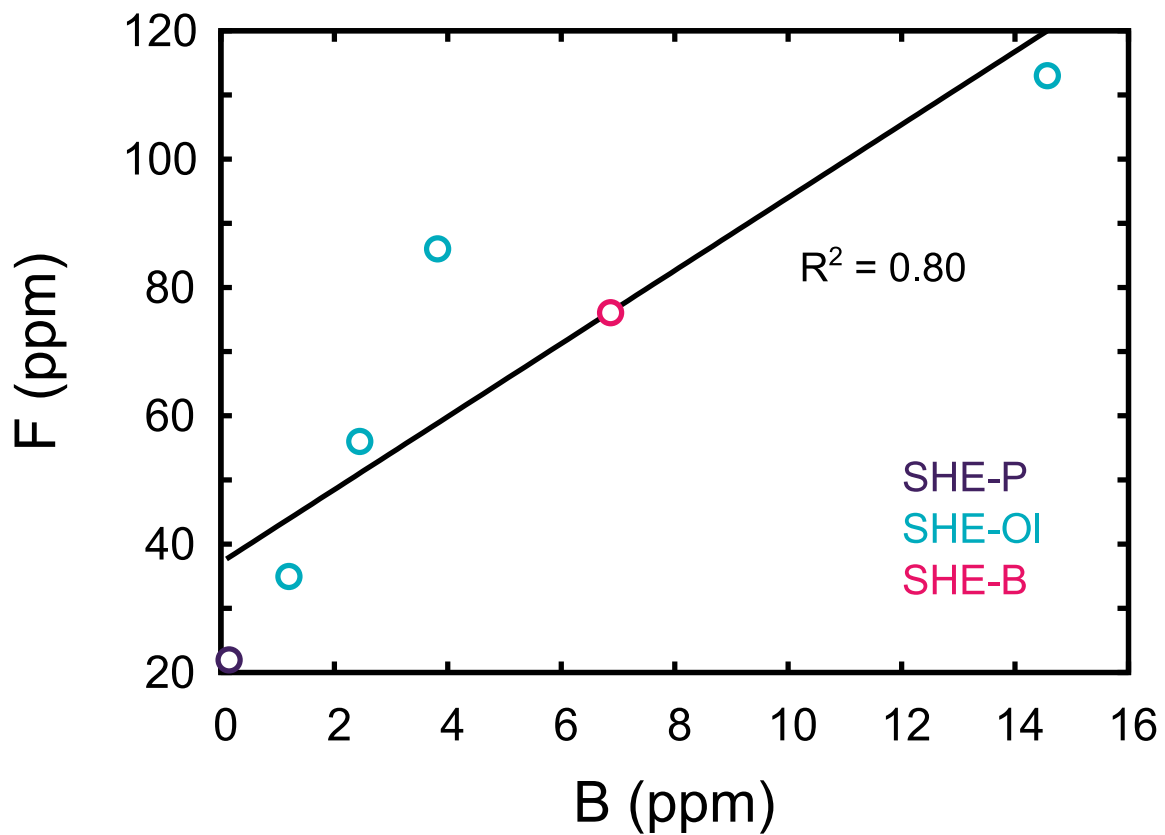


Fig. A9: Fluorine versus B contents in poikilitic, olivine-phyric and basaltic shergottites.

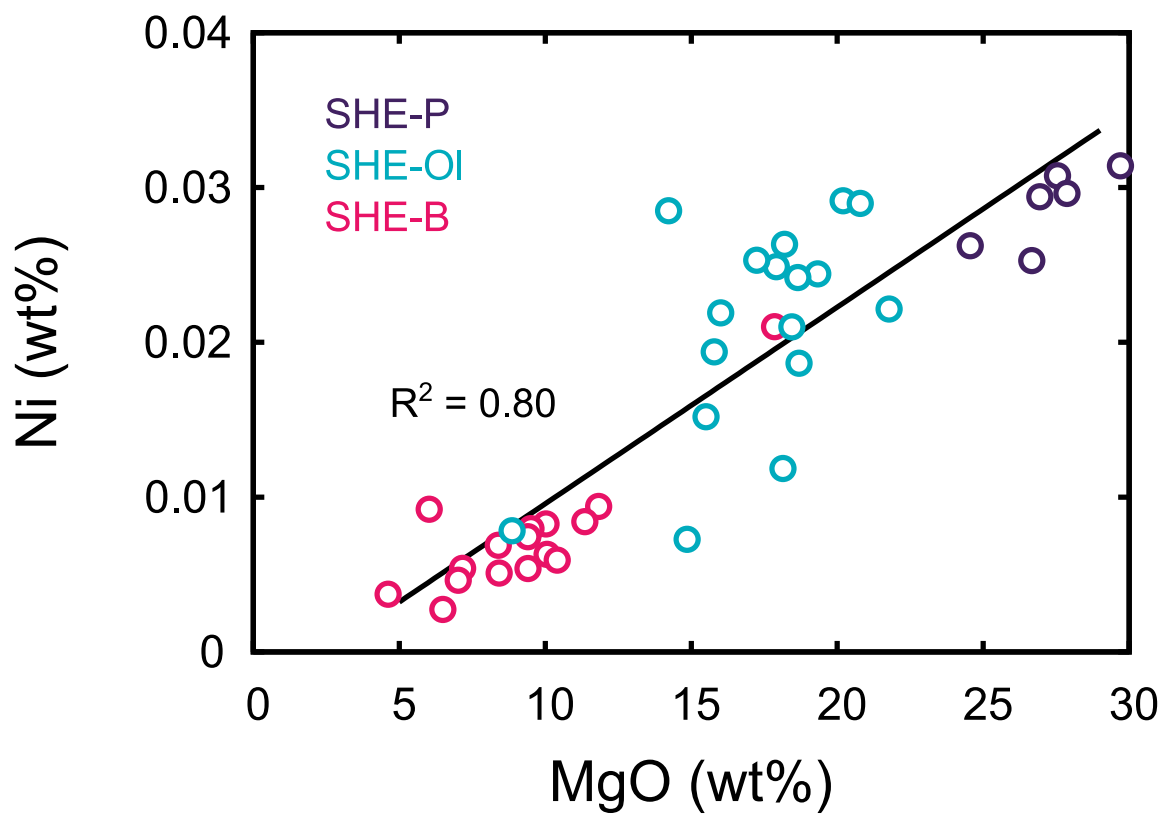


Fig. A10: Nickel versus MgO contents in poikilitic, olivine-phyric and basaltic shergottites.

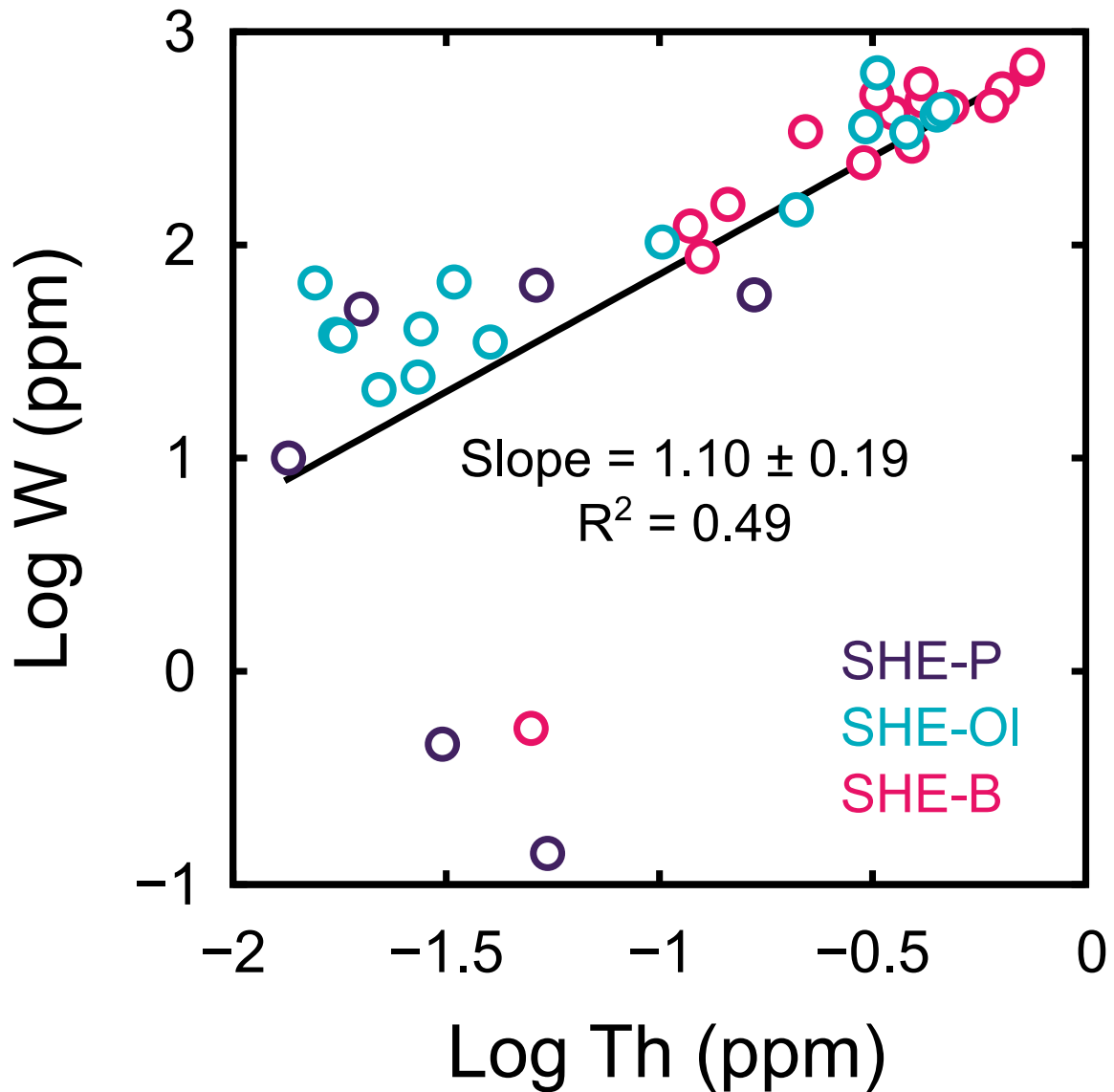


Fig. A11: Log-log plot of W and Th in poikilitic, olivine-phyric and basaltic shergottites.

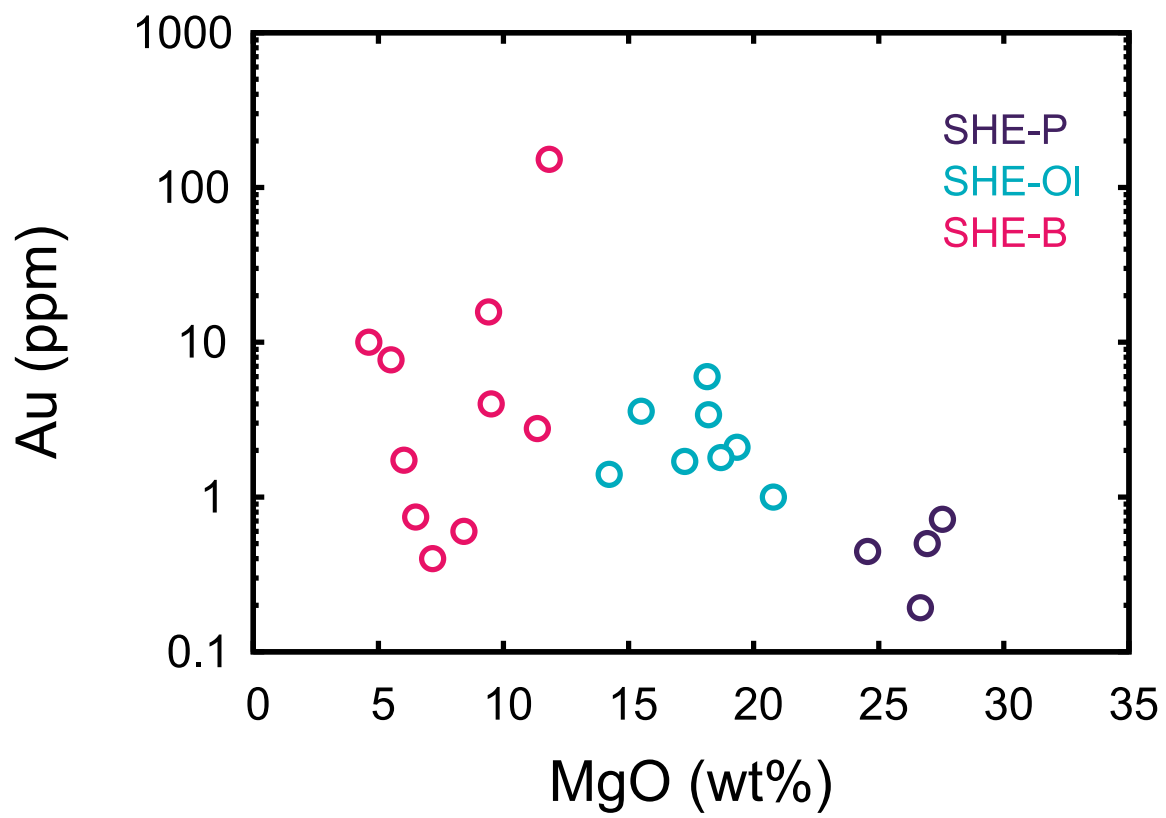


Fig. A12: Gold versus MgO contents in poikilitic, olivine-phyric and basaltic shergottites.

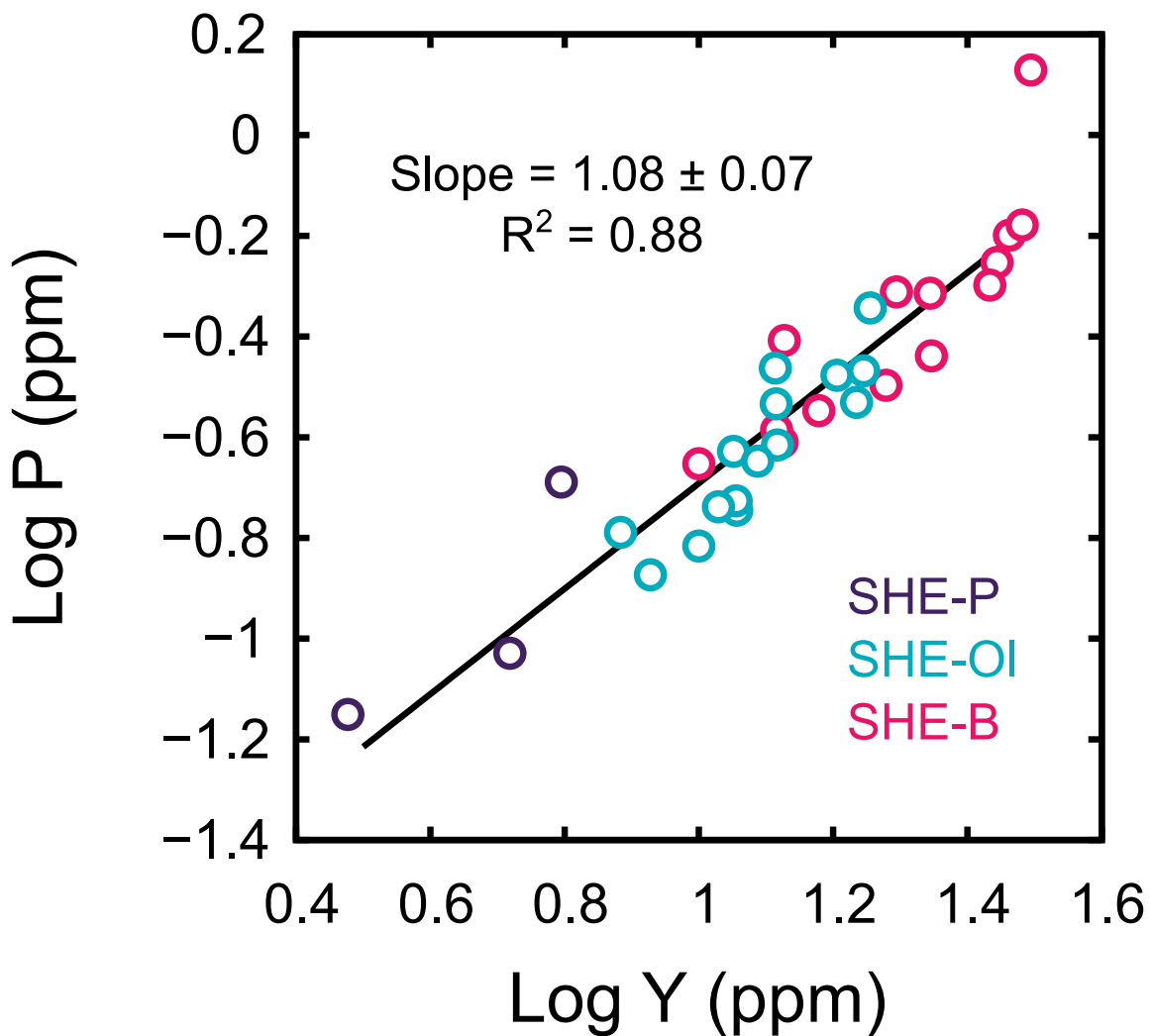


Fig. A13: Log-log plot of P and Y in poikilitic, olivine-phyric and basaltic shergottites.

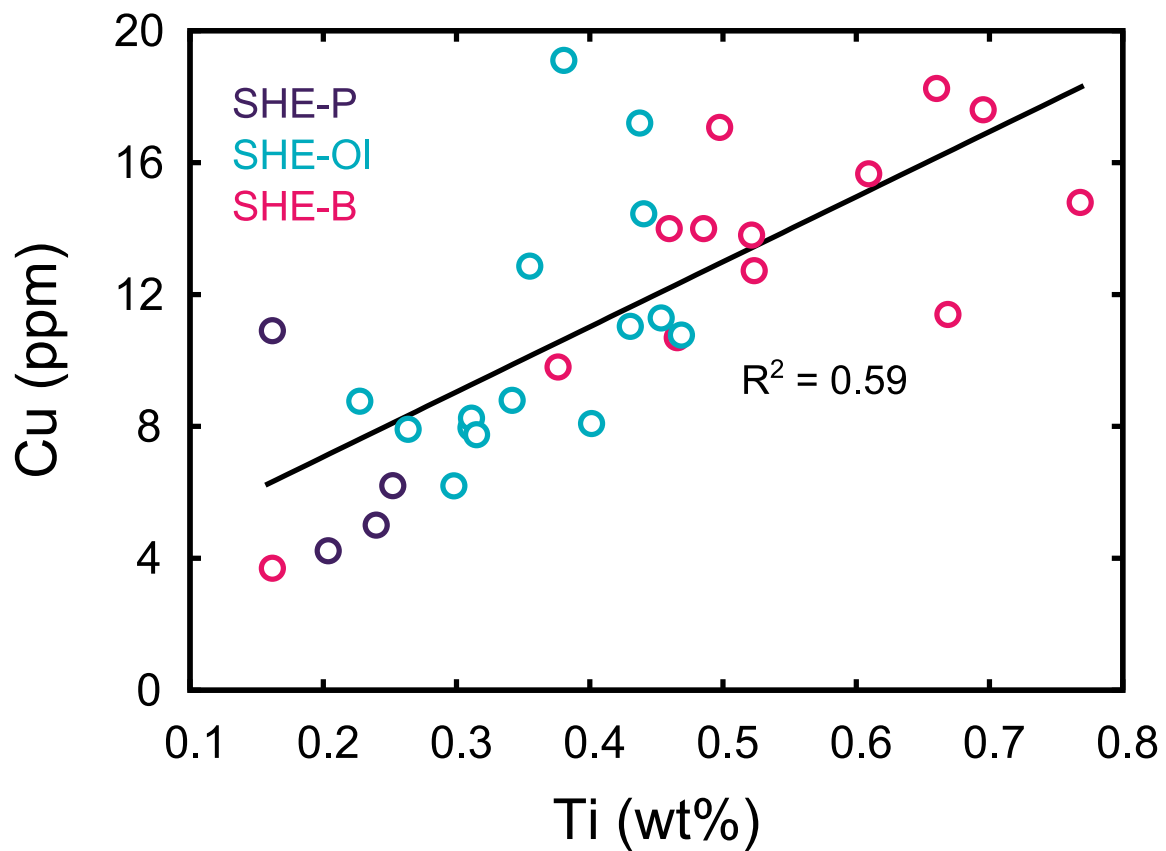


Fig. A14: Copper versus Ti contents in poikilitic, olivine-phyric and basaltic shergottites.

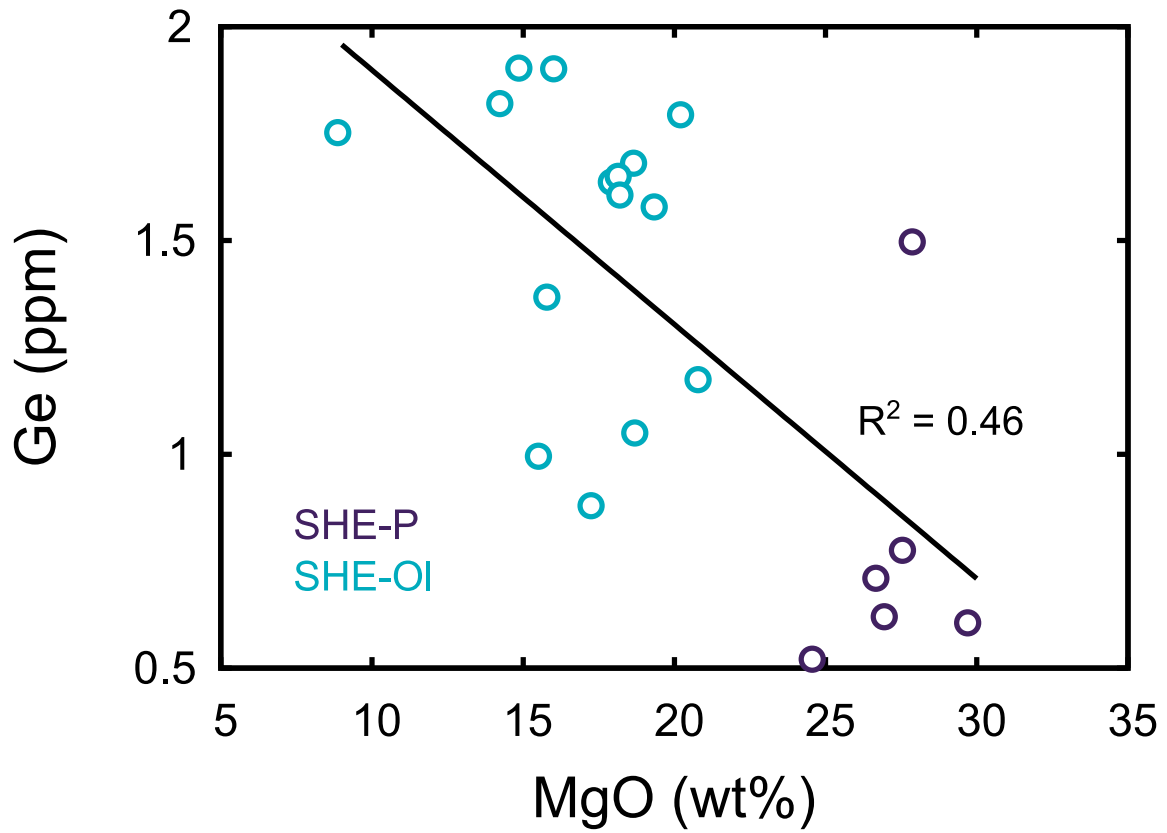


Fig. A15: Germanium versus MgO contents in poikilitic and olivine-phyric shergottites.

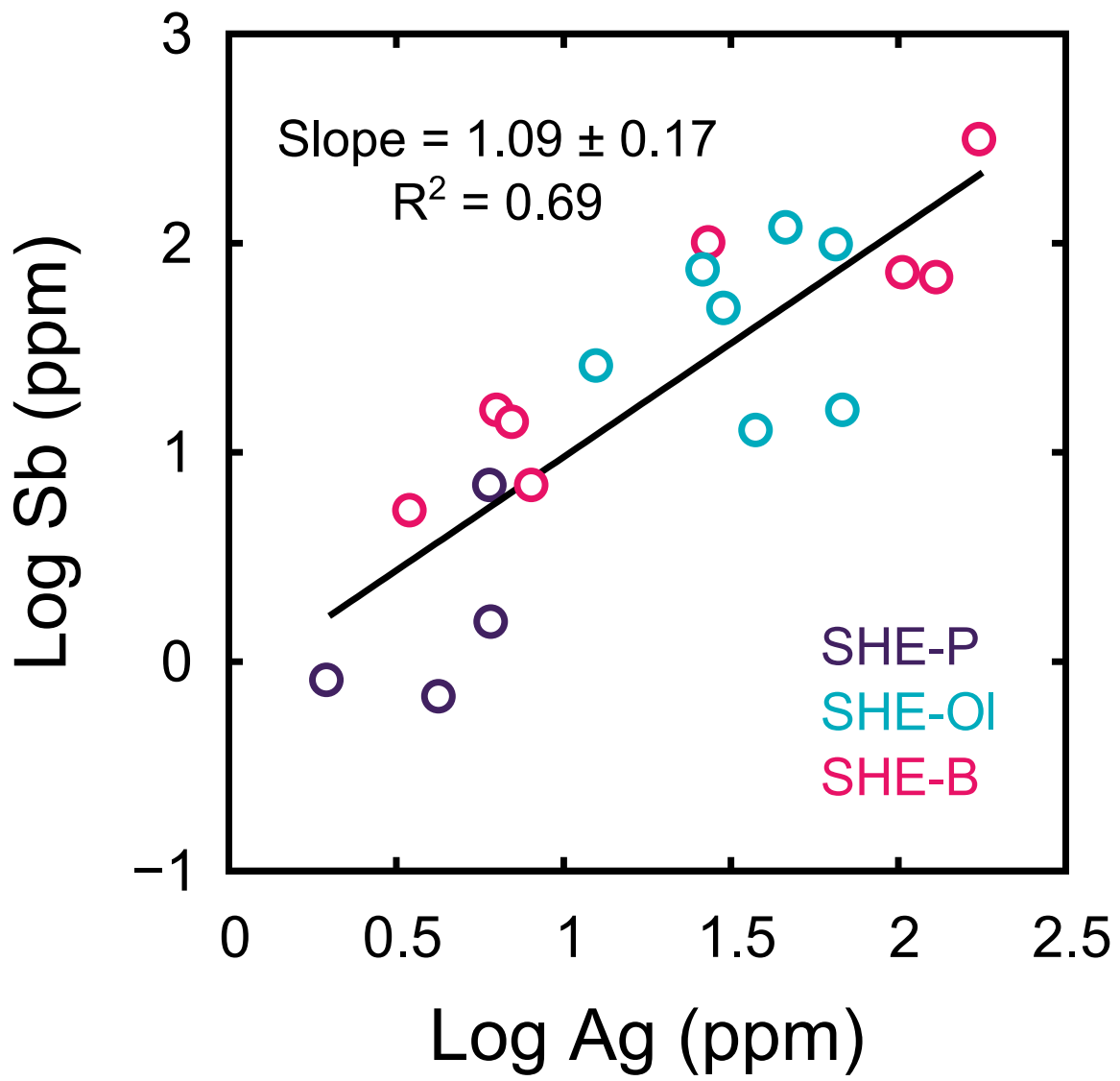


Fig. A16: Log-log plot of Sb and Ag in poikilitic, olivine-phyric and basaltic shergottites.

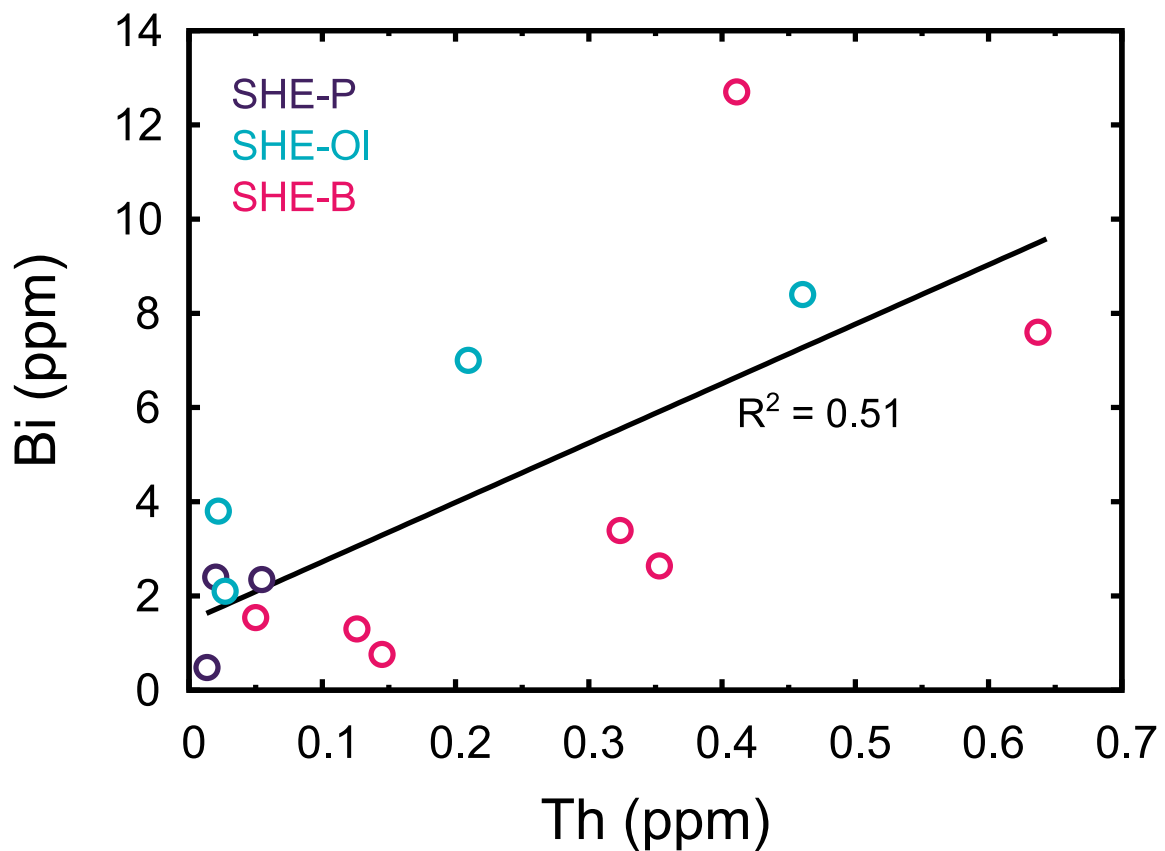


Fig. A17: Bismuth versus Th contents in poikilitic, olivine-phyric and basaltic shergottites.

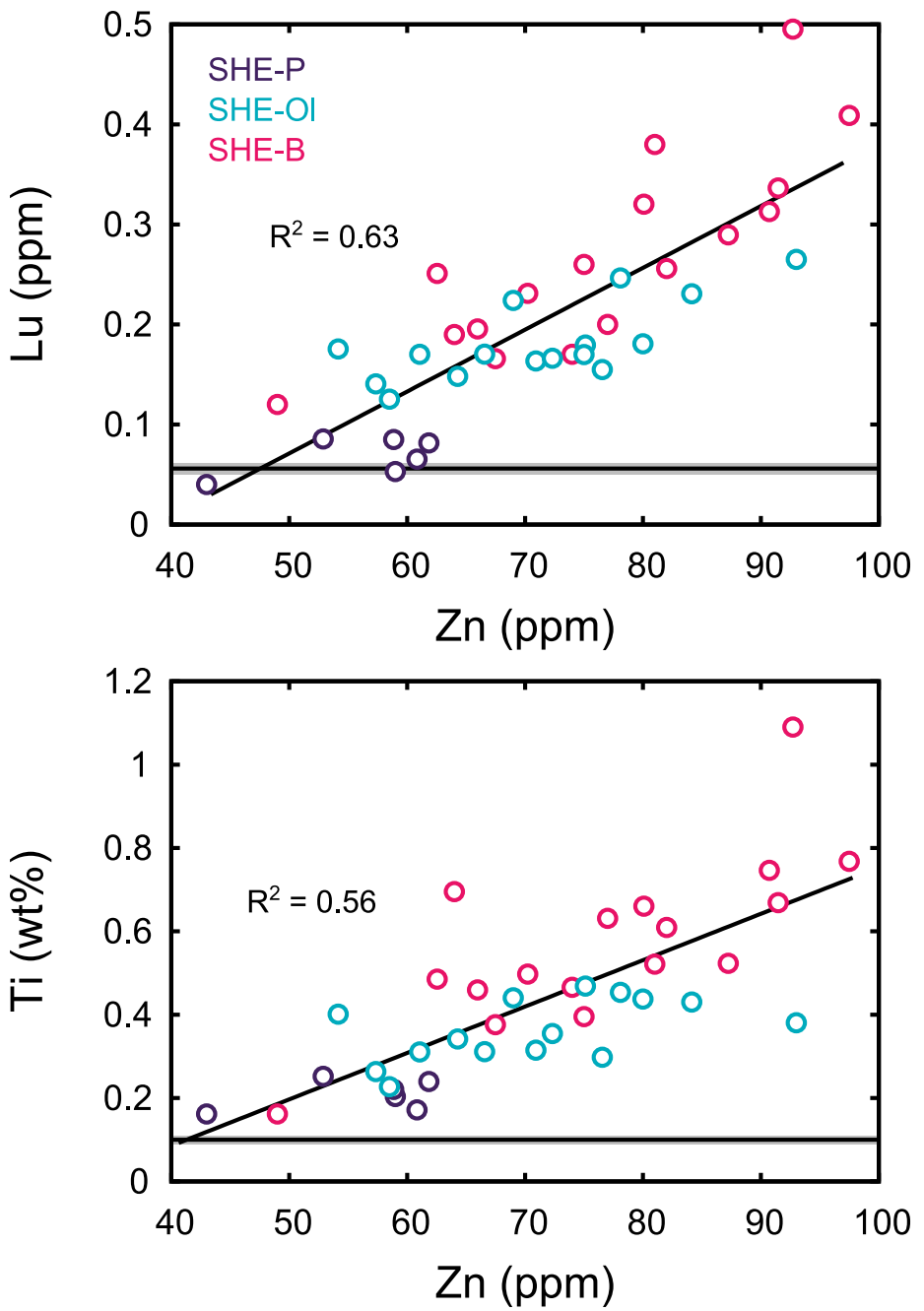


Fig. A18: Zinc versus Lu (top) and Zn versus Ti (bottom) contents in poikilitic, olivine-phyric and basaltic shergottites. Horizontal lines and gray bands present the BSM abundances of Lu and Ti, and their uncertainties, respectively (Table 5).

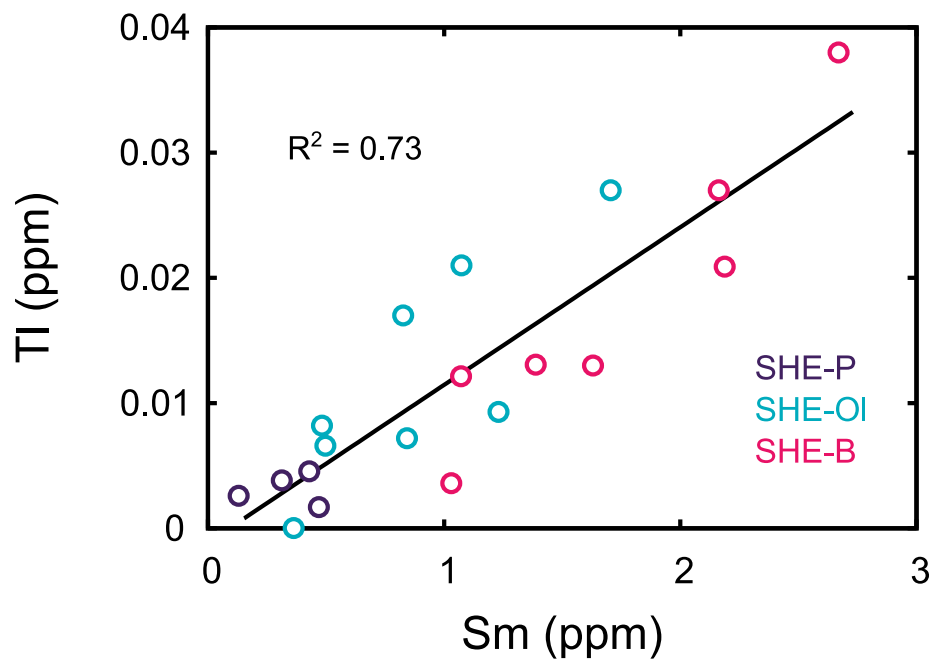


Fig. A19: Thallium versus Sm contents in poikilitic, olivine-phyric and basaltic shergottites.

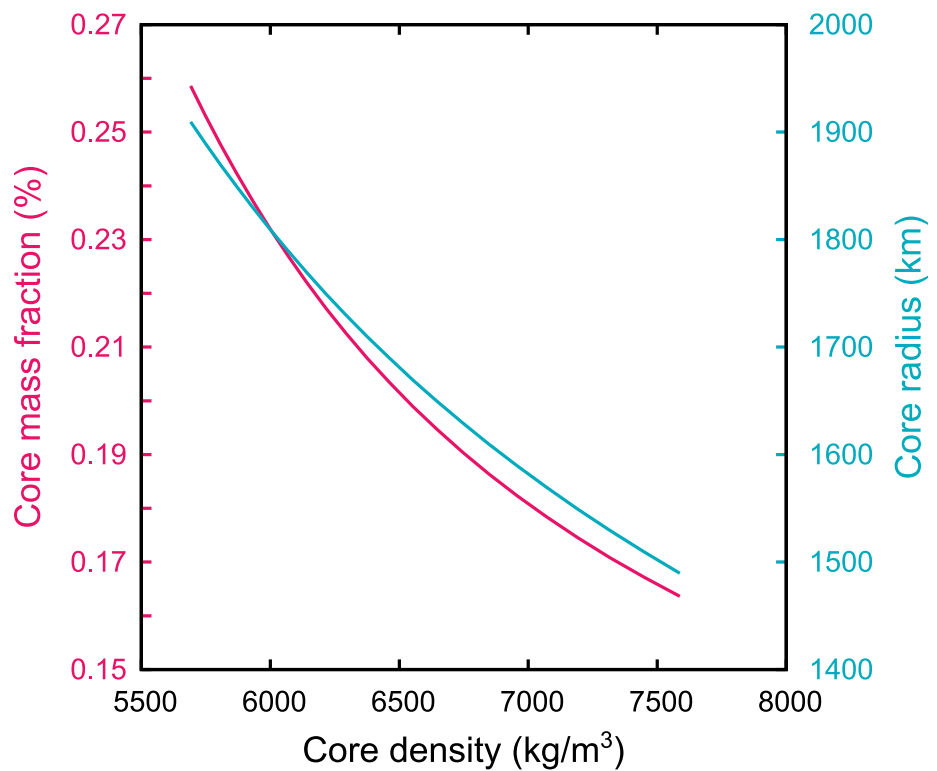


Fig. A20: Mass fraction and radius of the Martian core as a function of its density that are consistent with the BSM model presented in this study.